

LIBRARY Michigan State University

This is to certify that the dissertation entitled

He II Reverberation In NCG 5548

presented by

Aaron Patrick LaCluyzé

has been accepted towards fulfillment of the requirements for the

Ph.D. degree in Astrophysics and Astronomy

Major Professor's Signature

Date

Doctoral Dissertation

MSU is an affirmative-action, equal-opportunity employer

PLACE IN RETURN BOX to remove this checkout from your record. **TO AVOID FINES** return on or before date due. **MAY BE RECALLED** with earlier due date if requested.

DATE DUE	DATE DUE	DATE DUE
	<u> </u>	

5/08 K./Proj/Acc&Pres/CIRC/DateDue indd

HE II REVERBERATION IN NGC 5548

By

Aaron Patrick LaCluyzé

A DISSERTATION

Submitted to
Michigan State University
in partial fulfillment of the requirements
for the degree of

DOCTOR OF PHILOSOPHY

Astrophysics and Astronomy

2008

ABSTRACT

HE II REVERBERATION IN NGC 5548

By

Aaron Patrick LaCluyzé

Despite decades of study, the exact nature of the central engines of Active Galactic Nuclei (AGN) is still a mystery to be solved. Although great strides have been made, there are some outstanding questions that still need to be resolved, and new tools are needed to answer them. The goal of this project was to craft a new method to accurately measure highly blended weak emission lines in AGN. In particular, the reverberation behavior of He II $\lambda 4686$ and He II $\lambda 1640$ were investigated to reconcile a discrepancy between theoretical models, which predicted that the two lines should have the same lagtime and previous observational studies, which found that the optical line had a reverberation lag several times longer than the UV line.

The optical and UV He II emission lines were measured to have a reverberation lag time of 5 - 6 days, with good overlap between the two lines. Furthermore, a previously measured strong lines, C IV, which were also involved in the heavy blending, was measured to have a lagtime consistent with previous measurements. This helps to validate the technique that was used. This technique, which required a large software development effort, included using an automated fitting routine to simultaneously fit multiple emission line template profiles that were, themselves, created from observed data.

One rather surprising result was the clear indication that He II and C IV are not created by the same gas within the BELR. This is contrary to what was predicted by the typical model of the BELR but consistent with previous measurements.

Copyright by AARON PATRICK LACLUYZÉ 2008 For Lise, Dodger, Anna and Delenn

ACKNOWLEDGMENTS

First and formost, I must thank my wife, Jennifer, and my parents Paul and Mary. Without their help and support, I would not have made it this far. I also want to thank my advisor, Dr. Jack Baldwin. His patience has been saint-like.

There have been a great many graduate students over the years who have helped me though all of this. Thanks to Pete, Bob, Mike, Fred, Ryan, and Chuck, all of whom helped me understand what graduate school is all about. Brian, Chris, Ken, Nathan, and Katie helped me make it through the long years that followed. Thanks also to the current pool of grad students who have kept me sane while I finished. Special thanks goes to Charles, who was willing to answer my silly questions about software.

A very special thanks goes to Dan Reichart, who took a chance on me and has been very patient while I tied up loose ends.

I am grateful to the National Science Foundation for their support of this work under grant AST-0305833, and to NASA for their support under ADP grant NAG5-13075. I also thank Jack Baldwin, Mark Bottorff, Gary Ferland and Kirk Korista, the co-investigators on the latter grant, for their help.

Thanks to Christopher Waters for the LATEX class used to format this thesis.

TABLE OF CONTENTS

Li	st of Table	es	viii
Li	st of Figur	es	ix
1	Introduct	ion	1
	1.1	A Brief history of AGN	2
	1.2	AGN Standard Model	3
	1.3	Reverberation Mapping	6
	1.4	The Importance of He II Emission	9
2	Data Set	Description	16
	2.1	Background on AGN Watch and data set for NGC 5548	16
	2.2	Ultra-Violet Data From IUE and HST	17
	2.2.1	Non-linearity of IUE at Low Flux Levels	18
	2.3	Optical Data	23
	2.3.1	Corrections to the Optical Data	25
	2.3.2	Observed vs. Rest Frame	28
3	Data Fitt	ing and Measurement	29
	3.1	Automated Fitting Routine	29
	3.2	Building the Blend	32
	3.2.1	Fe II Template	33
	3.2.2	Other Templates	35
	3.2.3	Fitting Parameters	38
	3.2.4	Fitting Windows	40
	3.3	Minuit and the χ^2 Minimization	42
	3.4	Error Estimation	46
	3.5	Cross-Correlation Lags	47
4	Results		55
•	4.1	Cross Correlation Centroid Distribution	55
	4.2	Light Curve Error Estimation	59
	4.3	Sensitivity to Profile Templates	61
5	Discussio	n	67
6	Summary	·	72
A	Code for	contin.f	7 5
В	Code for	cfunk f	87

\mathbf{C}	Code for uvcontin.f	91
D	Code for uvfunk.f	104
${f E}$	Code for functions.f	108
F	Template Profiles	115
	References	137

LIST OF TABLES

1.1	Reverberation Lags From Previous Studies
1.2	Other C IV $\lambda 1549$ / He II $\lambda 1640$ Lag Ratios
2.1	IUE UV Data
2.2	Optical Data Site List
2.3	Optical Data
3.1	Fitting Windows
3.2	Optical Profile Summary
3.3	UV Profile Summary
4.1	CCCD Results
4.2	Profile Permutations
F.1	C IV BELR Template
F.2	He II BELR Template
F.3	He I BELR Template
F.4	H β BELR Template
F.5	C IV NELR Template
F.6	O III
F.7	He II NELR Template
F.8	O III 1663 BELR Template

LIST OF FIGURES

1.1	Simplified Cross-Sectional Representation of an AGN	5
1.2	Simplified Illustration of Reverberation Mapping	8
1.3	Simplified Grotrian Diagram of He II	10
1.4	NGC 5548 Optical Detail	11
1.5	NGC 5548 HST UV Detail	12
2.1	Typical UV spectrum	19
2.2	Ratio of IUE to HST flux levels as a function of IUE detector counts	21
2.3	Typical optical spectrum	24
3.1	Typical Optical Spectrum	30
3.2	Typical UV Spectrum	31
3.3	Fe II Optical Template	34
3.4	Fe II UV Template	35
3.5	Example Optical RMS Spectrum	36
3.6	UV RMS Spectrum	37
3.7	$H\alpha$ BLR Profile	38
3.8	He II BLR Profile	39
3.9	He I BLR Profile	40
3.10	C IV BLR Profile	41
3.11	Optical Fit Overlay	44
3.12	UV Fit Overlay	45
3.13	UV Continuum Light Curve	49

3.14	Optical He II Light Curve	50
3.15	UV He II Light Curve	51
3.16	C IV Light Curve	52
3.17	H β Light Curve	53
4.1	Composite Centroids for Optical and UV He II	56
4.2	Cross Correlation Centroid Distribution for C IV	58
4.3	Composite Centroids for Optical and UV He II and C IV	59
4.4	Cross Correlation Centroid Distribution for H eta	60
4.5	He II Error Estimation Test	61
4.6	He II Error Estimation Test	62
4.7	He II $\lambda 4686$ Profile Width	64
5.1	Standard LOC Model	70

CHAPTER 1: INTRODUCTION

Since their discovery by radio telescopes in the late 1950's, quasars have captivated researchers. Despite decades of intense study, only a general theoretical model exists with many details still unclear. Under the current standard model quasars are just one manifestation of a larger class of objects called active galactic nuclei (hereafter AGN). Because even the most nearby of AGN are at very large distances from us, direct imaging of their central cores is impossible. This makes verification of theoretical models difficult at best. We must therefore resort to indirect methods to attempt to gain insight into the actual physical workings within the core region. One technique that can be used to study the inner regions of AGN is reverberation mapping, where the lag time between a change in the driving continuum radiation and the response of an emission line is used to indirectly measure the distribution of gas around the central engine.

In this work, I present a new analysis of He II reverberation in NGC 5548, a relatively nearby and well studied low luminosity AGN, classified as a type 1 Seyfert galaxy. The remainder of this chapter will give a brief introduction to AGN, an overview of the reverberation mapping technique, and a discussion of why He II emission is both interesting and important to our understanding of AGN.

1.1 A Brief history of AGN

During the late 1950's, radio astronomy was beginning to produce vast catalogs of radio sources. Using these catalogs, astronomers attempted to match radio sources with optical counterparts. During this process, it became clear that several of the radio sources had fairly blue star-like point source optical companions. These strange objects were dubbed quasi-stellar radio sources (QSOs), or quasars for short. The most famous of these objects are 3C 48, the first to be observed, and 3C 273, the first to be identified with a bright ($m_v = 12.8$) stellar-appearing object; see Schmidt (1963), Oke & Schmidt (1963) and Greenstein & Schmidt (1964).

The spectra of these objects caused both initial confusion and decades of debate. Since the objects were star-like in appearance, the emission lines that were detected were not immediately identified. Schmidt and his collaborators made the first steps toward understanding by showing that in 3C 273 these unidentified emission lines were actually the well known Balmer lines of Hydrogen that had undergone a redshift of $z \simeq 0.158$. This sort of redshift had been seen before in galaxies, but a combination of being at a high redshift as well as being bright and stellar in appearance was both new and interesting. This led to debate within the community as to the nature of these objects. They could be extremely bright, distant objects with a redshift due to the Hubble flow (the expansion of the Universe itself.) This would explain the pointlike appearance, but would imply an extremely large luminosity. Or they could also be much less luminous star-like objects with the redshift arising from a large peculiar radial velocity relative to Earth. The latter hypothesis would imply a more ordinary luminosity, but would give no reason for the high velocity. While Schmidt and his colleagues assumed the former, there was no explanation at the time for how quasars could generate enough energy to be luminous enough to appear so bright at these vast extra-galactic distances. It is important to understand that like many objects in astronomy, the definition of a quasar was originally based mainly on appearance.

During the decades since, there have been a variety of objects discovered that have many properties in common with quasars. This much larger group of seemingly related objects are known collectively as active galactic nuclei. These AGN are galaxies in which the central core can outshine the rest of the stars in the galaxy combined. The defining characteristic is that the continuum radiation produced by these objects is not only luminous, but spans a large range in energies, extending from x-ray out to the far IR or radio regime. In most cases, there are also a variety of emission lines that, while common to most AGN, are of differing strengths depending on the object in question. The gas creating these emission lines is believed to be fed in from the host galaxy, making them a good tracer of chemical evolution in the central part of massive galaxies over a wide range of lookback times. (Hamann & Ferland, 1999; Hamann et al., 2002)

1.2 AGN STANDARD MODEL

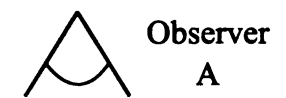
While there has been a great deal of debate on the exact structure of AGN, a "standard model" has been embraced by a large portion of the astronomical community. Under the standard model, all AGN, from radio galaxies to blazars, are the same type of object, with distance, viewing angle, and the total output energy being the major factors that dictate which classification each object is given. The object of interest in this study, NGC 5548, is a type 1 Seyfert galaxy. Seyfert galaxies are a type of AGN that show clear emission lines, nuclear x-ray emission, and sometimes a small-scale radio jet but are otherwise radio quiet. Seyfert galaxies are the most common type of AGN.

In the standard model (Gaskell, 2008, and references therein), the method of energy generation is accretion of matter onto a super-massive blackhole. This central black hole has a mass of about $10^6 - 10^8 M_{\odot}$ and is surrounded by an accretion disk that is on the order of a light day in diameter (see figure 1.1.) This size is inferred

from variations in the output intensity that are on the order of a day for lower energy objects like Seyfert galaxies, while more luminous QSOs show variability on time scales closer to a year, implying a correspondingly larger central engine. As gas falls in toward the black hole, it collapses into an accretion disk due to angular momentum conservation. Internal friction within this disk causes the gas to heat up and begin to emit radiation like a blackbody. The closer the gas is to the center, the higher its angular speed, and the higher the temperature. This creates a superposition of blackbody radiation of varying temperatures generating a powerful and relatively flat continuum. Secondary processes then convert some of this thermal radiation into additional x-ray, IR, and radio light. While some of this radiation escapes the AGN, some of it is reprocessed into emission lines by cooler gas that lies outside of the accretion disk.

The first region of gas that is encountered by the continuum radiation on its journey out from the accretion disk is the so called broad emission line region (BELR, sometimes written as BLR). This gas is in close to the accretion disk, at a distance of several light days to tens of light days from the central source in a typical Seyfert galaxy. Because the gas is in close to the central mass, it has a large velocity on the order of 10,000 km/s. This broadens any emission lines from the gas in the BELR, hence the name broad-line region. This Doppler-broadened emission, however, isn't seen in all types of AGN. The standard model postulates that outside the BELR there is a large dusty torus, a doughnut-shaped collection of gas and dust that blocks the emission coming from the interior. The angle of the object to our line of sight will dictate our ability to observe the broad emission lines. This is the primary classification difference between type 1 and type 2 Seyfert galaxies, with type 1 showing broad and narrow emission lines and type 2 showing only narrow lines (see figure 1.1.)

One consequence of the location of the BELR is that it is quite sensitive to any variability in the continuum emission. The emission lines are generated by gas that



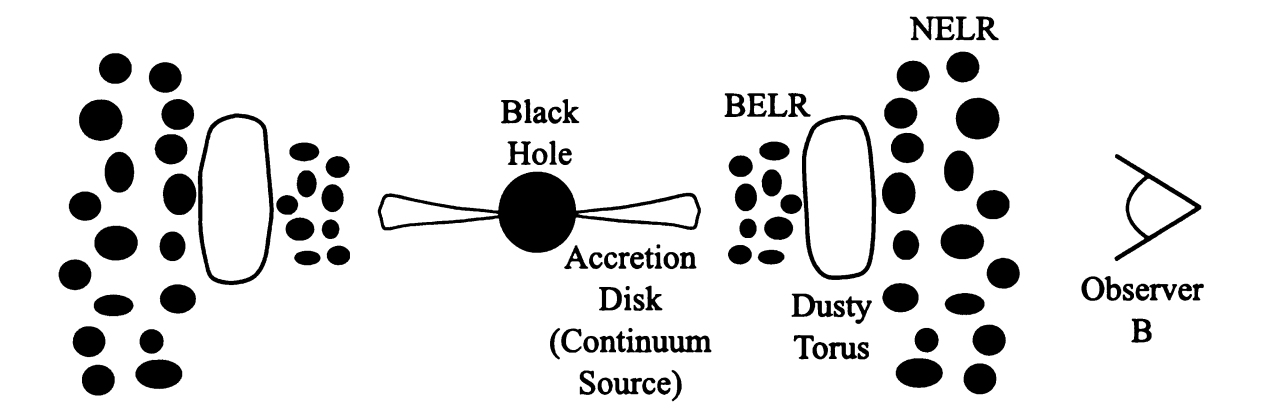


Figure 1.1 Simplified Cross-Sectional Representation of an AGN - This figure shows a typical AGN cross-section, seen edge-on. This figure is not to scale in any way and is meant as a general guide to the relative location of regions of interest in an AGN. When an observer is at position A, the emission from the interior BELR can be seen. When an observer is at position B, the dusty torus will block the BELR emission and only the lines from the NELR will be seen. This leads to a distinction between Seyfert 1 galaxies, which show BELR emission, and Seyfert 2 galaxies, which do not show BELR emission.

has been been excited by being continually bathed in radiation from the central engine. When the central engine's emission changes in intensity, the broad line emission also changes on a time scale directly related to the light travel time from the central source to the emitting gas. This variability in the central continuum is often seen in AGN, although the exact cause is not well known. It is also important to understand that the variability is not predictable or periodic as it would be in certain types of variable stars. As such, obtaining meaningful observations of this variability can be a long and difficult process spanning many months to years. Because this variability is not regularly periodic, extensive observations need to be made to ensure that the object is observed in both a quiet baseline state as well as during a period of more intense activity.

Outside of the dusty torus is another large region of gas that also reprocesses the continuum radiation into emission lines. This gas is much further from the central engine and as such does not exhibit the large Doppler broadening seen in the BELR. This region is therefore called the narrow emission line region (NELR, sometimes written as NLR). Unlike the BELR, the NELR is fairly insensitive to short term variations in the continuum intensity. As such, we can treat the narrow emission lines as being constant over the time scales during which the BELR is observed.

1.3 REVERBERATION MAPPING

Although AGN are very luminous, it was quickly deduced that for the core to coherently vary in brightness on timescales of days or weeks as observed, it must be very small, only light-days to light-weeks across (Terrell, 1967). This means that even the most nearby AGN have cores, including the BELR, that are on the sub-arcsecond scale and cannot be resolved by either ground or space based instrumentation. Direct imaging of the cores of AGN is simply inconceivable for the foreseeable future.

We can exploit the response of the BELR to changes in the continuum to indirectly measure the size of the BELR by making a few basic assumptions (Peterson & Horne, 2006). We assume that the continuum originates from a single central source. Because the size of the BELR is expected to be about a factor of 100 larger than the size of the accretion disk, this assumption is well justified.

We also assume that the most important time scale to be considered is the light travel time required for photons to travel a distance r from the central source to the BELR clouds:

$$\tau_{LT} = \frac{r}{c} \tag{1.1}$$

There are two other time scales that should be considered because they may at

first glance seem important. The first is the recombination time scale:

$$\tau_{rec} = (n_e \alpha_B)^{-1} \tag{1.2}$$

Here α_B is the Hydrogen case B recombination coefficient, and n_e is the particle density of the line producing gas. Case B describes the situation where low-density ionized clouds form Hydrogen emission lines such that the higher Lyman lines scatter often enough to be degraded into a Balmer line and either a Ly α or the two-photon continuum and the electron density must be low enough for collisions to be slow compared with spontaneous emission (Ferland, 1999). This is thought to describe line formation in most AGN (Osterbrock, 1989). A typical BELR density of $n_e \approx 10^{10} {\rm cm}^{-3}$ gives a $\tau_{rec} \approx 0.1 {\rm hr}$, much shorter than the light days of τ_{LT} .

A second possibly important time scale is the dynamical time scale for the motion of the BELR gas itself.

$$\tau_{dyn} \approx \frac{r}{\Delta V} \tag{1.3}$$

In the case of a typical Seyfert galaxy, the type of AGN of interest in this work, $\tau_{dyn} \approx 3$ – 5 years. This is much longer than the several months of the observing campaign used here, but can become an important factor with longer campaigns.

A final assumption that needs to be made is that there is a simple relationship between the observed continuum and the ionizing continuum. Because the ionizing continuum is driving the line variations, we must assume that the ionizing continuum and the observed continuum vary in phase with one another. There is some evidence that there is a delay between the long wavelength continuum and the shorter wavelength continuum variations (Gaskell, 2008), but the time scale of this is still significantly shorter than the timescale for the emission-line response.

To better understand the principle behind this technique, imagine a situation where we have three test clouds at a common distance r from the central engine (the

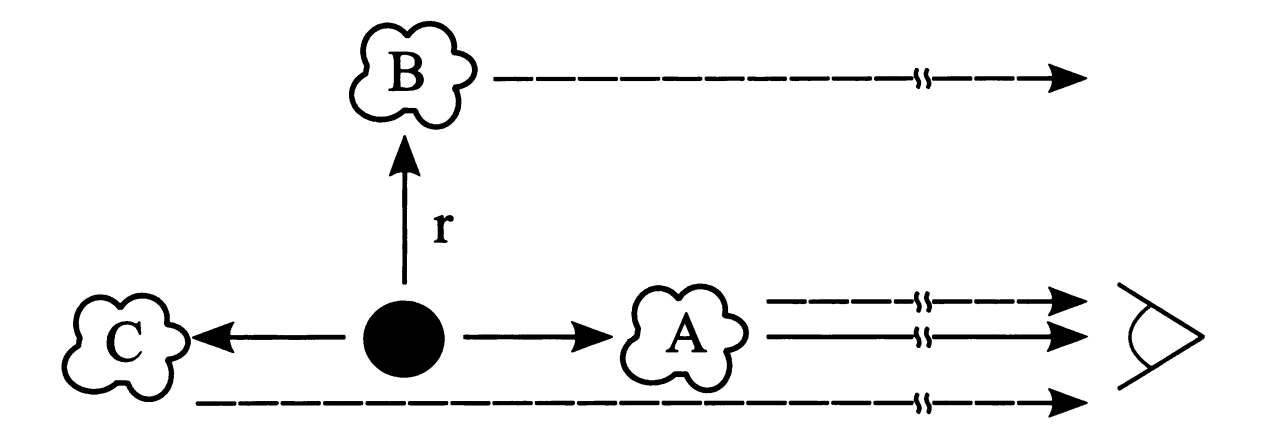


Figure 1.2 Simplified Illustration of Reverberation Mapping - The dark circle represents the accretion disk central engine of the AGN, producing the broad spectrum continuum radiation. The three objects labeled "A", "B", and "C" are representative BELR clouds all at the same distance r from the central engine. Because of the additional distance that lines emitted by clouds "B" and "C" must travel compared to "A", there is a delay in the response of the observed broad emission to a change in continuum luminosity.

black hole and its accretion disk, see figure 1.2.) If the central engine is variable and has a sudden increase in continuum luminosity, this pulse of increased intensity takes a finite amount of time to reach the gas which re-processes this continuum radiation, giving rise to the BELR lines. The pulse in the continuum luminosity continues onward to our observer at some distance which is large compared to r. The response of cloud "A" to the increased continuum is seen by our observer almost immediately after the increase in the continuum as cloud "A" is along the line of sight from the observer to the central engine. The response of cloud "B" is seen after an additional time r = r/c corresponding to the additional distance that the emission line radiation must travel. The response of cloud "C" has an additional distance of r compared to cloud "B", or 2r compared to cloud "A".

While it takes a finite amount of time for all of the gas to respond, the calculation of a cross correlation between the light curves of the continuum and the responding emission line yields a mean response time for the emitting gas, which is reported as the characteristic lag time. This is the principle behind reverberation mapping and

is the best tool currently available to study the inner structure of AGN.

This generalized discussion of the nature of the BELR is for the most part speculative. Very little is actually known about the true structure of this region. While the cartoon picture of discrete clouds is useful for illustrative purposes, it may not reflect the true nature of the region.

1.4 The Importance of He II Emission

In order for an emission line to be produced efficiently, there must exist a specific combination of gas density and incident radiation strength. This is the crux of the "Locally Optimally-emitting Cloud" (LOC) model put forth by Baldwin et al. (1995). If the gas is too diffuse, there is not enough reprocessing to significantly affect the radiation output. If the gas is too far from the central engine, there isn't enough incident flux to cause significant excitation or ionization/recombination. This is the central premise behind several models of the inner regions of AGN. Each emission line has an optimal location in space around the central engine where it can be produced efficiently. This corresponds to a characteristic distance from the center, assuming a roughly spherically symmetric distribution of gas. This distance is set by the ionization parameter, the ratio of incident ionizing flux to the gas density.

In this work, the primary goal is to measure the reverberation lags of He II $\lambda 4686$ in the optical region and He II $\lambda 1640$ and C IV $\lambda 1640$ in the ultraviolet region in NGC 5548. The He II lines are produced by singly ionized helium which is hydrogenic in nature. This means that, having only one electron, He II behaves in many ways similar to hydrogen and is therefore relatively easy to understand. Theoretical predictions (Baldwin et al., 1995) show that the optimal conditions for producing both the $\lambda 4686$ and the $\lambda 1640$ lines are virtually identical as both emission lines should be produced by the same recombination and radiative cascading process (MacAlpine, 1981), as illustrated in figure 1.3. This means that they should both have about the same

reverberation lag times. In addition, Bottorff et al. showed that plasma simulations assuming a simple model for the BELR gas distribution (see discussion of LOC model in chapter 5) suggest that the He II lines (λ 1640 and λ 4686) should have a similar reverberation lag as C IV (λ 1549).

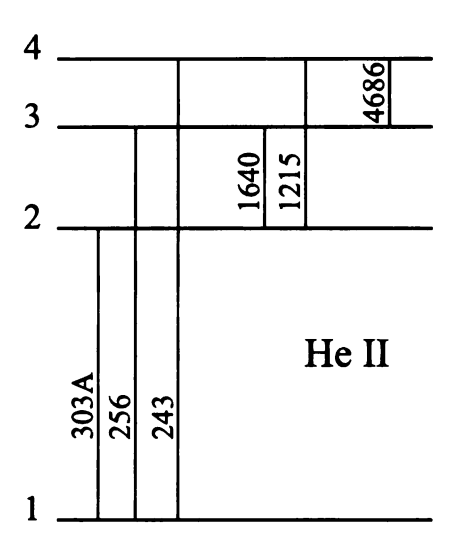


Figure 1.3 Simplified Grotrian Diagram of He II, showing only the first four energy levels. The lines between energy levels are labelled by the approximate wavelength of the photons emitted when an electron drops from the higher to the lower energy level, or the wavelength of light absorbed to move an electron from the lower energy level to the higher one. Of particular note are the paths that would lead from level 4 to level 3 and from level 3 to level 2 that would produce $\lambda 4686$ and $\lambda 1640$.

From an observational standpoint, there is only one object, NGC 5548, where the $\lambda 1640$ and $\lambda 4686$ lines have been measured in the same campaign. Because the BELR is changing over time, it is important to measure both lines during the same time period in order to accurately measure the lag ratio. Wamsteker et al. (1990) studied the intensity ratio of the He II $\lambda 1640$ and $\lambda 4686$ in observations from both IUE and ground based data sources from 1978 - 1986. While reverberation mapping was not the goal of that study, the authors did find that the intensity ratio of the two lines, $f(\lambda 1640)/f(\lambda 4686)$, varied from 4 to 10 during the study. A changing flux ratio would imply that the two lines are responding to the continuum changes on different time scales, implying different reverberation lag times for the two He II lines. While

Wamsteker et al. did some fit synthetic profiles to some of the blended emission lines, they did so by using several generic line components rather than true template profiles generated from the observations.

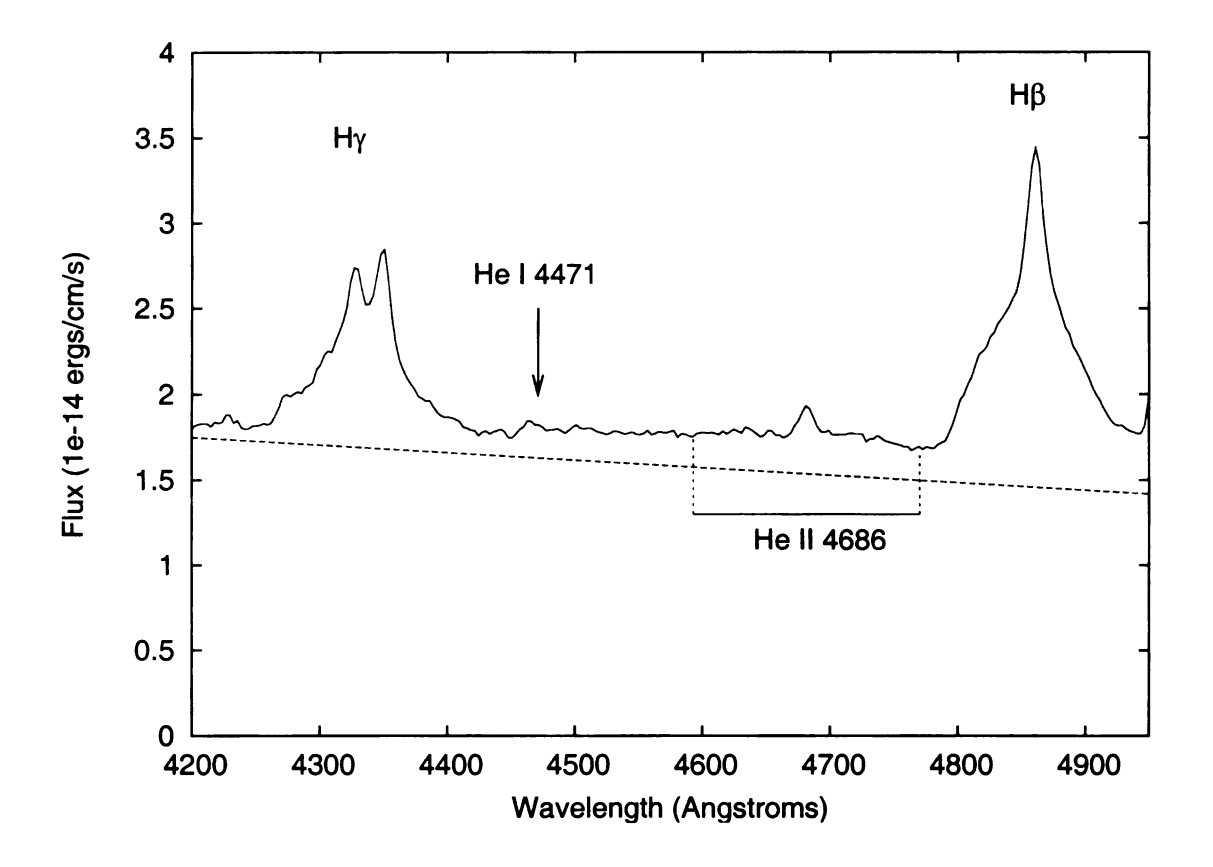


Figure 1.4 NCG 5548 Optical Detail - Example of NGC 5548 optical spectrum, as used in Dietrich et al. (1993). The continuum was approximated as a straightline under the region of interest (dashed line.) The He II λ 4686 emission was defined to be in a simple bin above this pseudo-continuum from 4593 - 4770 Å. This area includes contamination from the wing of H β as well as He I and a weak iron multiplet that is contaminating the entire region.

NGC 5548 was later a target for study by the International AGN watch (see chapter 2 for more information on this data set.) The UV He II λ 1640 and C IV λ 1549 (Clavel et al., 1991) and the optical He II λ 4686 (Dietrich et al., 1993) were among the emission lines studied to determine their reverberation lag times. These two studies found that the two He II lines may have different reverberation lags (between 4-10 days for the UV line and 7 days for the optical) and the He II λ 1640 did not agree well

with C IV (between 8-16 days). The authors did caution, however, that blending with other nearby emission lines is an issue (see figure 1.4.) The emission lines were defined to be in a simple wavelength bin, and all flux above a straight-line pseudo-continuum was assumed to be from the line in question. This does not correctly account for the wings of surrounding lines that could be contaminating the measurement. The optical He II λ 4686 line is contaminated by H β , He I, and a Fe II multiplet that is under the entire region (see section 3.2 for more discussion on these contaminants.)

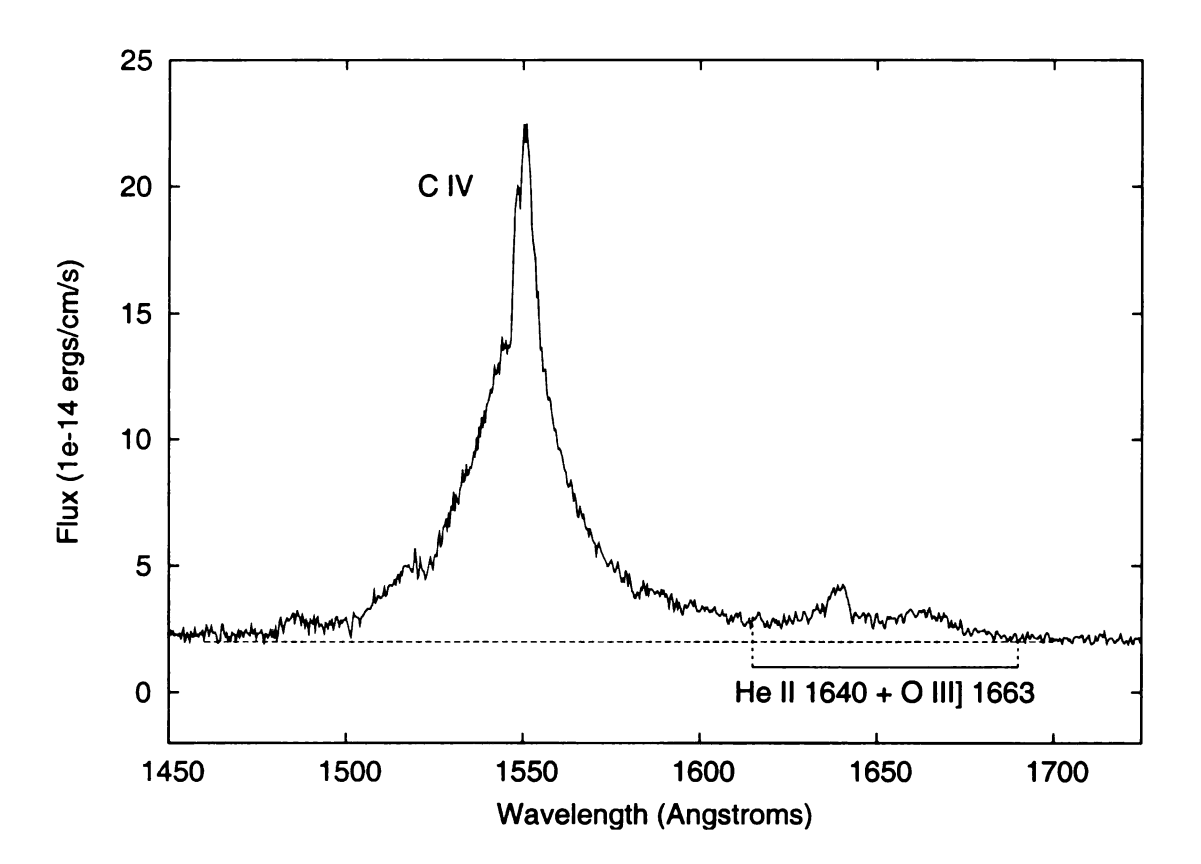


Figure 1.5 NCG 5548 HST UV Detail - Example of NGC 5548 UV spectrum, as used in Korista et al. (1995). The continuum was approximated as a straightline under the region of interest (dashed line.) The He II $\lambda 1640$ emission was defined to be in a simple bin above this pseudo-continuum. This area includes contamination from the wing of C IV $\lambda 1549$ as well as O III] $\lambda 1663$ and a weak iron multiplet that is contaminating the entire region.

Korista et al. (1995) did a similar analysis for the UV data, but included measurements from HST as well as IUE. Once again, a straight line continuum and wavelength

bins were used in a manner similar to the Dietrich et al. study (see figure 1.5.) In the case of the UV spectrum, the He II $\lambda 1640$ line is heavily blended with the O III] $\lambda 1663$ emission as well as the wing of C IV and a weak Fe II multiplet that is contaminating the entire region. In this case, no attempt has been made to deblend the O III] $\lambda 1663$ emission, and the effects on the reverberation lag were simply estimated.

Table 1.1: Reverberation Lags From Previous Studies - This table, taken from data in table 1 of Peterson & Wandel (1999), shows the best measured values for the reverberation lags of several emission lines from NGC 5548 using the 1989 AGN Watch data set.

Line	Lag (days)
He II $\lambda 1640$	$3.0^{+2.9}_{-1.1}$
He II $\lambda 4686$	$8.5^{+3.4}_{-3.4}$
C IV λ1549	$9.5_{-1.0}^{+2.6}$

The AGN watch data was also further analyzed by Peterson & Wandel (1999) in order to estimate the mass of the central black hole. During this study, more careful attention was paid to the reverberation lag measurements. These values are shown in table 1.1. While it is true that the two He II lines do agree within formal errors, the UV He II and the C IV do not overlap, which is not predicted by simulations (Bottorff et al., 2002). In fact, Bottorff et al. argue that if this discrepancy is real, it is a significant failure in a general picture that otherwise fits together all of the reverberation results. Under any situation where the $\lambda 1640$ and $\lambda 4686$ lines are formed by cascades following recombination, as is thought to be the case, the two lines must be formed in the same volume of gas and therefore should vary together with the same reverberation time scales. Bottorff et al. further show that the C IV $\lambda 1549$ should be produced under conditions similar enough to the region that favors He II

production and there should therefore be only a small difference in the reverberation lag times of C IV and either He II.

While the He II $\lambda 1640$ and $\lambda 4686$ lines do formally overlap in the one object where both line are measured in the same campaign, there are several other AGN where only the He II $\lambda 1640$ and the C IV $\lambda 1549$ were measured. These measurements are summarized in table 1.2. In each case, the lag ratio of C IV $\lambda 1549$ to He II $\lambda 1640$ differs from unity by a convincing margin.

Table 1.2: Other C IV $\lambda 1549$ / He II $\lambda 1640$ Lag Ratios - This table, taken from Bottorff et al. (2002) summarizes the (C IV $\lambda 1549$)/(He II $\lambda 1640$) lag ratio for several objects, which Bottorff et al. considered to have reliable lag measurements of both lines. It is clearly shown that this ratio is greater than 1 in all of the objects.

Object	(1549)/(1640) Lag Ratio	References
NGC 5548	3.3	Bottorff et al. (2002)
NGC 3783	5.0	Reichert et al. (1994)
Fairall 9	3.4	Rodriguez-Pascual et al. (1997)
NGC 7469	2.4	Wanders et al. (1997)
3C 390.3	3.8	O'Brien et al. (1998)
Average	3.6	

The conclusions of Bottorff et al. (2002) concerning the existing data were that, "the best estimate of the lag times is that the $\lambda 1640$ feature varies 3 times more rapidly than $\lambda 4686$ " and that "the He II $\lambda 1640$ lag times are measured to be several times shorter than those of C IV $\lambda 1549$ ". The first of these points would be extremely surprising, while the difference between the He II and C IV lag times is not predicted by the simplest models of the BELR.

One possibility, tested in this work, is that the He II lag measurements are simply in error. The He II emission lines are quite weak compared to most of the well-studied AGN emission lines. There is also considerable contamination by surrounding emission lines. In the case of He II λ 4686, it is contaminated by the blue wing of H β (and possibly to a some extent the red wing of H γ), He I λ 4471 and a Fe II multiplet. The UV He II λ 1640 line is similarly contaminated by C IV λ 1549 and O III λ 1663 as well as a Fe II multiplet. Previous measurements of these lines, such as those described above, have not fully accounted for these blending problems. Emission lines were defined either by a simple bin or approximated using a blend of Gaussian profiles. Neither of these methods fully account for contamination by other emission lines that may be varying at slightly different rates.

In this work, we present a new re-analysis of archival data of NGC 5548, a nearby, well observed, type 1 Seyfert galaxy. Careful attention has been paid to separating contamination from the He II emission so as to present the most careful measurement of the reverberation lags to date. This has also been done in a more automated fashion than in previous studies in order to remove some of the the human subjectivity that is always present in data analysis. The software tools that were developed were designed to be compatible with previously existing software that is used by several collaborators.

Chapter 2: Data Set Description

This chapter will outline the basic details of the data used for this study. It is important to understand that gathering the amount of data needed for a study like this is a huge undertaking. For example, several years of observations are needed to get a really good baseline covering multiple reverberation events, and these should have a time sampling of at least one observation every few nights. In this case, archival data from a previous effort were used. This archival data set, despite some of its shortcomings, is the most complete set of observations in terms of both spectral and temporal coverage of any AGN that has been taken.

2.1 Background on AGN Watch and data set for NGC 5548

The archival data set used here was taken as part of a project instigated by the International AGN Watch, a consortium of scientists who were interested in studying several AGN in detail, with careful consideration given to sufficient time resolution of observations. To this end, one of the objects chosen for study was NGC 5548, a nearby Seyfert 1 galaxy. NGC 5548 is of interest because it is close ($z = 0.017175 \simeq 71 \text{ Mpc}$) and although it is a fairly typical type 1 Seyfert galaxy, it is also highly variable. This allows for extensive study using reverberation mapping techniques. This work spanned more than a decade and produced a series of papers entitled "Steps Toward

Determination of the Size and Structure of the Broad-Line Region in Active Galactic Nuclei I-XVI". Clavel et al. (1991), Peterson et al. (1991), Peterson et al. (1992), and Dietrich et al. (1993) are of particular interest for the study described here.

Because of the need to compare lines in the optical as well as the ultraviolet, data from both ground and space based observations are necessary. The Earth's own atmosphere blocks far too much UV radiation to allow for observations in this wavelength regime to be taken from the ground. The UV data used here were taken using the International Ultraviolet Explorer (IUE), with some additional observations taken with the Hubble Space Telescope (HST).

2.2 Ultra-Violet Data From IUE and HST

The International Ultraviolet Explorer (IUE) satellite was launched in January of 1978. It carried an 18-inch telescope with a UV spectrograph. Although it initially had an expected service life of three years, it remained in operation until it was decommissioned on September 30, 1996. During 1988-1989, the AGN Watch used it for regular observations of NGC 5548 for roughly eight months (Clavel et al., 1991, and references therein.) During this time, a coordinated effort was made to obtain ground-based optical observations of NGC 5548 to complement the UV data from IUE.

This IUE data set is the longest regularly sampled set of observations of NGC 5548 in the UV. Although the resolution is somewhat low at roughly 2 Å per pixel, it is difficult to ignore this large data set. The observations span Julian Dates 2447510 - 2447745 (14 December 1988 - 7 August 1989) and were taken quite regularly about four days apart, with a total of 60 different days with observations. On any given day, one LWP (1900-3300 Å) and at least one SWP (1170-1970 Å) spectrum were taken. Observations were taken in low resolution mode (1000 km s⁻¹ FWHM) with the large aperture (10" x 20".) In the analysis described here, the SWP and LWP

spectra from any given day were combined together to create a single spectrum for each date, with multiple SWP spectra averaged together when more than one was taken on the same day.

One drawback, in both the IUE and optical data sets, is the sampling rate. Ideally, observations would be taken on a time scale shorter than the shortest reverberation lag that is being studied in order to ensure sufficient temporal coverage of the emission line's reaction to the changes in the continuum. In the case of IUE, spectra were taken quite regularly at about four day intervals. The primary lines of interest for the original AGN Watch study have lag times on the order of tens of days and would be adequately sampled by measurements every four days. Due to the techniques used for the reverberation analysis, this data can still be used for He II, and aliasing due to the regular sampling also should not be an issue (see section 3.5 for further discussion of this point.)

2.2.1 Non-linearity of IUE at Low Flux Levels

The IUE data have a variety of known problems. Because of the age and nature of the instrument, several different corrections need to be made to the raw data before they are useful for scientific measurements. These corrections can be as complex as taking into account the angle of the instrument relative to the magnetic field of the Earth. These corrections are well known and have been applied to the data obtained from the AGN Watch.

Koratkar et al. (1997) made a detailed comparison of near simultaneous spectra of several AGN taken with both IUE and the HST FOS. They found that there were three objects that had observations taken with both instruments no more than 24 hours apart. These objects were Mrk 509, NGC 3783, and NGC 5548. While detailed comparisons of the two instruments had previously been done, such as Bohlin et al. (1990), they were typically done with bright spectrophotometric standard stars. It

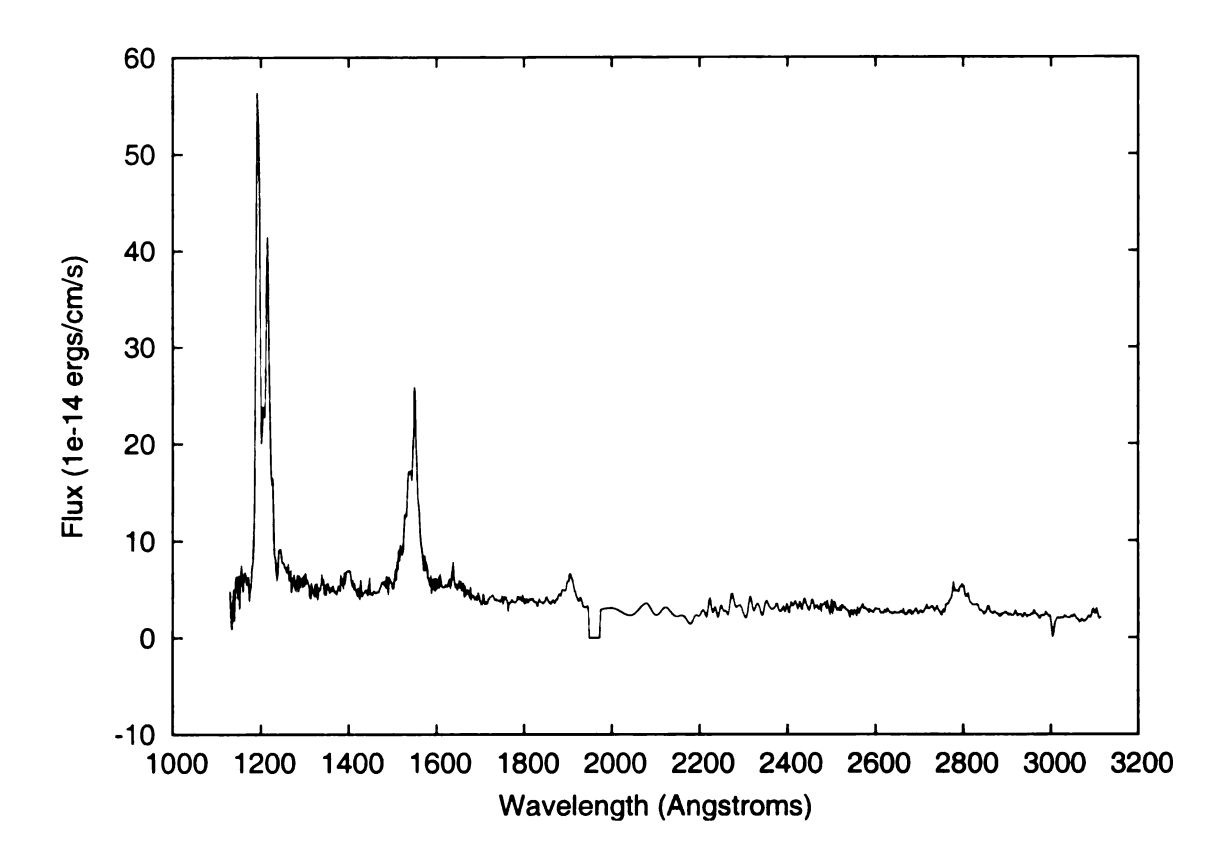


Figure 2.1 Full Typical UV Spectrum - While the emission lines of interest all lie on the left half of this spectrum, the extended coverage allows a more accurate fit of the ionizing continuum.

was thought that since the spectral energy distribution of AGN is both significantly different in shape and much fainter than that of standard stars, a direct comparison of actual AGN might be more illustrative of the differences between IUE and HST. Koratkar et al. found that while the IUE and HST measurements of strong emission lines agreed to within 15%, the results for weaker lines disagreed by a much greater amount, reaching a factor of six for the faintest lines.

Koratkar et al. concluded that IUE did have a nonlinear response at low flux levels, but they were unable to characterize it well enough to accurately evaluate its effect on their data set. Koratkar et al. analyzed the reduced, flux-calibrated spectra, in which the total counts in each pixel had been divided by the exposure time and multiplied

by a detector response function. However the actual non-linearities in IUE's SIT-Vidicon detectors are expected to depend only on the charge on the photocathode, which is proportional to the counts recorded after conversion in the ADC. We therefore repeated their analysis in terms of raw detector counts to see if a better non-linearity correction function could be derived.

The data for this comparison came from near simultaneous observations of NGC 5548 using both IUE and HST on 5-6 July 1992, observations that were also used by Koratkar et al. in their 1997 paper. The IUE observation (LWP23450) was retrieved from the archive in both the raw format and as a NEWSIPS (de La Pena et al., 1994) extracted final spectrum. IRAF was used to extract a spectrum from the raw file and parameters were adjusted until the extracted spectrum matched the NEWSIPS spectrum as well as possible as a way of finding the number of raw counts that went into each pixel in the fully-reduced NEWSIPS extracted spectrum. This was, unfortunately, a very subjective process, but should be sufficient to decide if further investigation would be fruitful. In the end, we simply wish to determine if the ratio of the flux from IUE to the flux from HST is a simple function of raw detector counts.

The HST data have 0.4 Å per pixel resolution, much higher than those of IUE. To better facilitate a comparison, a boxcar smoothing was applied to the HST data until a resolution similar to that of the IUE data was achieved. A scale factor was applied so that the HST and IUE data had similar flux levels for the Mg II emission around 2850Å before a ratio of the IUE flux to the HST/FOS flux was computed for each separate pixel in the IUE spectrum. This ratio was then plotted as a function of the raw count numbers from the raw IUE spectra (see figure 2.2). This did show a good deal of discrepancy at low counts (less than 100 raw counts). At very low count levels, this ratio varied drastically. There was no apparent pattern to the fluctuations, and as such there was no straightforward way to remove this effect. While the IUE detector does have some problems at low count levels, no systematic non-linearities

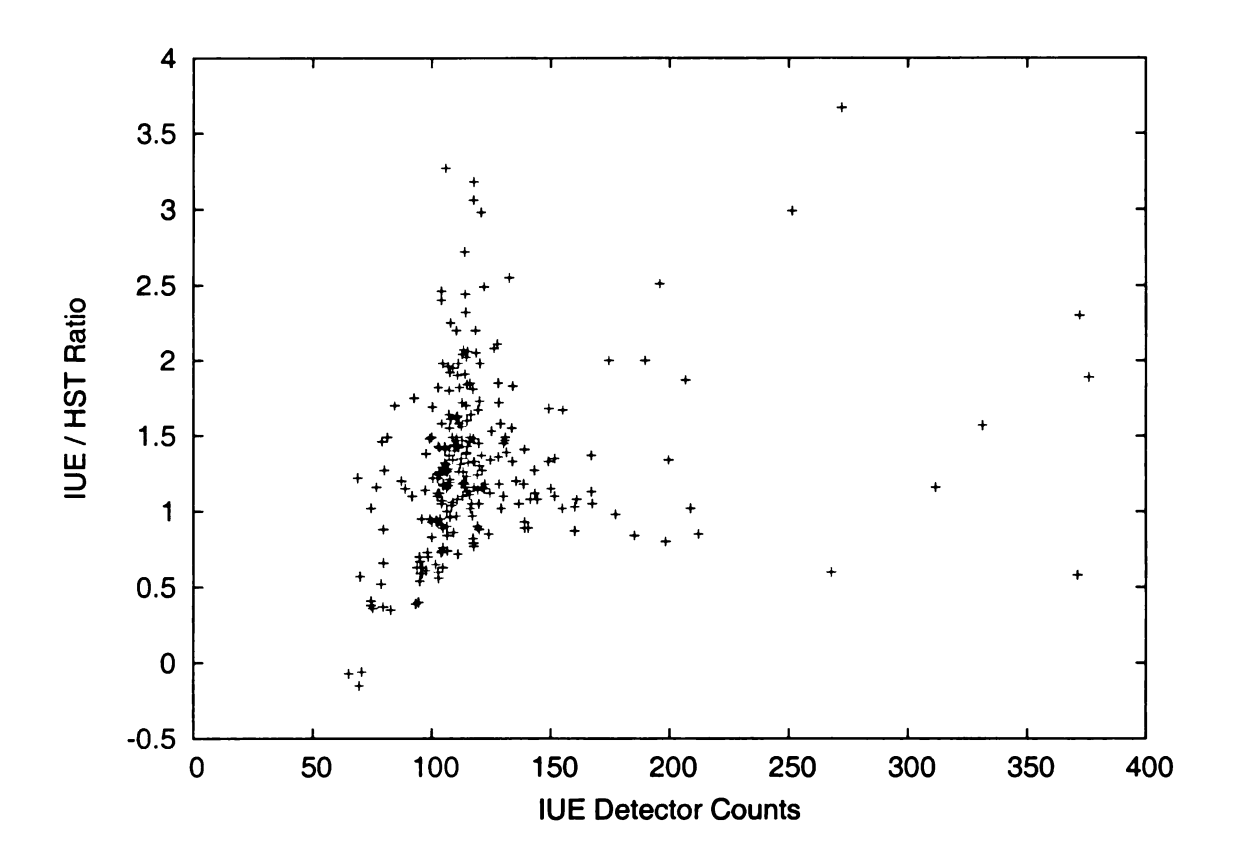


Figure 2.2 Ratio of IUE to HST flux levels as a function of IUE detector counts for near simultaneous observations of NGC5548 - It is clear that there is an issue with nonlinearity at low count levels, but it is unclear how to accurately characterize this effect in order to correct for it.

were measurable above the noise level. Fortunately, since even the relatively faint emission lines such as He II 1640Å are floating atop the continuum, these problems with extremely low raw counts should not be significant in this present study.

The IUE data are too important to ignore, but they must be used with care due to both the low resolution and the known linearity issues. The HST data have much higher resolution and are of better quality. Unfortunately, while sampled daily, there is only about one month of data. This is far too short a time period to do significant reverberation mapping.

Table 2.1: IUE UV Data - The following is a list of all IUE UV observations that were used in this study along with the Julian dates of the observations.

File	JD	File	Of.	File	Ωſ	File	JD
r57510uv.imh 2447510.15	2447510.15	r57569uv.imh	2447569.9	r57629uv.imh	2447629.81	r57688uv.imh	2447688.81
r57514uv.imh 244751	2447514.14	r57573uv.imh	2447573.77	r57633uv.imh	2447633.98	r57692uv.imh	2447692.81
r57517uv.imh	2447517.99	r57577uv.imh	2447577.92	r57637uv.imh	2447637.98	r57696uv.imh	2447696.81
r57522uv.imh	2447522.15	r57581uv.imh	2447581.91	r57641uv.imh	2447642.02	r57700uv.imh	2447700.81
r57526uv.imh	2447526.15	r57586uv.imh	2447586.06	r57645uv.imh	2447645.97	r57705uv.imh	2447705.48
r57530uv.imh	2447530.07	r57590uv.imh	2447590.06	r57649uv.imh	2447649.9	r57709uv.imh	2447709.4
r57534uv.imh	2447534.06	r57594uv.imh	2447594.06	r57653uv.imh	2447653.9	r57713uv.imh	2447713.39
r57538uv.imh	2447538.3	r57598uv.imh	2447598.06	r57657uv.imh	2447657.57	r57717uv.imh	2447717.37
r57543uv.imh	2447543.28	r57602uv.imh	2447602.07	r57661uv.imh	2447661.56	r57721uv.imh	2447721.39
r57546uv.imh	2447546.07	r57606uv.imh	2447606.07	r57665uv.imh	2447665.59	r57725uv.imh	2447725.4
r57549uv.imh	2447549.89	r57609uv.imh	2447609.93	r57669uv.imh	2447669.57	r57729uv.imh	2447729.73
r57553uv.imh	2447553.2	r57613uv.imh	2447613.75	r57673uv.imh	2447673.56	r57733uv.imh	2447733.74
r57557uv.imh	2447557.22	r57617uv.imh	2447617.63	r57677uv.imh	2447677.57	r57737uv.imh	2447737.72
r57561uv.imh	2447561.91	r57621uv.imh	2447621.65	r57680uv.imh	2447680.81	r57741uv.imh	2447741.65
r57565uv.imh	2447565.92	r57625uv.imh	2447625.65	r57684uv.imh	2447684.96	r57745uv.imh	2447745.61

2.3 OPTICAL DATA

The optical data taken for the AGN Watch to complement the UV data were obtained at a variety of sites scattered around the globe. Telescopes used in the AGN Watch study ranged in size from 1.8m to 6m and a variety of spectrographs were used. A complete listing of all observatories used in the AGN Watch study can be found in the notes for table 1 in Peterson et al. (1991). Because of the range of resolution and quality, only a subset of these observations were chosen for analysis in this work. This subset is listed in table 2.2, and the actual observations used are listed in table 2.3. Both the signal to noise and the spectral coverage varied substantially from site to site. Even within one site's data, spectral coverage could be different from one set of observations to the next. Because He II was not the line of primary interest in the original project, the optical observations are not entirely ideal for its measurement. Even so, there are some observations with both sufficient signal strength and spectral coverage to make an attempt at a He II measurement. After carefully comparing the merits of the different data sets, we chose to use only the subset of observations that were used in Dietrich et al. (1993), paper IV of the larger AGN Watch study.

The file names listed in table 2.3 include a letter designating the observatory site code given in table 2.2. In some cases, more than one observation was taken on a given night at a given site. In this case, not only will there be a letter suffix to denote site, but an alphabetical letter is added to uniquely identify it. If more than one observation was taken from a given site and they were all usable for this study, the multiple observations were averaged together before fitting and a suffix of "x" was added. In the cases where more than one observation was taken on a given night from multiple sites, the spectra were fit individually and the resultant flux measurements were averaged together before the cross correlation function was calculated.

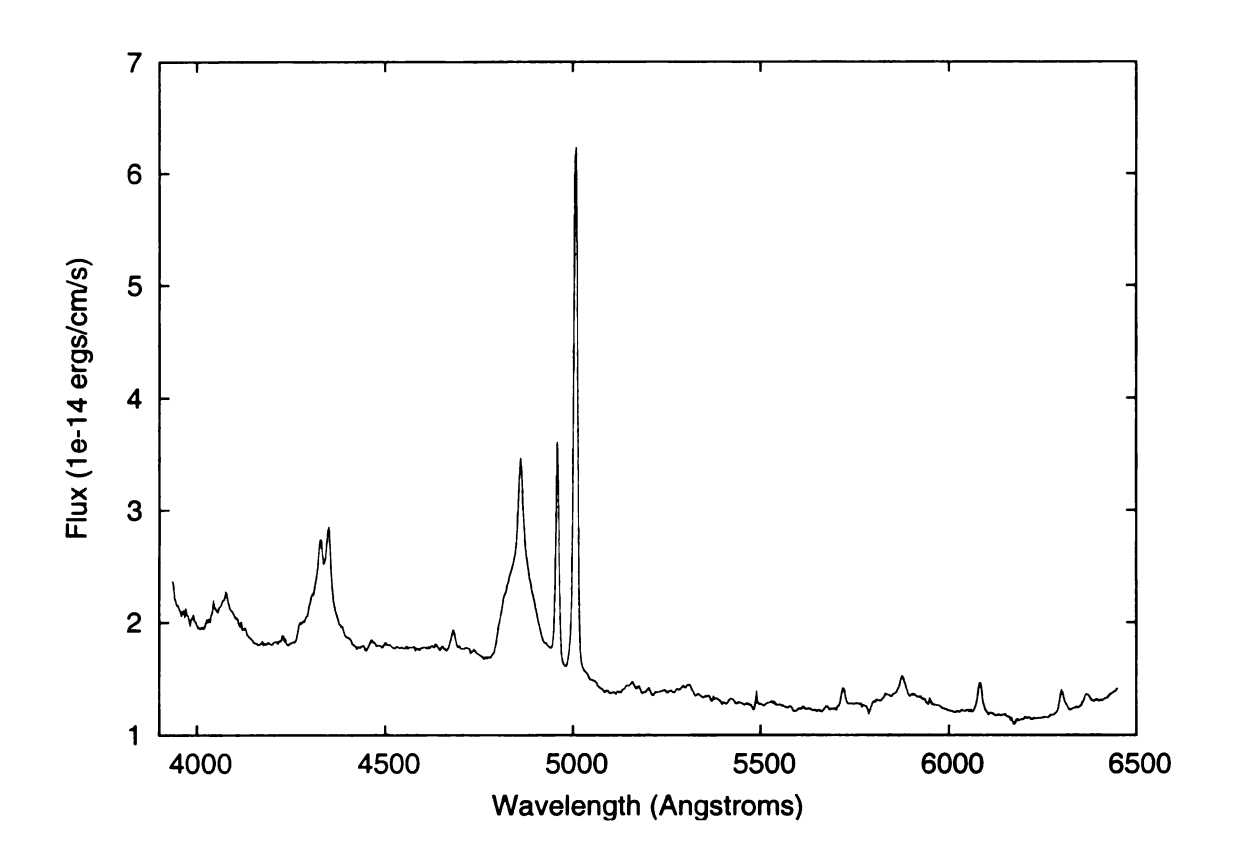


Figure 2.3 Full Typical Optical Spectrum - This optical spectrum was taken from site H, which has fairly good signal to noise and spectral coverage. Not all of the optical observations are of this quality.

Table 2.2: Optical Data Site list - This lists the site code as well as the correction scale factor for the optical observations found in table 2.3 as derived in Dietrich et al. (1993)

Data Source	Site Code	P.A.	Aperture Geometry	Scale Factor
Ohio State CCD	A	90°	5.0" x 7.6", 1.0" x 7.6"	0.953 ± 0.020
INT 2.5m	\mathbf{C}	0,72.1,75.4	1.5 x 6.0	0.930 ± 0.000
Hale 5m	D	61, 66.9	$1.0 \times 4.0, 1.0 \times 7.0$	0.918 ± 0.000
			4.0 x 8.0	
Ohio State IDS	G	•••	$\emptyset, 7.0$	0.953 ± 0.020
3m Shane	Н	$59, \ldots, 130$	2.1 x 7.9	0.903 ± 0.064
Steward	I	60, 90, 130	4.5 x 27.2	0.924 ± 0.053

Table 2.2: Optical Data Site List (continued)

Data Source	Site Code	P.A.	Aperture Geometry	Scale Factor
MDM	K	0	$1.7 \times 3.0, 2.4 \times 3.0,$	0.949 ± 0.014
			6.7×3.0	
Calar Alto	M	0,90	1 x 10.0 4 x 10.0	1.000 ± 0.000
1m Nickel	N	0	4.6 x 19.2	0.963 ± 0.000
McDonald CCD	J	0,90	$8.0 \times 9.0, 7.0 \times 7.2$	1.116 ± 0.000
McDonald IDS	Q	90	4.4 x 4.4	0.920 ± 0.000

2.3.1 Corrections to the Optical Data

Unlike the IUE data which were taken from a very stable environment above the Earth's atmosphere, the optical spectra are affected by transmission changes and smearing due to the atmosphere, and also by instrumental flexure as the telescope tracks the object. Some differences in the instruments used for the optical observations, such as spectrograph slit width, also must be taken into account. The UV data set does not need this sort of correction because the UV observations were all taken with a single instrument.

In order to accurately compare the optical data, they first needed to be rescaled and wavelength corrected. Since observing conditions may have changed from one observation to the next, the strong [O III] line at $\lambda 5007$ was used both to scale the flux and to fix any minor wavelength calibration issues that might exist. Because [O III] is formed in the narrow line region, it should remain insensitive to the short time scale variations that are powering the BELR variations and should therefore have the same flux in all observations. This rescaling was accomplished by manually measuring the flux and the central peak using IRAF. All observations were then scaled

such that their slit width corrected flux (see discussion below) for [O III] $\lambda 5007$ was the canonical value of 5.53×10^{-13} erg/s/cm². This value is taken from Dietrich et al. (1993).

Table 2.3: Optical Data - The following is a list of all optical observations that were used in this study along with the Julian dates of the observations.

File	Ωſ	File	Ωſ	File	Ωſ	File	JD
f57509hx.imh	2447510	f57592m.imh	2447593	f57660ix.imh	2447661	f57748c.imh	2447748
f57509hc.imh	2447510	f57599kx.imh	2447600	f57663mx.imh	2447663	f57757m.imh	2447758
f57524ix.imh	2447525	f57613ix.imh	2447614	f57664ma.imh	2447664	f57766ix.imh	2447767
f57525ia.imh	2447526	f57614h.imh	2447615	f57665g.imh	2447666	f57766n.imh	2447767
f57539m.imh	2447540	f57616dx.imh	2447617	f57700n.imh	2447701	f57767ix.imh	2447768
f57546m.imh	2447547	f57620q.imh	2447620	f57701n.imh	2447702	f57777h.imh	2447778
f57549m.imh	2447550	f57621h.imh	2447621	f57702k.imh	2447702	f57778a.imh	2447779
f57556hx.imh	2447557	f57622q.imh	2447622	f57703ia.imh	2447704	f57778ix.imh	2447779
f57574ix.imh	2447575	f57628hx.imh	2447629	f57704i.imh	2447705	f57779ia.imh	2447780
f57574m.imh	2447575	f57631n.imh	2447632	f57711ax.imh	2447711	f57797h.imh	2447798
f57576m.imh	2447577	f57643h.imh	2447644	f57716h.imh	2447715		
f57583n.imh	2447584	f57645ix.imh	2447646	f57719ax.imh	2447720		
f57587m.imh	2447588	f57655ax.imh	2447656	f57725ax.imh	2447726		
f57589m.imh	2447590	f57655q.imh	2447656	f57742c.imh	2447742		
f57592j.imh	2447593	f57658hx.imh	2447659	f57746m.imh	2447746		

There are a variety of challenges associated with using the ground based optical data. Due to variations in observing conditions, the absolute flux level from one observation to the next must be corrected. A strong narrow line such as $O[III] \lambda 5007$ can be used as a reference standard to scale the data. Since the narrow emission line region is both large in size and at a large distance from the central source, it is relatively insensitive to continuum variations on short time scales (Peterson, 1993). We can therefore assume that the flux in |O| III $\lambda 5007$ remains constant over the time it was observed. Furthermore, we can use this line to correct for any errors in the wavelength calibration since its peak wavelength should also not change. Unfortunately, the NELR that generates [O III] narrow lines is of a large enough angular size that the amount of flux recorded is influenced by the slit width of the spectrograph used. This means that in order to make any meaningful comparison between the various ground based sites, a correction for slit width must be made to the narrow lines. Dietrich et al. (1993) went to great lengths to determine these correction factors for slit width, and we use their corrections here (as listed in the last column of table 2.2) before scaling the observed spectra to have the same flux in [O III].

Another important limitation of the optical data is the same as that of the IUE data, poor spectral resolution. Even the best of the ground based optical data only have a resolution of about 2 Å per pixel. Some of the lower resolution data from the AGN watch archive were not suitable for accurately measuring the He II emission.

2.3.2 Observed vs. Rest Frame

While NGC 5548 is relatively nearby, it is still far enough away that cosmological redshift needs to be taken into account. It lies at a redshift of z = 0.017175 (de Vaucouleurs et al., 1991) which needs to be corrected for in order to put the emission into a rest frame. To accomplish this, the IRAF task "dopcor" was utilized.

Chapter 3: Data Fitting and Measurement

Previous reverberation measurements (e.g. Clavel et al., 1991; Dietrich et al., 1993, and many others) directly show that the emission lines from different ions respond to continuum variations on different timescales. This is interpreted to mean that the BELR covers a wide range of distances from the continuum source, and lines coming from different ionization states are formed at different radial distances. Since the He II lines are spectroscopically observed in blended features that also include emission lines from ions of very different ionization levels (e.g. Fe⁺, H⁺, C⁺³, and O⁺²), it is crucial to be able to accurately measure the flux in each of the separate components in the blend in order to accurately measure the He II reverberation time scale. Some previous studies simply defined continuum-subtracted wavelength ranges, or bins, for each emission line. While this method is a decent approximation, it does not accurately measure contamination from adjacent emission lines. In order to more accurately fit these highly blended varying emission lines, new software tools as well as reasonable approximations of the individual emission line profiles were needed.

3.1 Automated Fitting Routine

The central difficulty to be overcome is the de-blending of spectral lines in the data. The emission spectrum of an AGN is a very complicated structure since there can be multiple overlapping emission lines that vary with slightly different lagtimes. To accurately de-blend these components, one must fit each component individually at

every time slice. This can be done by hand, but it would be both time consuming and very subjective; a fit by hand does not give a true "best fit" to the observations but instead is simply what the observer feels looks best. An automated fit using some mathematical technique would be efficient, consistent, and give at least some measure of the quality of the fit.

To create the automated fitting routine, it was important to build upon existing software tools used by my advisor and his collaborators. This would both make the automated fitting routine useful for purposes other than this study and allow easy use of previous measurements of NGC 5548 as a starting point. This should help to explain the sometimes cryptic nature of the input parameters as well as the choice to use FORTRAN.

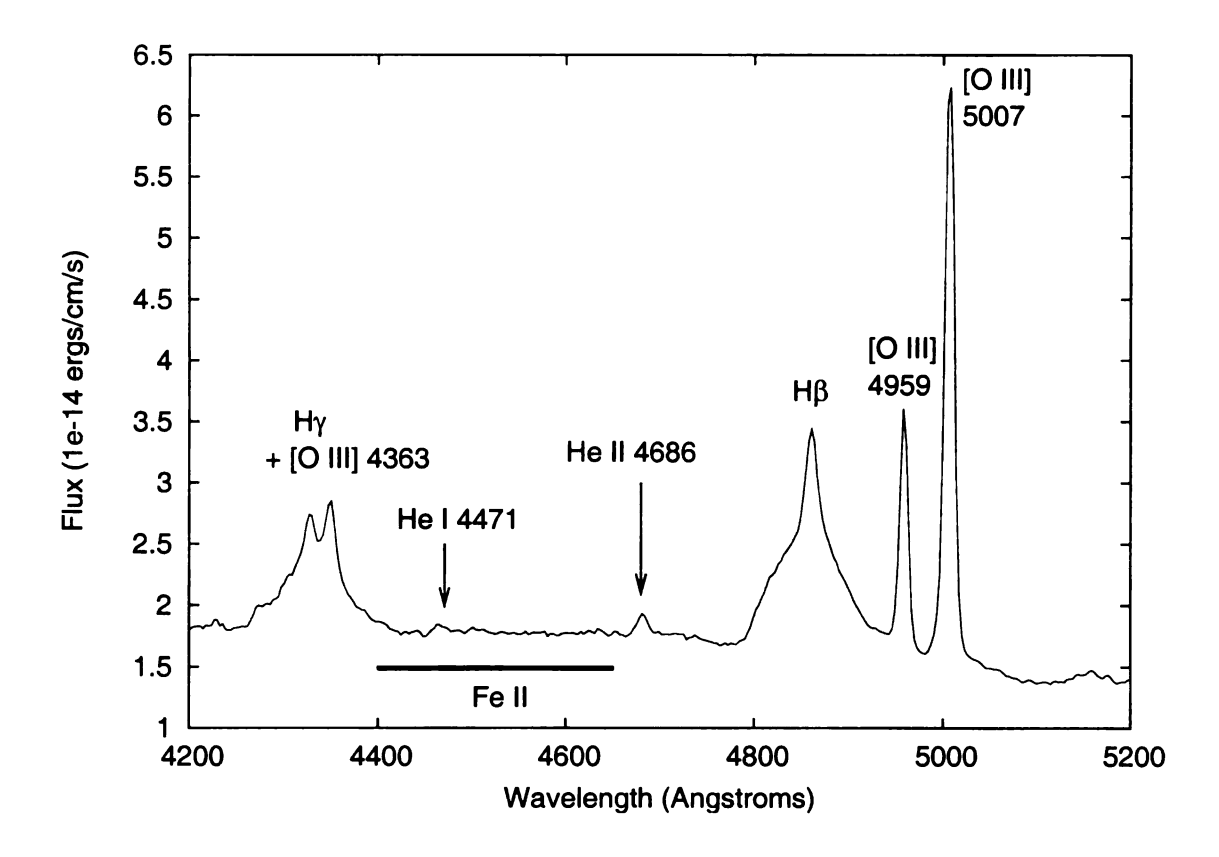


Figure 3.1 Typical Optical Spectrum of NGC 5548 - This spectrum, from the file n57621h, is a detail region of a typical NGC 5548 optical spectrum. Several of the important emission lines are labeled.

Figure 3.1 shows a portion of a typical optical spectrum for NGC 5548. While the primary feature of interest for this study is the $\lambda 4686$ He II line, it is surrounded by contamination from other lines in the blend. The wing of the Balmer H β line as well as a Fe II multiplet and the He II line from the NELR all contribute to the measured flux around $\lambda 4686$. There is also contamination from the He I $\lambda 4471$ as discussed by Vestergaard & Peterson (2005). To properly measure the flux from the He II $\lambda 4686$ line, all of the other contaminating lines must be fitted as well. In addition, the underlying continuum component, which is also variable, was included in the fit.

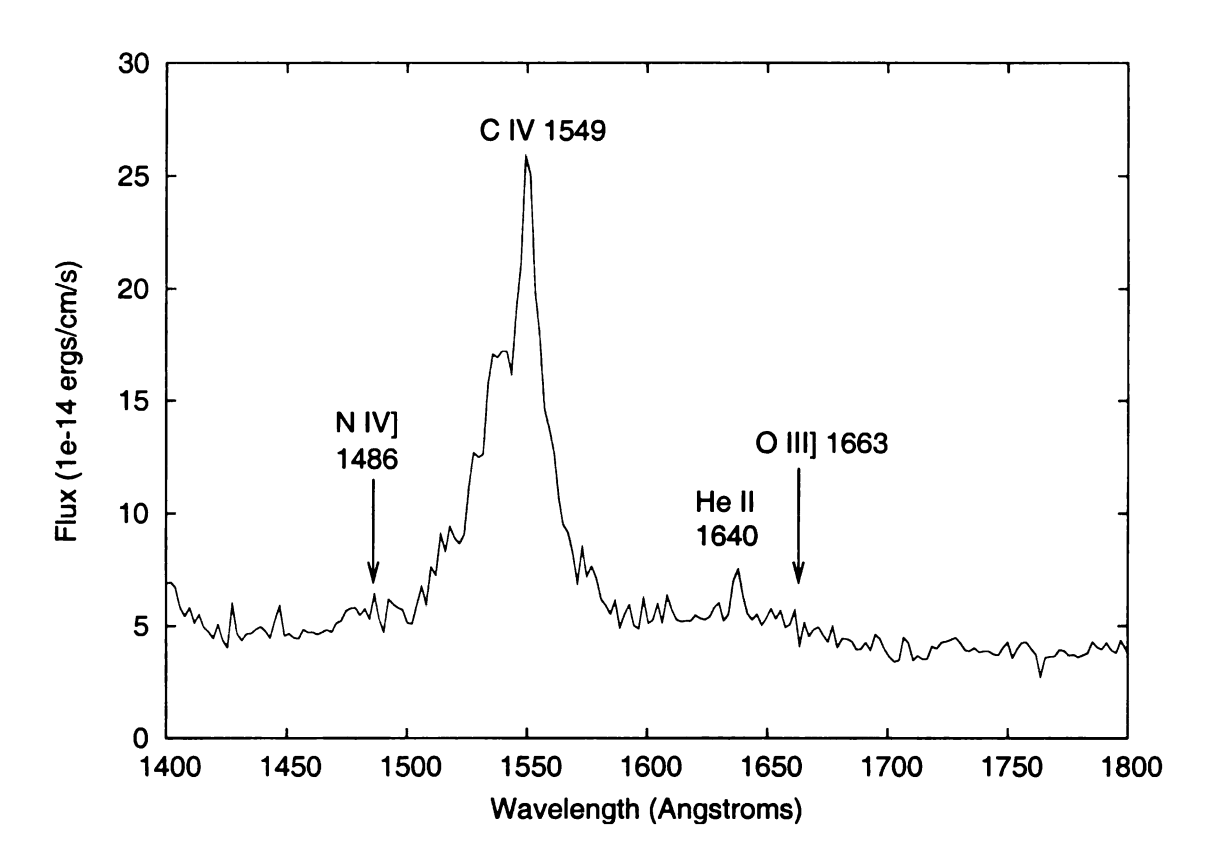


Figure 3.2 Typical UV Spectrum of NGC 5548 - This spectrum, from the file r57530uv, is a detail region of a typical NGC 5548 UV spectrum. Several of the important emission lines are labeled.

At its core, the automated fitting routine (hereafter AFR) uses a χ^2 minimization technique to fine tune an initial guess at the fit. The goodness-of-fit statistic χ^2 is

basically defined as:

$$\chi^2 = \sum_{i=1}^n \left(\frac{A_i - B_i}{\sigma}\right)^2 \tag{3.1}$$

where A and B are the data spectrum and the blend built from profiles, respectively. The σ is some measure of the noise in the data spectrum. In the UV, since all of the spectra were taken with the same instrument, this value was simply estimated by looking at a relatively flat, uncontaminated area, and a value of 0.5×10^{-14} was chosen. Because the optical data come from different instruments, this value was estimated in the program by applying a boxcar smoothing to the data in the fitting windows and seeing how far the observed values deviated from this smoothed version. This value would stay the same for any individual spectrum that was fit, so the actual value of σ is not all that important.

3.2 Building the Blend

The continuum radiation was modeled as a simple power law:

Continuum =
$$A \left(\frac{\lambda}{5600}\right)^{\gamma}$$
 (3.2)

with both A and γ allowed to vary within reasonable ranges. While the exact form of the continuum emission from the central engine is not known, it is thought to be a superposition of blackbody spectra of nearly continuously varying temperatures coming from an accretion disk undergoing viscous heating. A power law does not precisely describe this situation mathematically, but it is a reasonable approximation for the relatively small wavelength ranges at which we are looking and is a good deal more accurate than a simple straight line approximation which is often used.

To make the fit as realistic as possible, template profiles of the emission lines are used whenever practical. In some previous studies (such as Dietrich et al., 1993), emission lines, including both those arising from the NELR and BELR, were measured

in a simpler way. If the emission line was deemed to be weak, a wavelength range (or bin) was defined for that line, and all flux within that range that was above the continuum level (which was itself defined as a straight-line under the bin) was assumed to be from the emission line in question. Contamination from adjacent lines was either ignored or simply estimated. If the line was deemed to be strong, it was sometimes modeled using a superposition of several Gaussians. If the shape was complicated, more Gaussians were added until a shape that more closely approximated the true shape of the actual emission line was created. Neither of these techniques truly described the physical situation, and a new approach was needed. To this end, it was decided to use observed spectra from actual AGN to create template profiles that more accurately reflected the shape of the real observed emission lines.

3.2.1 FE II TEMPLATE

First noted by Phillips (1977, 1978), the Fe II multiplet of Seyfert 1 galaxies are very similar from object to object. The primary difference between any two given Seyfert 1 AGN is the amount of Doppler broadening. With this fact in mind, the Seyfert 1 galaxy I Zw 1 has long been of interest in order to generate a template profile for the Fe II emission in AGN. I Zw 1 has quite narrow broad lines such as Fe II and $H\beta$, some of the narrowest permitted lines observed in any Seyfert 1 galaxy. Phillips demonstrated that if the Fe II profile was Doppler broadened to match the width of $H\beta$, the I ZW 1 template fit other Seyfert 1 galaxies well. Véron-Cetty et al. (2004) have created a revised and improved version of the I Zw 1 optical template (see figure 3.3.) Vestergaard & Wilkes (2001) created a similar template for the UV emission from data of I Zw 1 taken with HST (see figure 3.4) Vestergaard & Peterson (2005) used these templates successfully to study the Fe II emission in NGC 5548 using the same AGN watch data set used in this study. Although their focus was not He II, they did find that the use of these templates improved the measurement of other

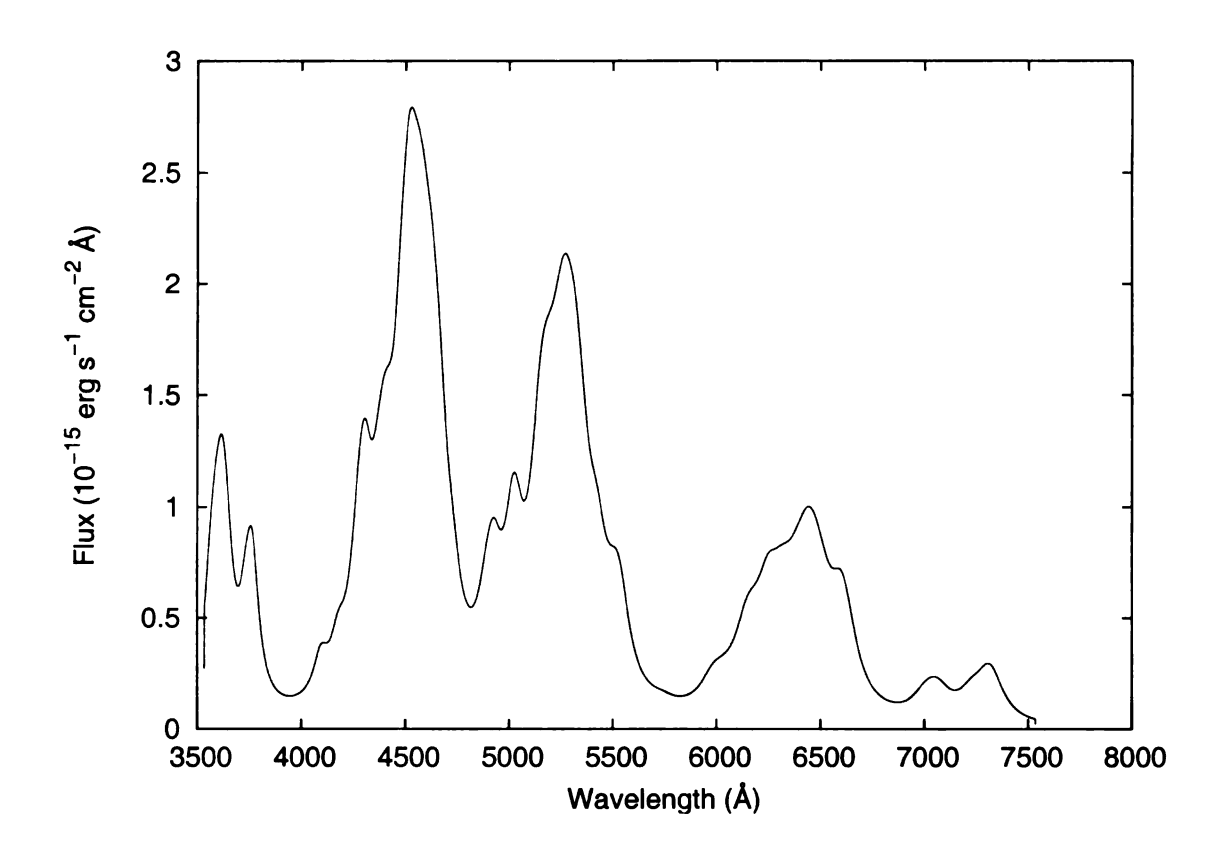


Figure 3.3 Fe II Optical Template - based on a broadened version of the Véron-Cetty et al. (2004) optical template.

emission lines in the regions contaminated by Fe II.

This present work is the obvious extension of that idea, using all of the template profiles at our disposal to disentangle these multiple overlapping lines. M. Vestergaard kindly provided us with a set of Fe II template profiles with a variety of different Doppler broadenings. We used the same templates that were used by Vestergaard & Peterson (2005) in their study of NGC 5548 using a Doppler broadening of 6250 km/sec, similar to the broadening used in their paper and which seemed to give a good fit to the NGC 5548 data. The templates shown in figures 3.3 and 3.4 show this particular broadening.

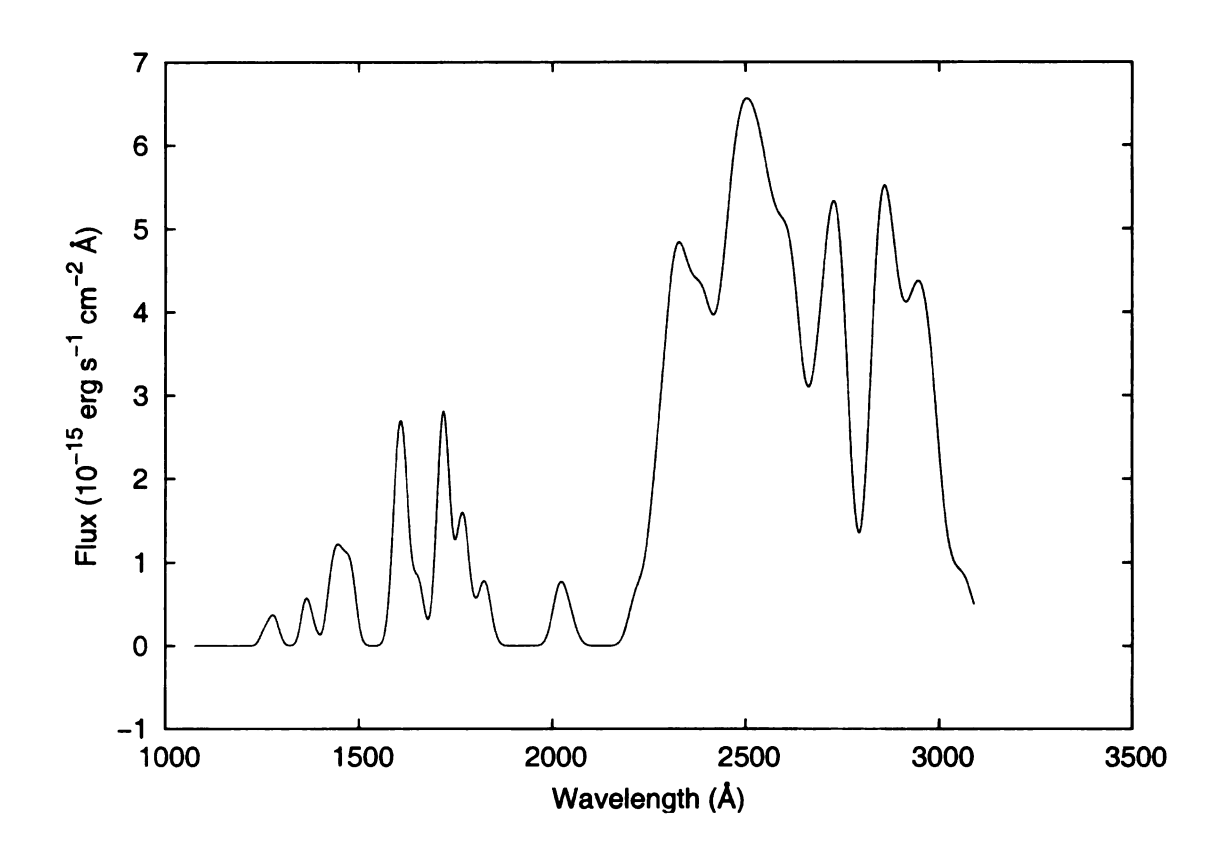


Figure 3.4 Fe II UV Template - based on a broadened version of the Vestergaard & Wilkes (2001) UV template.

3.2.2 OTHER TEMPLATES

The creation of the remainder of the template profiles was a rather subjective procedure. As a starting point, a RMS (root mean squared) spectrum was created from scaled and shifted data spectra (see figures 3.5 and 3.6.) In this way, we are left with primarily the highly variable BELR emission with the nearly constant NELR emission removed. From there, some smoothing was typically applied, and any sharp upturns remaining on the edges were clipped to try to leave a smoothly changing template profile. As this was a fairly individualized process, tabular copies of the templates used are included in appendix F of this work.

The strong H α line, seen on the right side of figure 3.5, was used to create a template for the Hydrogen Balmer lines (see figure 3.7.) The Balmer lines should all

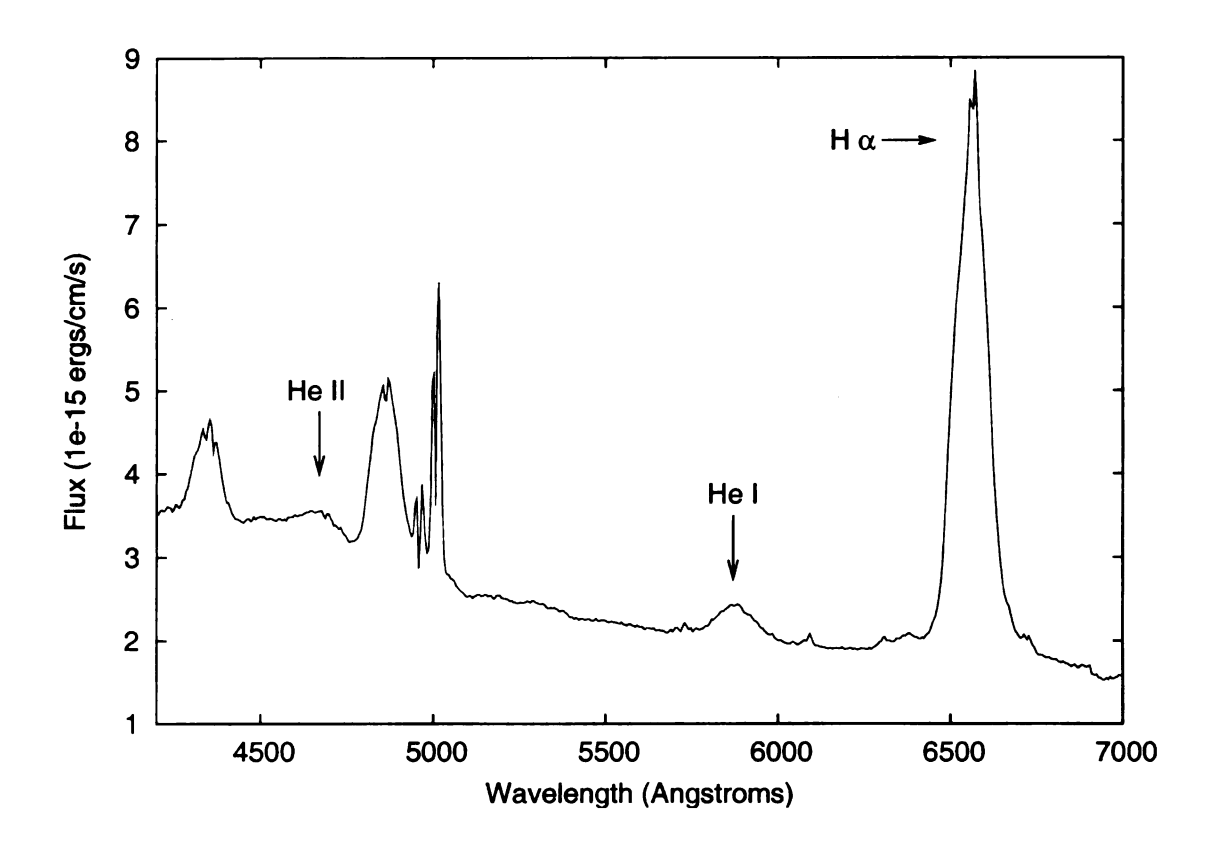


Figure 3.5 Optical RMS Spectrum - Most of the non-variable NELR lines have been eliminated, leaving only the highly variable BELR emission. This can be used to construct template profiles for the BELR emission that give a better approximation of the true shape of the emission lines. The regions used for the creation of the $H\alpha$, He I, and He II BELR templates are marked.

have similar profile shapes because they are all emitted by the same gas. This profile can therefore be rescaled to fit $H\beta$ or $H\gamma$ as needed.

The He II $\lambda 4686$ emission from the RMS spectrum was used to generate a BELR He II template (see figure 3.8) for fitting both the $\lambda 4686$ and the $\lambda 1640$ broad line components. This is important to note, as we have used the exact same template profile to fit both the UV and the optical He II emission lines. Because we expect the emission to originate from the same region within the AGN, they should have the same shape.

The relatively strong He I line at $\lambda 5876$ was used to create a He I template (see figure 3.9) for fitting the He I line at $\lambda 4471$, a line which contaminates the

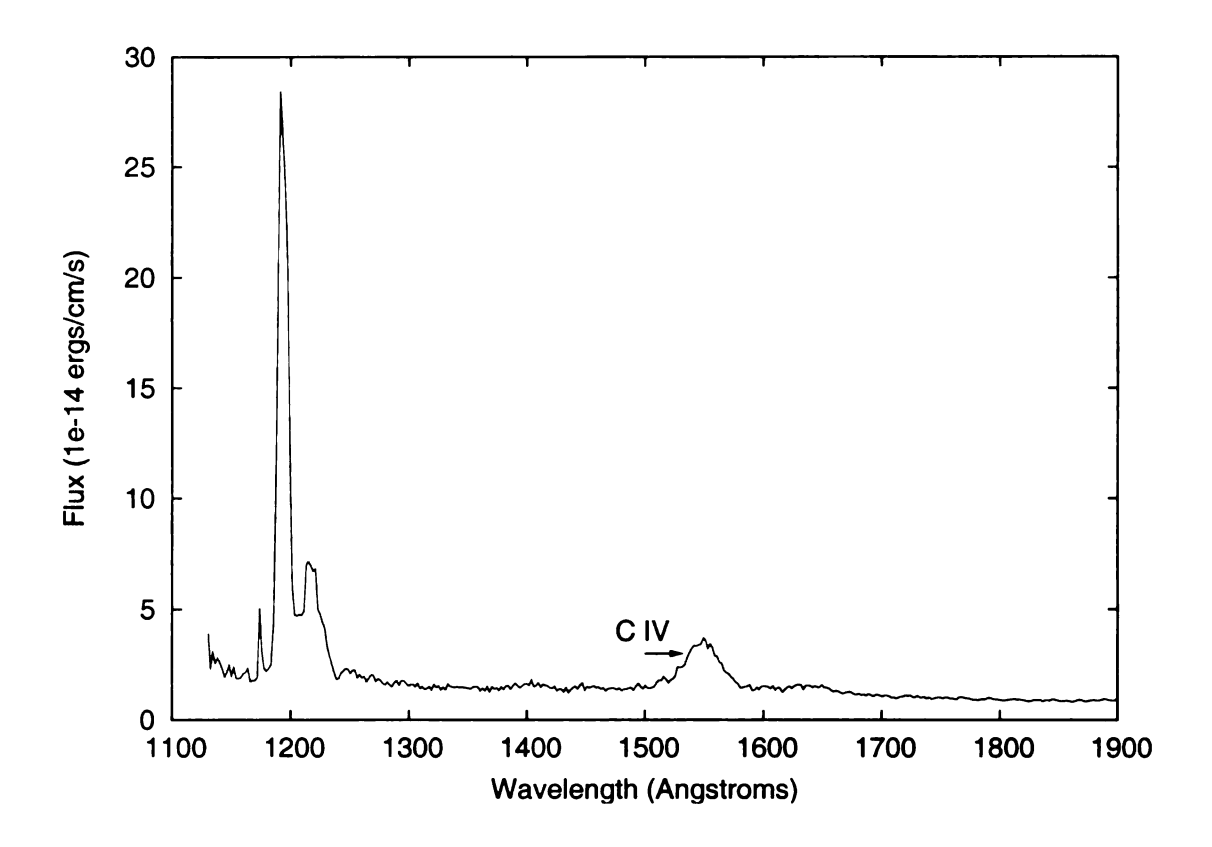


Figure 3.6 UV RMS Spectrum - This is a detail of the region of interest of the UV rms spectrum. Most of the non-variable NELR lines have been eliminated, leaving only the highly variable BELR emission. Like the optical rms spectrum, this can be used to construct template profiles for the BELR emission. The C IV BELR profile was created from the strong emission labeled in this spectrum.

measurement of the He II $\lambda 4686$ emission line.

Templates for O III] $\lambda 1663$ and the narrow line component of the He II $\lambda 1640$ blend were created in a similar manner, but an average rather than an RMS spectrum was used as the starting point. In an average spectrum, the NELR emission is not removed as in a RMS spectrum. These lines could also have been described with a simple Gaussian or blend of Gaussians of appropriate widths, if necessary.

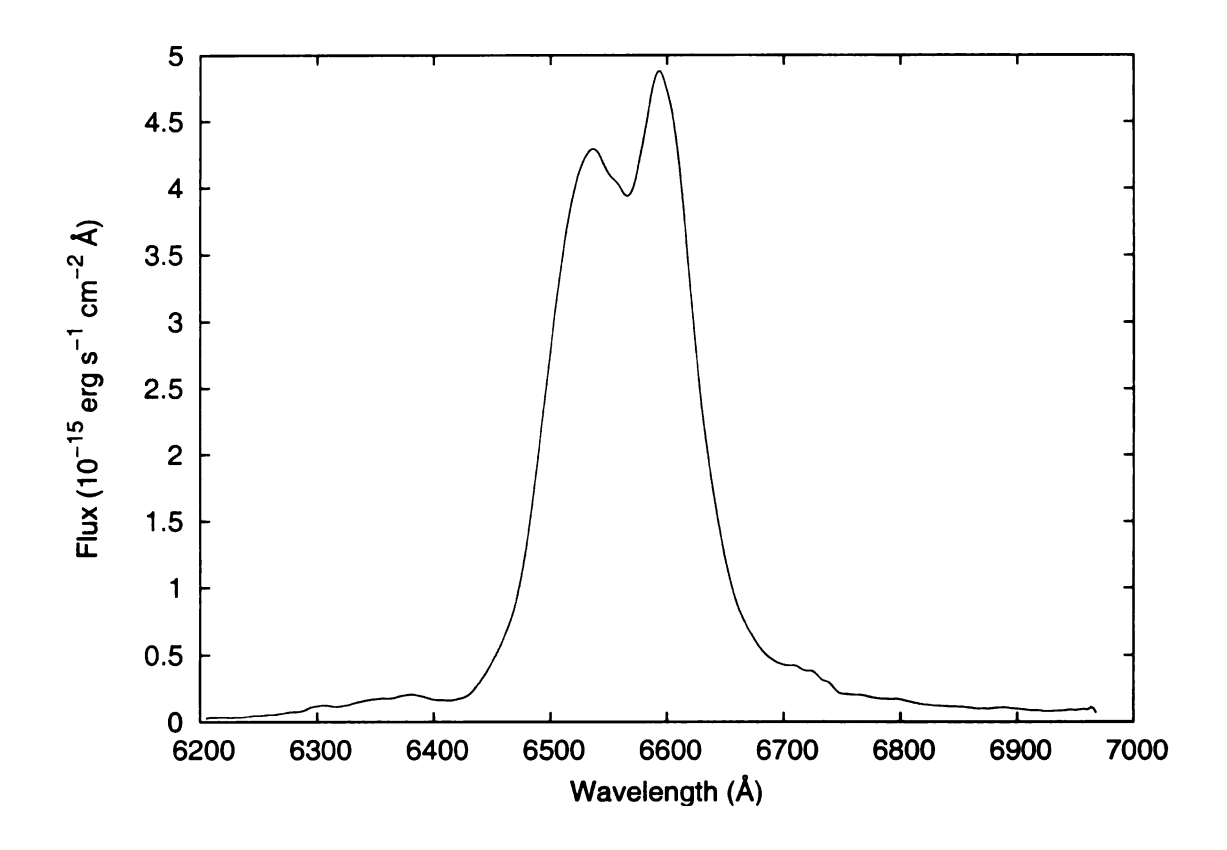


Figure 3.7 H α BELR Profile

3.2.3 FITTING PARAMETERS

Each profile will be shifted in wavelength (actually in velocity) and scaled by a multiplicative factor as part of the automated fitting procedure. So for each template profile that is to be used, we have to specify an original wavelength ($\lambda_{\rm old}$), a shifted wavelength ($\lambda_{\rm new}$), and a multiplicative constant. These parameters are given in the input file, called "blends.in". While three parameters are input, only the last two are allowed to vary. In the input files for the fitter, the multiplicative constant is actually expressed as a fraction of the total flux in the data spectrum. For example, if a particular emission line carries 10% of the total flux, the scaling factor would be 0.1. This method is used in order to mirror more accurately the input files used in the program *Blends*. (*Blends*, and several of the subroutines called by the automated fitter were developed by Dr. Jack Baldwin. They are used extensively by both him

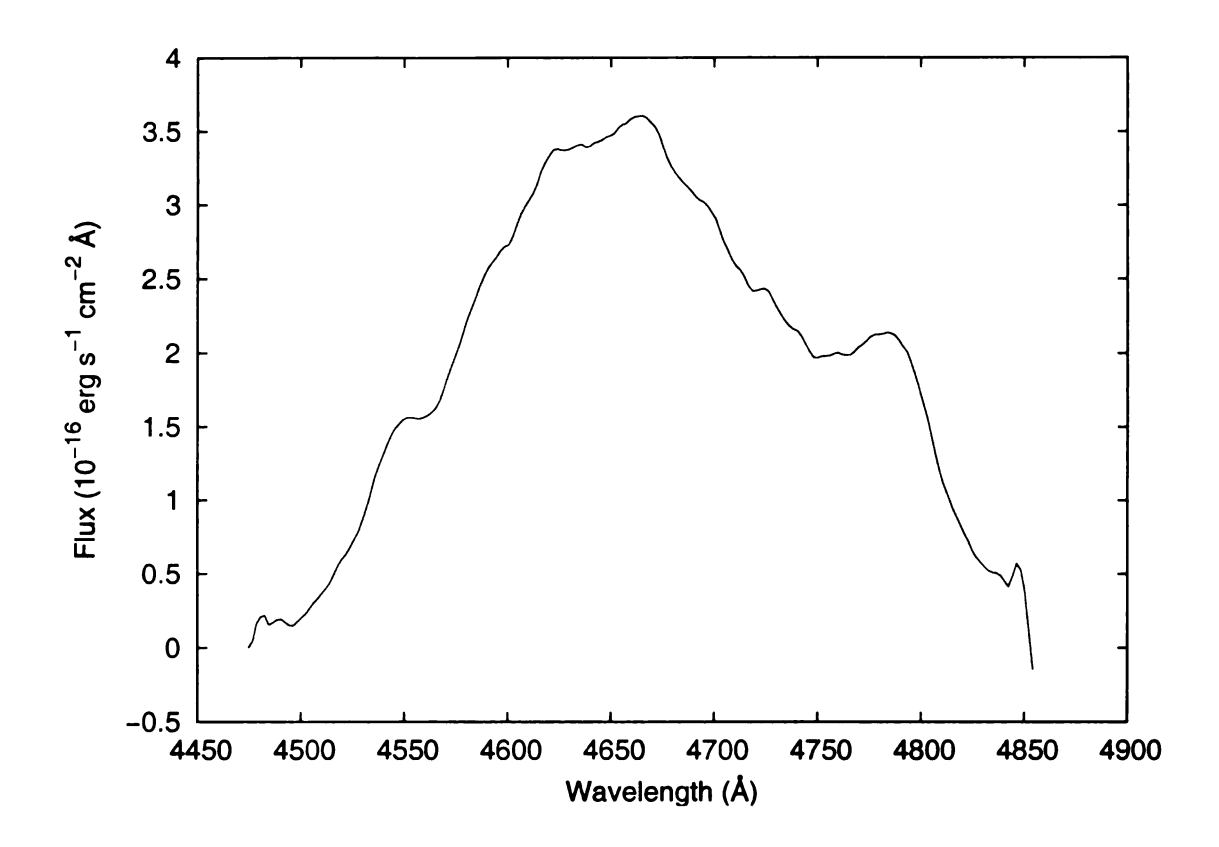


Figure 3.8 He II BELR Profile

and his collaborators, the author of this work included.) The only significant change of which to be aware is that *Blends* assumes that the continuum shape has been removed and that there is only an additive constant still included. This constant continuum level is one part of the input file for *Blends* but is ignored by the AFR which instead fits a power-law continuum described by equation 3.2. It still must be included in the input file to preserve formatting. The long term aim here was to produce a general-purpose automated fitting program for which the starting values could be determined by using the existing *Blends* program to fit by hand, and then the *Blends* output file would be used as the input file for the automated fitter.

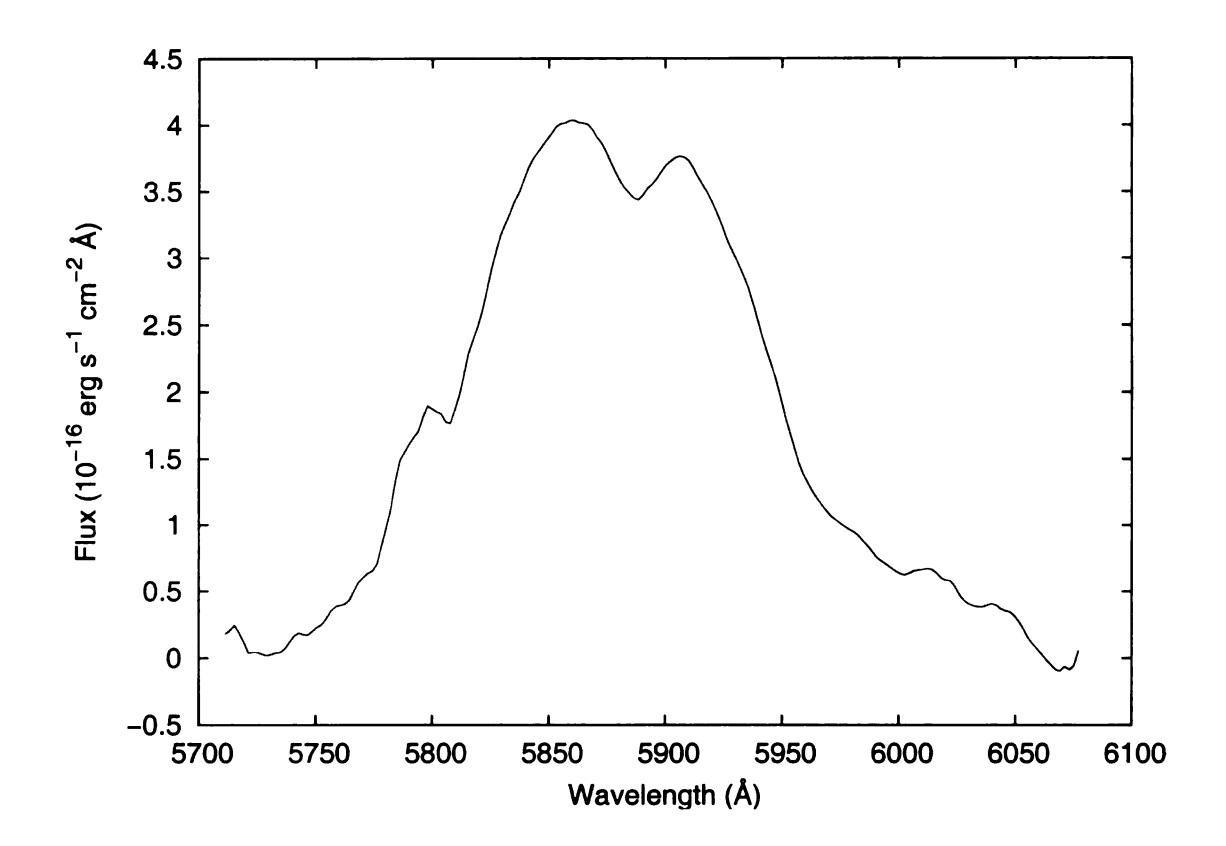


Figure 3.9 He I BELR Profile

3.2.4 FITTING WINDOWS

While the spectra we are using may cover several thousand angstroms, we are typically only interested in a small region around an interesting emission feature. In addition, we may need to fit in areas away from the line of interest in order to constrain the shape of the continuum. There also may be regions of the spectrum where we do not have a profile for the emission that is present. To accommodate these facts better, the AFR does not calculate contributions to χ^2 everywhere in the spectrum but rather only in certain regions of interest specified by an input file to define fitting windows. These windows are defined by a pair of wavelengths, a starting and an ending wavelength, with one pair per line in an input file called "window.txt".

In choosing what regions to fit, it is important to fit only in areas where we have profiles or where there is little or no emission (just continuum.) During testing, it was

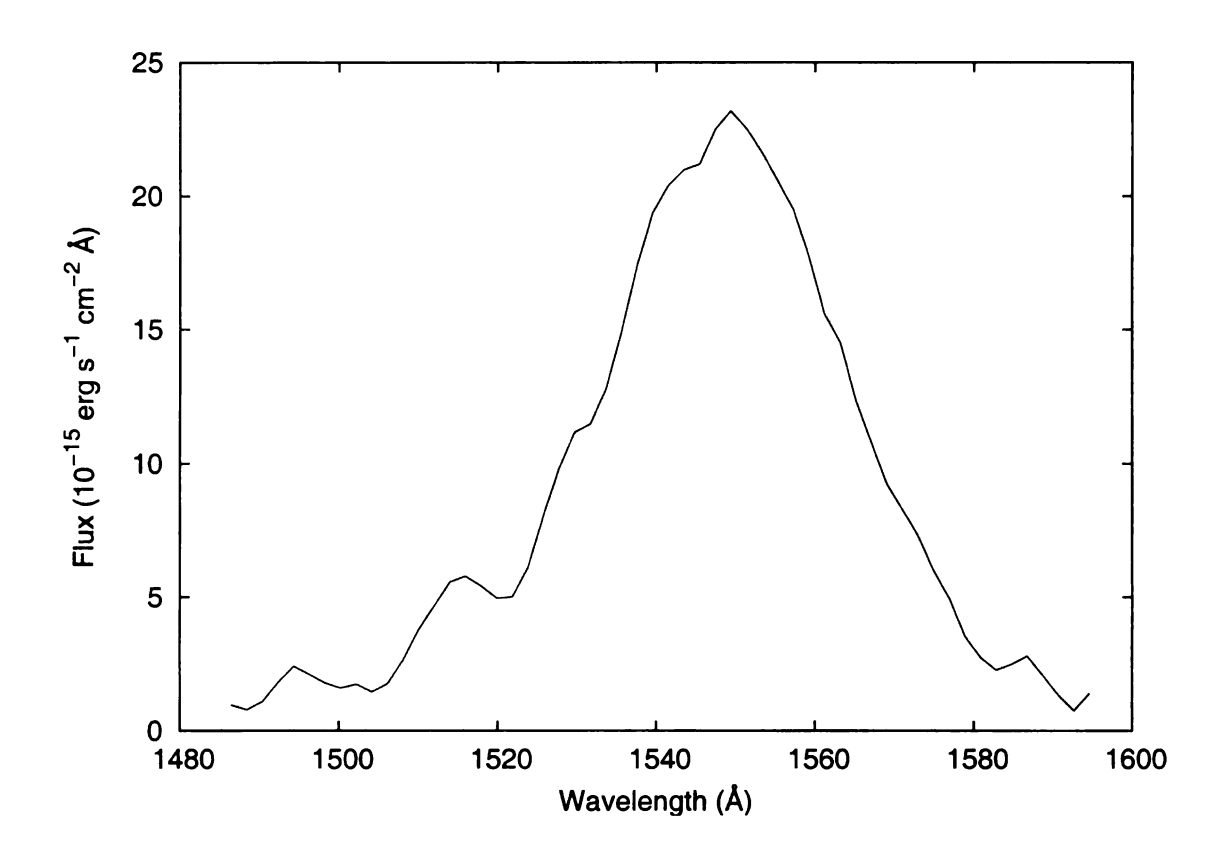


Figure 3.10 C IV BELR Profile

found that the NELR lines can cause difficulties with the automated fitter in some circumstances. The width of the NELR lines is directly tied to the width of the slit used on the spectrographic detector. Because a number of different instruments with different slit widths were used for the optical observations, a single template narrow line cannot be used for all of the optical spectra. Since these lines are formed far away from the continuum source, they are essentially constant in flux over the timescales we are investigating. Therefore, fitting them in each individual spectrum is unnecessary, and when possible only the wings corresponding to the broad line emission are fit. In this way we are fitting only the broad edges of the emission line, which is, after all, the part in which we are interested. This is fairly easily accomplished with the optical spectra, where the NELR lines create well defined spikes, typically near the center of the BELR line. The UV spectra, taken with IUE, don't suffer from the changes in

NELR line width that affect the optical data. In this case, the He II narrow line is included in the fit, but kept constant. This is possible because the UV observations were all taken with the same slit width on the same instrument.

The actual values used for the fitting windows are listed in table 3.1. In addition to these values, the file "window.txt" requires a number at the end of each line specifying the amount of smoothing to apply when estimating the amount of noise in the fitting region for the purposes of calculating χ^2 . This number must be odd, and a value of 7 was chosen for the optical data. This value is ignored in the actual fit of the UV data (the amount of noise is hardcoded in) but a value must still be present in the input file.

Table 3.1: Fitting Windows - This table summarizes the windows in which χ^2 is actually calculated. It is important to fit only in regions where we have template profiles or where very little emission is contaminating the continuum. In the case of the optical data, we have left gaps where the NELR emission occurs.

Optical (Å)	UV (Å)
4225 - 4275	1425 - 1730
4420 - 4676	1798 - 1836
4703 - 4838	2400 - 2650
5100 - 5170	
5650 - 5700	

3.3 Minuit and the χ^2 Minimization

Once all of the physical corrections have been made to the observations and template profiles as well as fitting windows have been chosen, the automated fitter takes over.

At its heart is a function minimization package called Minuit. Minuit was developed at CERN, the European Organization for Nuclear Research as a generalized multiparameter function minimizer for use with FORTRAN programs. It is important to understand that Minuit is only a function minimizer; it does not know any of the actual details of the function it is minimizing. It is up to the end user to come up with a useful quantity to calculate as well as some way of bringing all of the pieces together. To that end, a fitter for the optical data called "contin.f" (see appendix A) and a fitter for the UV data called "uvcontin.f" (see appendix C) were developed. These each call the Minuit package as a subroutine. As mentioned in the previous section, we are able to fit the NELR emission in the UV spectra. Because of this, there are some additional constraints that we can put on some of the components of the blend. It is for this reason that there are two different versions of the fitting code. A more elegant generalized version of this fitter should be able to handle both the optical and the UV, and will hopefully be the subject of a future project.

When the fitter is run, it takes a list of input spectra from the file "sorted2.in". The spectra listed in this file must be in IRAF ".imh" format because of some of the subroutines that are used to read in the data. The fitter also takes the list of input template spectra and the windows it should use for calculating χ^2 ("blends.in" and "window.txt", discussed in the two previous sections.) If no fitting windows are specified, the fitter assumes that it should attempt to fit the entire spectrum. The initial guesses at the parameter values for each of the template profiles, as well as any constraints on those parameters, are then put into arrays that are passed to Minuit. Minuit in turn passes these values to a user-supplied subroutine where the function to be minimized is calculated. In the case of the optical data this subroutine is called "cfunk" (see appendix B) and in the case of the UV data this subroutine is called "uvfunk" (see appendix D).

The subroutine then takes the parameters it is given and creates the blended

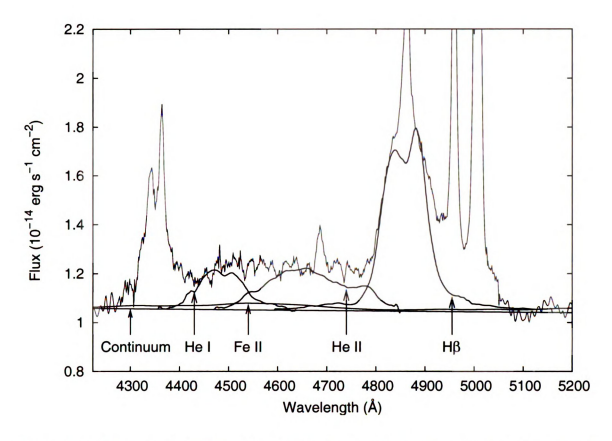


Figure 3.11 Optical Fit Overlay - This figure shows the relative postions of the various components in the optical blend.

spectrum. This is done by first shifting the emission line template spectrum in velocity space using a subroutine adapted from Blends. This "align" routine (as well as several other useful subroutines) can be found in the listing for "functions.f" (see appendix E). The routine from Blends was used because it has been well debugged and properly handles the complexities of flux correction when moving a spectrum in velocity space. The template is then scaled by some factor. This is done for each of the templates in the "blends.in" list. A power-law continuum as described by equation 3.2 is then added together with each of the shifted and scaled templates to create the final blended spectrum. (Examples can be seen in figures 3.11 and 3.12 for the optical and UV spectra respectively. Compiled lists of templates used can be found in tables 3.2 and 3.3 at the end of this chapter.) The subroutine then compares the blended

spectrum's flux value in each wavelength bin with that of the input spectrum that is being fit (from "sorted2.in") to calculate χ^2 . This χ^2 value is then handed back to Minuit. Minuit makes adjustments to the parameters and then calls the subroutine again. This process is repeated until the value being returned is no longer changing by more than some threshold value or until a set number of iterations has been reached (each of these parameters are set by the user in the main fitting program code.) The values used to create the blend are then used to calculate the flux in the template profiles as well as in the power-law continuum. These are then output into a file called, for historical reasons, "slope.txt". This entire process is then repeated with the next input spectrum from "sorted2.in."

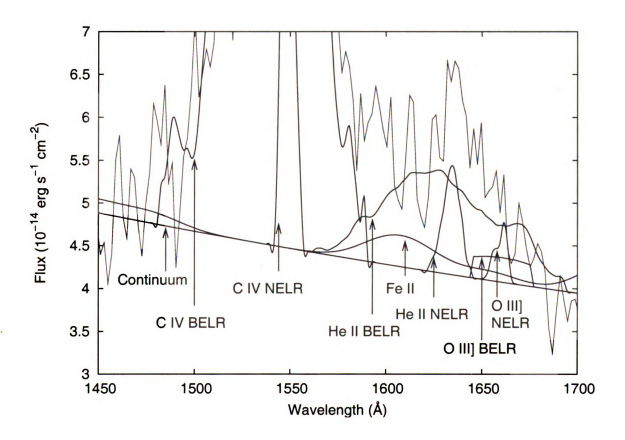


Figure 3.12 UV Fit Overlay - This figure shows the relative positions of the various components in the UV blend.

Unfortunately, due to the nuances of data output when using FORTRAN, the

output file "slope.txt" is in a less than optimal state. Some simple manipulation with, for instance, a Perl script can put this into a more user friendly format that can be used for further analysis. In the end, we need separate light curve files that contain the Julian date and flux in each emission line, as well as one for the continuum. The Julian dates for each observation was deduced using a combination of IRAF header information, file naming convention, and records from previous papers, in particular Dietrich et al. (1993). These dates are listed in tables 2.1 and 2.3.

Some constraints were put on Minuit to keep results within physically plausible ranges. The wavelength λ_{new} was only allowed to shift by $\pm 7\text{Å}$, and the initial guess for the flux in a line was only allowed to vary within a range of 0.1x and 6x of the original value. This was done because it was found that weak lines in a noisy spectrum could easily be driven to zero or pushed well away from their intended area of fitting. In addition, the NELR lines in the UV fit were held to constant values. These values were chosen by first allowing them to change flux during a fit and seeing what the median value was. This value was tweaked as necessary to allow for a good fit and then hardcoded into the "uvcontin.f" and "uvfunk.f" files. Because of the higher quality overall of the calibration of the UV data, certain lines were also tied together in λ_{new} to prevent Minuit from driving them outside of physical ranges. The lack of resolution and quality of the calibration prevented this in the optical data, so only the wavelength range was constrained.

3.4 Error Estimation

Minuit determines statistical errors during its fitting such that a change in a parameter that results in an increase of 1 in the reduced χ^2 is treated as a 1σ change in the parameter. We have made several design choices that make this value given by Minuit a bit suspect. In order both to make the final emission lines physically reasonable and to ensure that the fitter does not accidentally set a weak line to zero to generate

a fit that looks better, we had to constrain the range of values that most parameters could have. This is something that is not recommended by the author of the Minuit Reference Manual, as it can lead to strange results for the error bars. It was, however, necessary to ensure that weak lines such as He II 4686 would not be lost when fitting these low resolution, noisy spectra. The error in any given parameter is also influenced by how well the fitter has done at fitting the adjacent blended lines. These factors seem to help explain the perplexing error values that we found from Minuit. The error bars on the parameters, when used to recalculate the integrated flux in any given line can be orders of magnitude smaller or larger than the calculated flux. This renders these error bars essentially useless for the purposes of further calculation.

Due to these issues, the error in the flux needs to be estimated. As will be shown in the discussion of the cross correlation function, the final reverberation lag is insensitive to modest changes in the size of the error bars, so it is only important that we arrive at a value that is reasonable physically when we take into account the quality of the source data. Given these facts, we have chosen to take as an error 10% of the median flux value for the line in question. This error is similar to the value estimated by Dietrich et al. (1993).

3.5 Cross-Correlation Lags

As was well illustrated by Kaspi (2007), Blandford & McKee (1982) first gave a name to and laid down the mathematical foundation that governs the technique of "reverberation mapping". The response of an emission line to continuum variations is described by

$$L(v,t) = \int \psi(v,t-\tau)C(\tau)d\tau \tag{3.3}$$

.

Here, $C(\tau)$ is the continuum light curve and L(v,t) is the responding emission-line light curve. The quantity $\psi(v,\tau)$ is defined as the transfer function; that is to say the function that governs the response of the emission-line, where v is the velocity field of the BELR that causes the shape and broadening of the BELR emission. This definition assumes that the object is able to be studied in great detail, with very well sampled light curves over a long period of time. In practice this is not typically the case. When using low resolution spectra and poorly sampled light curves, the two-dimensional transfer function, $\psi(v,\tau)$ collapses to a one-dimensional transfer function, $\psi(\tau)$. This is expressed as the single parameter of the time lag between the continuum light curve and the emission-line light curve.

$$F_{CCF}(\tau) = (N\sigma_C\sigma_L)^{-1} \sum_t C(t)L(t+\tau)$$
(3.4)

Here, N is the number of points in the sum, τ is the lag, and σ_C and σ_L are the rms of the light curves of the continuum and the emission-line respectively. The centroid of this CCF is the measure of the size of the BELR, and is often denoted as R_{BLR} or R_{BELR} .

Using this formalism, we are able to calculate a characteristic radius at which an emission-line is produced by creating a light curve for both the continuum and the emission-line in question and calculating a cross-correlation function for them.

Dr. Brad Peterson and his collaborators have developed software to compute this CCF in a standardized way. There are two basic techniques, discussed in detail in Peterson (1993). In the first method, the light curves for the actual observations are interpolated into a smoothly varying function. This function is then sampled regularly to calculate the cross-correlation function. In the second method, called the discrete correlation function (DCF) method, only real data points are used without any interpolation. The DCF method has some further subtleties such as exclusion of points that have a zero time difference, that is to say it will not attempt to correlate

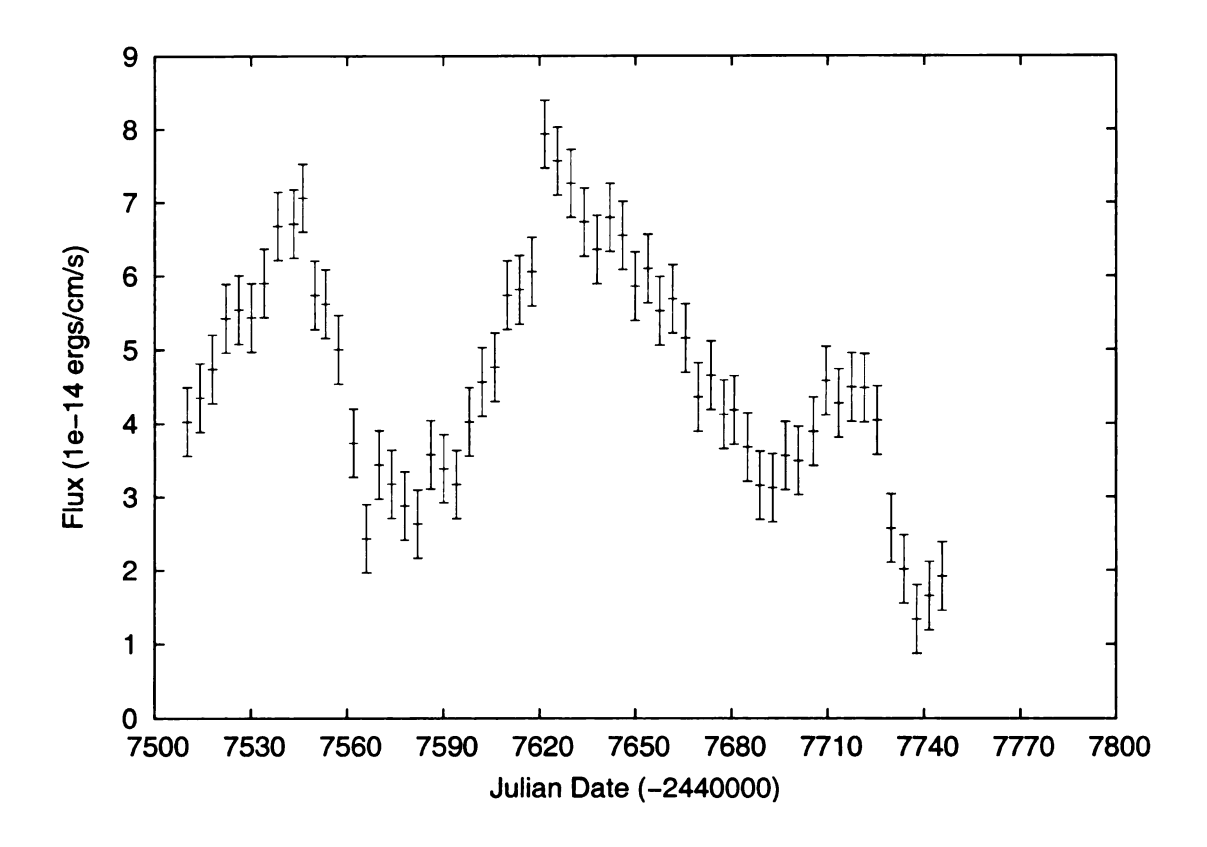


Figure 3.13 UV Continuum Light Curve - as measured at λ 1337, as per Dietrich et al. (1993).

points taken from the same spectrum. This is done to eliminate artificial "lags" at very short times due to correlated errors in the measurement or calibration of the spectrum. Unfortunately, as noted by Peterson (1993), the DCF method does not work well when used on poorly sampled data. Because the data used in this study does not have a sampling rate that is much smaller than the expected reverberation lag time, we used only the interpolated method.

The implementation of the interpolated method was kindly provided to us by B. Peterson in the form of code called *lagerr6*. This code allows for the comparison of two light curves for the purposes of calculating a cross correlation centroid distribution (CCCD.) The interpolation method makes repeated attempts at the creation of a cross correlation function. On each attempt *lagerr6* first performs a flux randomization of

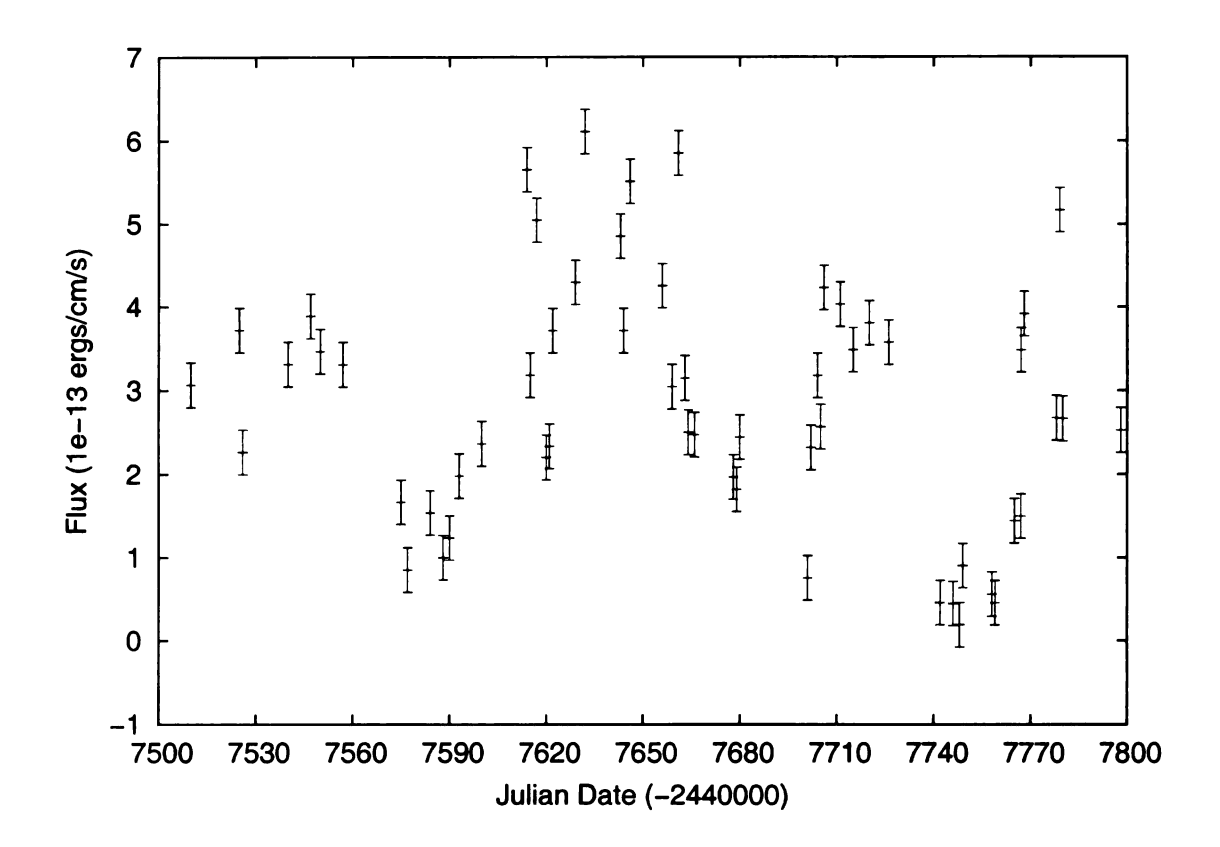


Figure 3.14 Optical He II Light Curve

the input data curve. It allows each point to have a value within the error bars provided with a Gaussian weighting before creating a smooth interpolation between the points and taking a subsample for the purposes of calculating the cross correlation function. If the CCF is above some target threshold, in this case a CCF factor of 0.4, it is deemed a "good" CCF. For a CCF that is "good", a centroid of the distribution above some cutoff value is determined. In the case of this study, the threshold is set at 0.8 of the maximum. An alternate method is to simply look at the peak value of the CCF rather than the centroid of the CCF. The relative merits of the two methods has long been debated, however, B. Peterson has a preference for the centroid method (see the discussion in the appendix of Peterson et al., 2004). Therefore we constrain our discussion here to the centroid method.

The process above is then repeated some large number of times, in this case

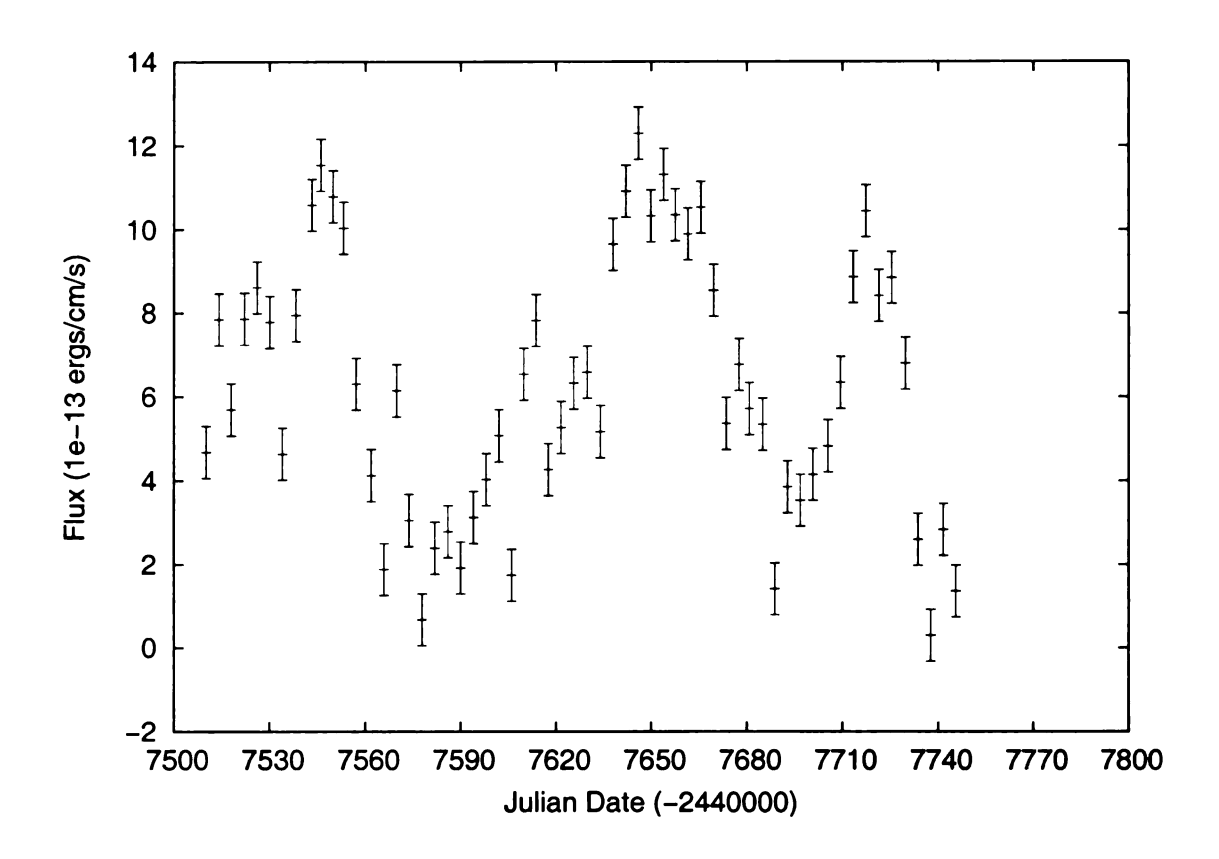


Figure 3.15 UV He II Light Curve

10,000 iterations. This leaves us with a distribution of cross correlation centroids. During the above process, interpolation of just one of the light curves can be done or both can be done simultaneously. In order to counteract any problems that may occur by interpolating the light curves, the process is typically repeated twice; once interpolating the driving light curve and once interpolating the responding emission line light curve. The value of $\tau_{\rm cent}$ is defined to be the centroid of the CCCD. The error in this value is a 1 σ value where 67% of the centroids fall within 1 σ of the value of $\tau_{\rm cent}$. The results of the two separate interpolation runs are then averaged to give the final characteristic reverberation lag time.

When running *lagerr6*, it is important to ensure that the maximum shift that is tested for is at least twice the expected reverberation lag, so as to avoid skewing the centroid calculation if the CCF has broad wings. In the case of the He II lines, a

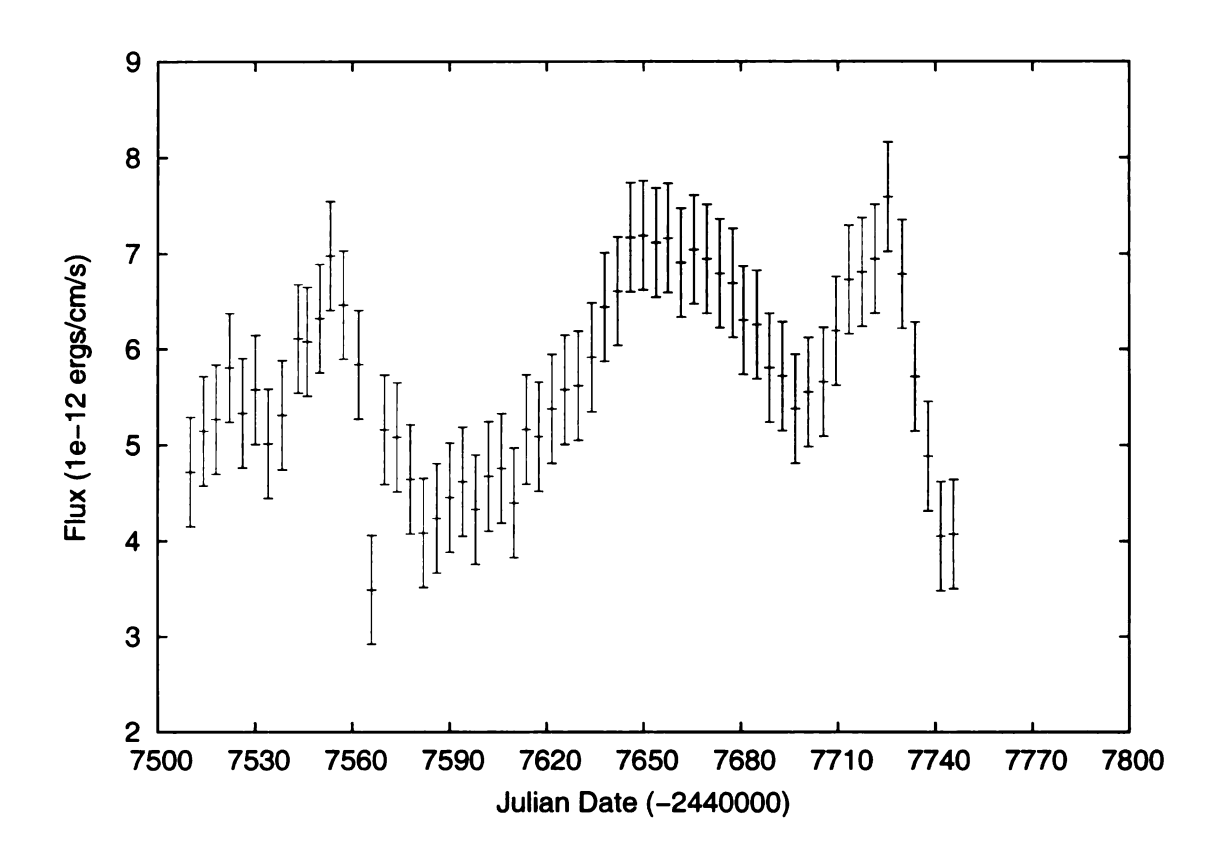


Figure 3.16 C IV Light Curve

maximum shift of twenty days was used. Thirty days was used for C IV and fifty days was used for H β . In each case a resolution of one day was used because of the relatively sparse sampling rate of the original data.

Peterson (2006) noted that as the continuum source in an AGN gets brighter, it also gets harder. This is to say that the amplitude of variability is larger at shorter wavelengths. Therefore, the UV flux rather than the optical flux should be a better measure of the ionizing flux from the central engine. With this detail in mind, all reverberation analysis done in this work uses the UV continuum as the driving light curve.

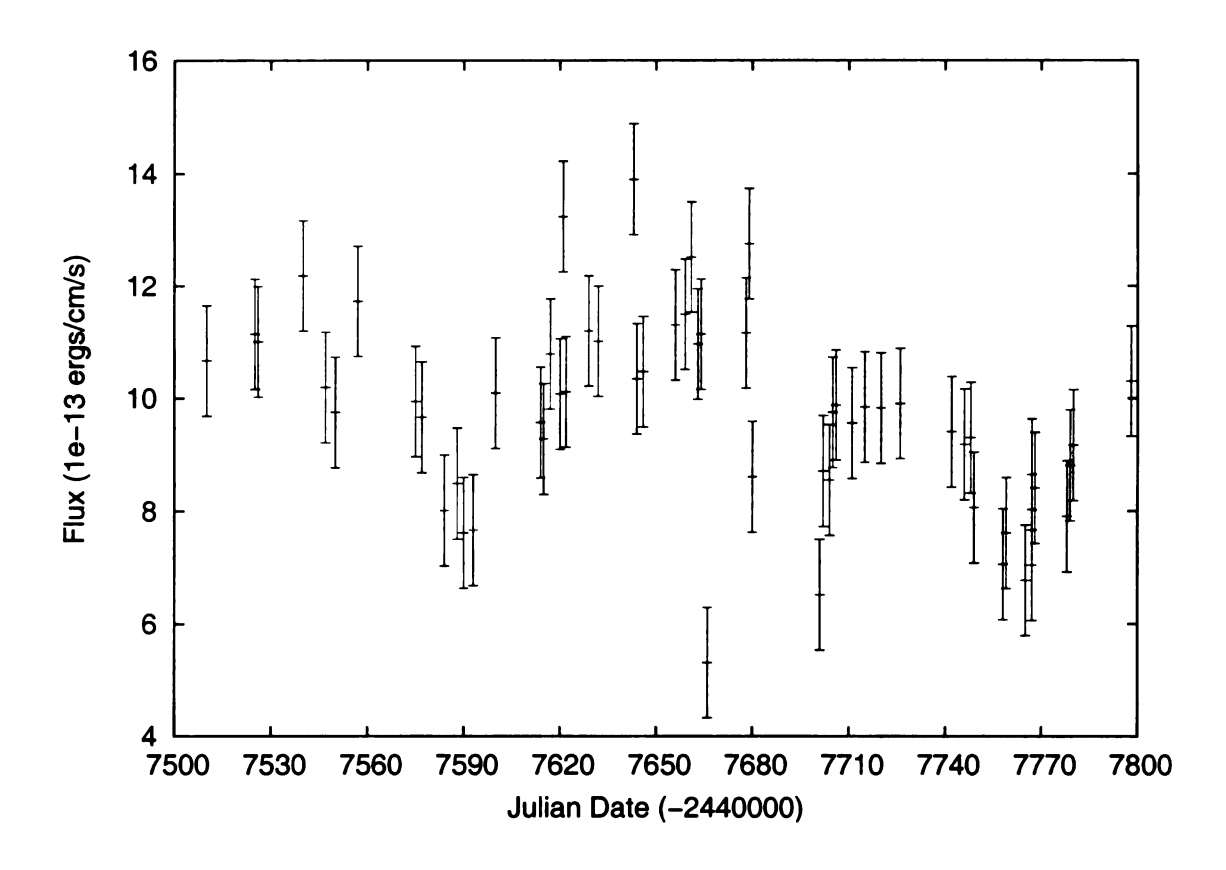


Figure 3.17 H β Light Curve

Table 3.2: Optical Profile Summary - This table compiles a list of the various optical template spectra as well as the spectra used to generate them. The Fe II multiplet is from Véron-Cetty et al. (2004).

Profile Name	Emission Line	From	Notes
smooth_4686.imh	He II $\lambda 4686$ BELR	Optical RMS	
$Fe2_Opt_22.imh$	Fe II Multiplet	External Source	
$smooth_halpha.imh$	$_{ m Heta}$ BELR	Optical RMS	
smooth_5876.imh	He I BELR	Optical RMS	

Table 3.3: UV Profile Summary - This table compiles a list of the various UV template spectra as well as the spectra used to generate them. The Fe II multiplet is from Vestergaard & Wilkes (2001). The O III] BELR and NELR were generated from an rms and an average of several selected spectra that showed prominent O III] emission.

Profile Name	Emission Line	From	Notes
smooth_4686.imh	He II $\lambda 1640$	Optical RMS	
${\rm Fe2_UV_new.imh}$	Fe II Multiplet	External Source	
$c4_blr_smooth.imh$	C IV $\lambda 1549$ BELR	UV RMS	λ tied to He II BELR
$c4_1549_obs2.imh$	C IV $\lambda 1549$ NELR	UV Average	λ tied to He II BELR, flux constant
o3-1663.imh	O III] $\lambda 1663$ NELR		λ tied to He II BELR, flux constant
$narrow_he2.imh$	He II $\lambda 1640~{ m NELR}$	UV Average	λ tied to He II BELR, flux constant
o3_blr.imh	O III] $\lambda 1663$ BELR		λ tied to He II BELR

CHAPTER 4: RESULTS

In the preceding chapter, we laid out a formalism for how to calculate a characteristic reverberation lag time for each of the emission lines we are intersted in studying. In this chapter, we present the results of the cross correlation centroid distribution calculations. It is important, however, to note that this is simply a *characteristic* radius. For any given emission line, there will be a region of some size where the conditions are favorable for emission by the ionized gas within the BELR. The $\tau_{\rm cent}$ discussed in this chapter is simply a parameter used to characterize this region. It can be thought of as the distance in light-days from the central engine to where the line is emitted, but it is important to keep in mind that the emission comes from a region around $\tau_{\rm cent}$ rather than coming only from a distance of $\tau_{\rm cent}$.

4.1 Cross Correlation Centroid Distribution

Figure 4.1 shows the cross correlation centroid distribution (CCCD) for the optical He II emission line (λ 4686) and the UV He II emission line (λ 1640.) In the case of this and subsequent CCCD figures shown in this chapter, the actual CCCD plotted is one generated when both the driving continuum light curve and the responding emission light curve are interpolated. While the final value of $\tau_{\rm cent}$ was determined by averaging the two separate CCCD plots, one interpolating the driving continuum only and one interpolating the responding emission line only, the general shape and location of the peak are similar in the case where both of the light curves are inter-

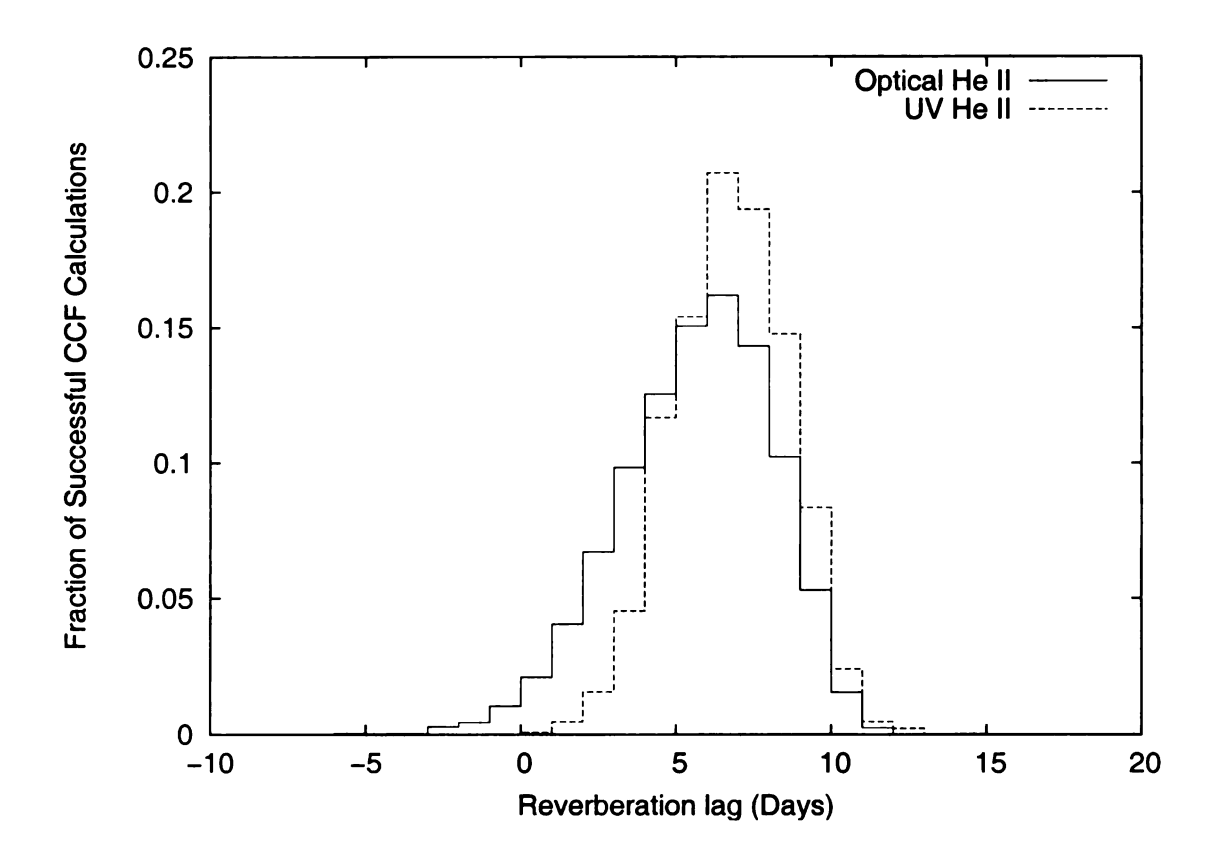


Figure 4.1 Composite CCCD for Optical and UV He II - It is important to note that the optical and UV He II emission-lines fall nicely on top of each other, implying that they are produced with the same lag time, and therefore the same distance from the central engine. Once again, please note that the CCCDs that are shown are for the case where both the driving and responding light curves are interpolated.

polated simultaneously. Therefore, the plots where both light curves are interpolated are used as representative of the important concepts that need to be illustrated.

Both the optical He II CCCD and the UV He II CCCD seem to be quite well behaved, with well defined Gaussian-like shapes. This is a good indication that we have found a strong correlation. The actual values for $\tau_{\rm cent}$ for each of the interpolation cases, as well as the final averaged value for each of the emission lines, are shown in table 4.1.

Table 4.1: CCCD Results - The results of the cross correlation centroid distribution calculated by the *lagerr6* code are shown for three cases; interpolating only the first (driving continuum) array, only the second (responding emission line) and both. The final value for each emission line's τ_{cent} was determined from an average of the 1st array and 2nd array cases. The prior results in column 1 are taken from table 1 of Peterson & Wandel (1999), summarizing the 1989 AGN Watch data set. We consider the values for H β to be unreliable, as discussed in the text.

Emission Line	Prior Result	1st Array	2nd Array	Both Arrays	Final Value
He II λ4686	$8.5^{+3.4}_{-3.4}$	6.2 ± 2.7	3.9 ± 2.8	5.2 ± 2.5	5.0 ± 1.9
He II $\lambda 1640$	$3.0^{+2.9}_{-1.1}$	6.5 ± 1.8	5.7 ± 2.3	6.3 ± 1.8	6.1 ± 1.5
C IV	$9.5^{+2.6}_{-1.0}$	11.9 ± 3.0	11.8 ± 4.6	11.9 ± 3.4	11.8 ± 2.8
${ m H}eta$	$19.7^{+2.0}_{-1.4}$	12.7 ± 7.5	10.5 ± 8.0	11.5 ± 7.0	11.6 ± 5.5

We also see that they both overlap quite well, indicating that the gas emitting each of these lines comes from the same region within the BELR. This fact is further reflected when the actual final values for $\tau_{\rm cent}$ are calculated for each of the lines (table 4.1). The values agree well within the range of error values. When compared with prior results (column 2 of table 4.1), we see that the He II λ 4686 has decreased slightly and the He II λ 1640 has increased. This result is not unexpected, as we assert that prior studies have failed to adequately remove all of the contamination from surrounding lines. Any contamination from a line with a slightly different reverberation lag time will cause a shift in the observed cross correlation function.

The CCCD for C IV is shown in figure 4.2. Like the He II CCCDs, it is also fairly well behaved, although it has a slightly broader shape. The value of $\tau_{\rm cent} = 12.514 \pm 2.730$ is slightly longer than previous measurements, however it still agrees within errors. When the CCCD for C IV is overlayed on the plot of the two He II

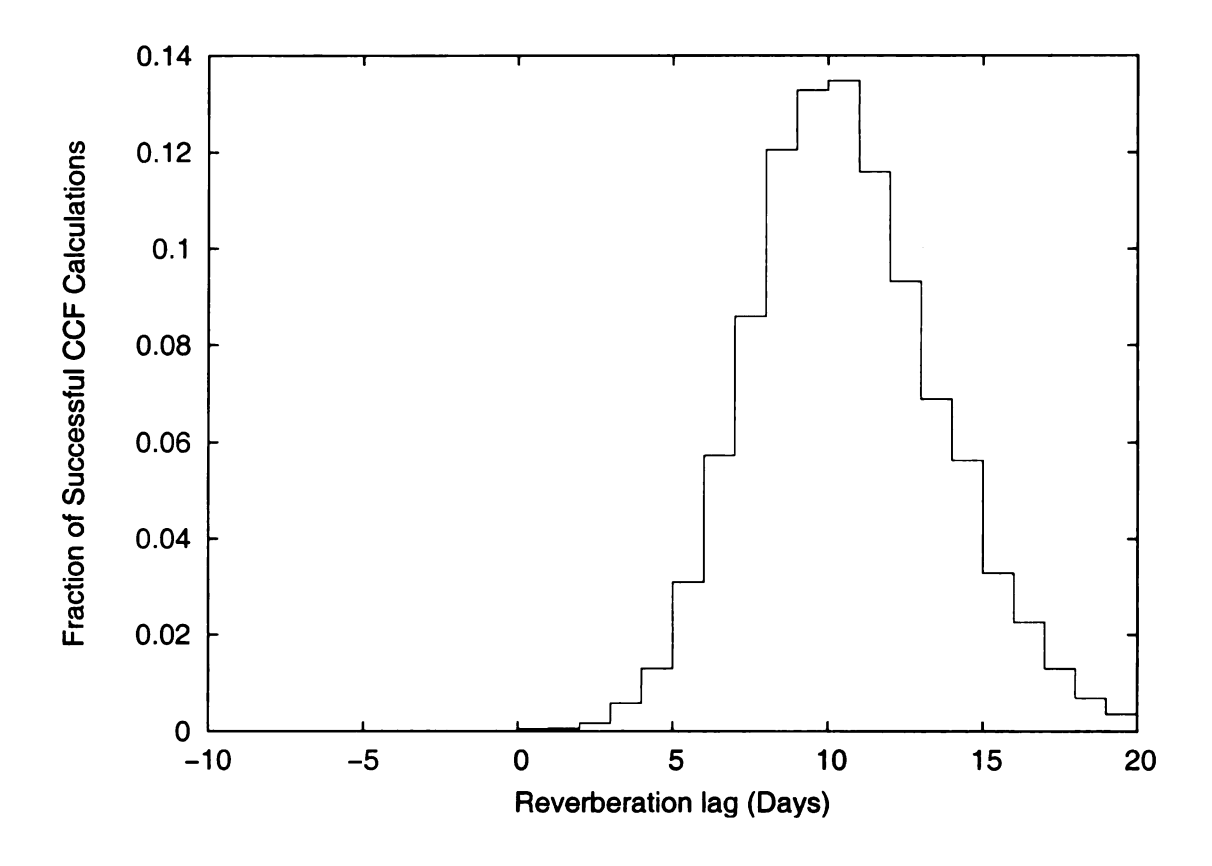


Figure 4.2 Cross Correlation Centroid Distribution for C IV - This plot shows the results for interpolation of both the driving and the responding light curves. The final $\tau_{\rm cent}$ is 12.514 ± 2.730

CCCDs, it becomes quite clear that the He II emission lines and the C IV line do not arise from gas at the same $\tau_{\rm cent}$ (see figure 4.3).

The CCCD for H β is shown in figure 4.4. This is a good example of a situation where this straightforward approach can fail. The CCCD appears to be a combination of two Gaussians. One is fairly weak and is centered around 4 days. The other is much stronger and is centered near 15 days. The shorter, weaker peak, is most likely due to inadequate deblending of the H β emission line. Because we were only interested in H β as a contaminant for He II λ 4686, only the blue wing of H β was fit. A simple centroid of this CCCD would yield a characteristic lag time ($\tau_{\rm cent}$) that is too small. We note that the peak of the H β CCCD shown in figure 4.4 is at about 15 days,

which is closer to the previously observed 19.7 day lag.

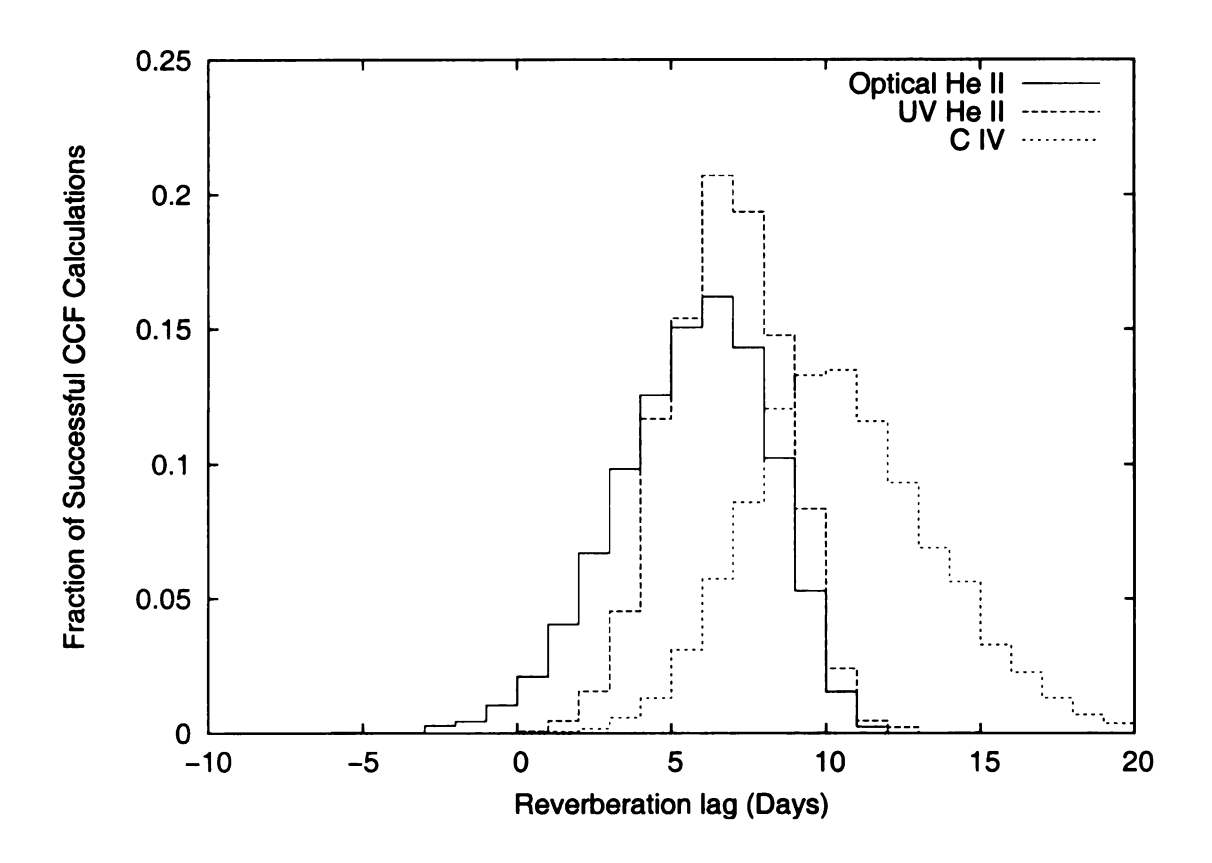


Figure 4.3 Composite Centroid Distribution for Optical and UV He II and C IV - While is seems clear that the UV and optical He II come from the same characteristic radius, it also seems clear that these two emission lines arise from a different region than the region producing C IV.

4.2 LIGHT CURVE ERROR ESTIMATION

It was noted in chapter 3 that the errors on the continuum and emission line light curves were estimated. It was further suggested that the exact value of those error bars was not particularly important, so long as they stayed within physically plausible bounds. In order to demonstrate this, the errors on both the UV continuum, the He II $\lambda 1640$ and the C IV emission lines were both doubled and halved. This gives us a range of error estimates from 5% to 20%. The cross correlation analysis was then

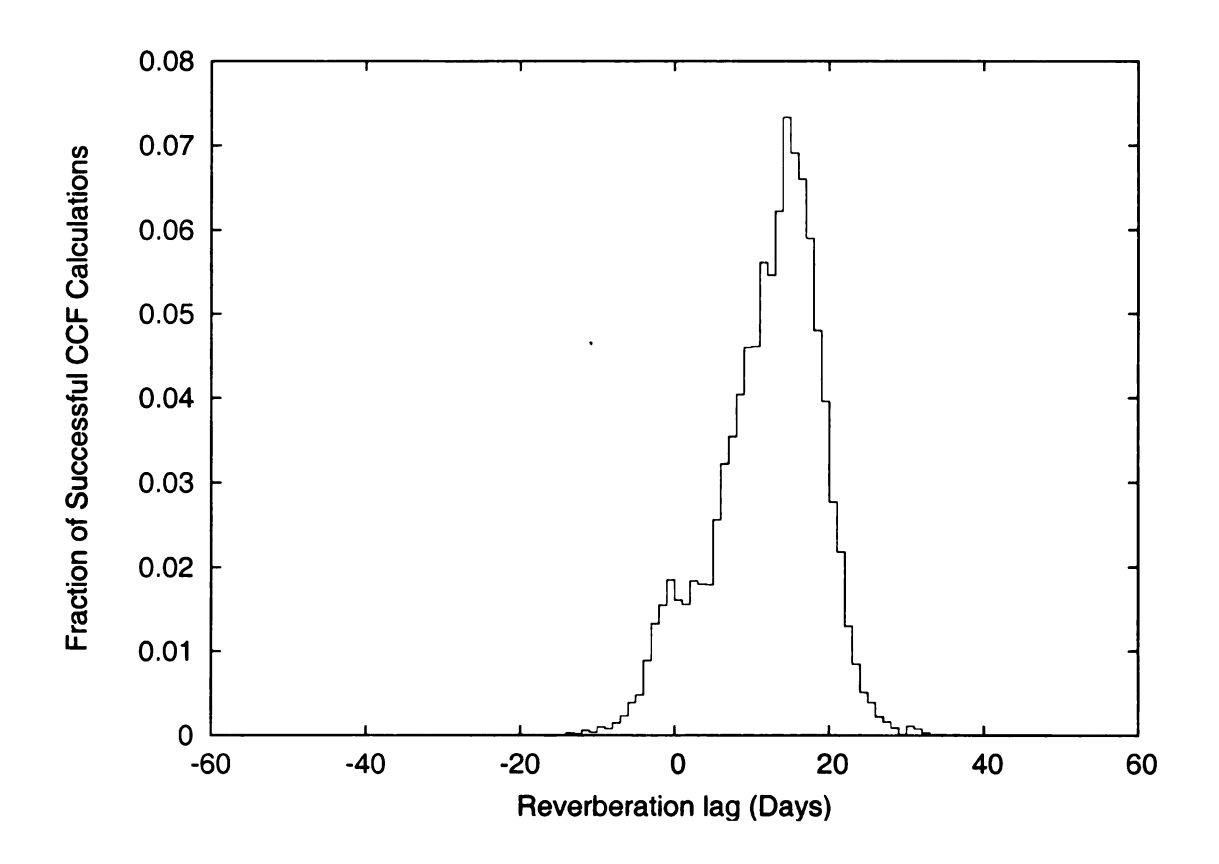


Figure 4.4 Cross Correlation Centroid Distribution for H β - This plot shows the results for interpolation of both the driving and the responding light curves. The final $\tau_{\rm cent}$ was calculated by first fitting a pair of Gaussians to the CCCD. The center and σ values for the larger peak were then averaged to yield a final value of $\tau_{\rm cent} = 15.3 \pm 4.3$. The peak with the shorter lag time is most likely due to inadequate deblending with another feature.

repeated using these values. The results can be seen in figure 4.5 for the He II and figure 4.6 for the C IV. From these plots, we can see that the exact value of the error bars on the light curves does not change the intrinsic result. The gas producing the He II UV emission line is not the same gas that is producing the C IV emission line. It is clear from the C IV figure that as the error bars on the input light curves get larger, the error associated with the width of the CCCD also increases.

With this result in hand, we feel confident that the 10% error that we have estimated for our fits is reasonable and that it gives a reasonable result for the value of $\tau_{\rm cent}$. The exact size of the error bars on our light curves can be debated, but that

does not change the intrinsic result.

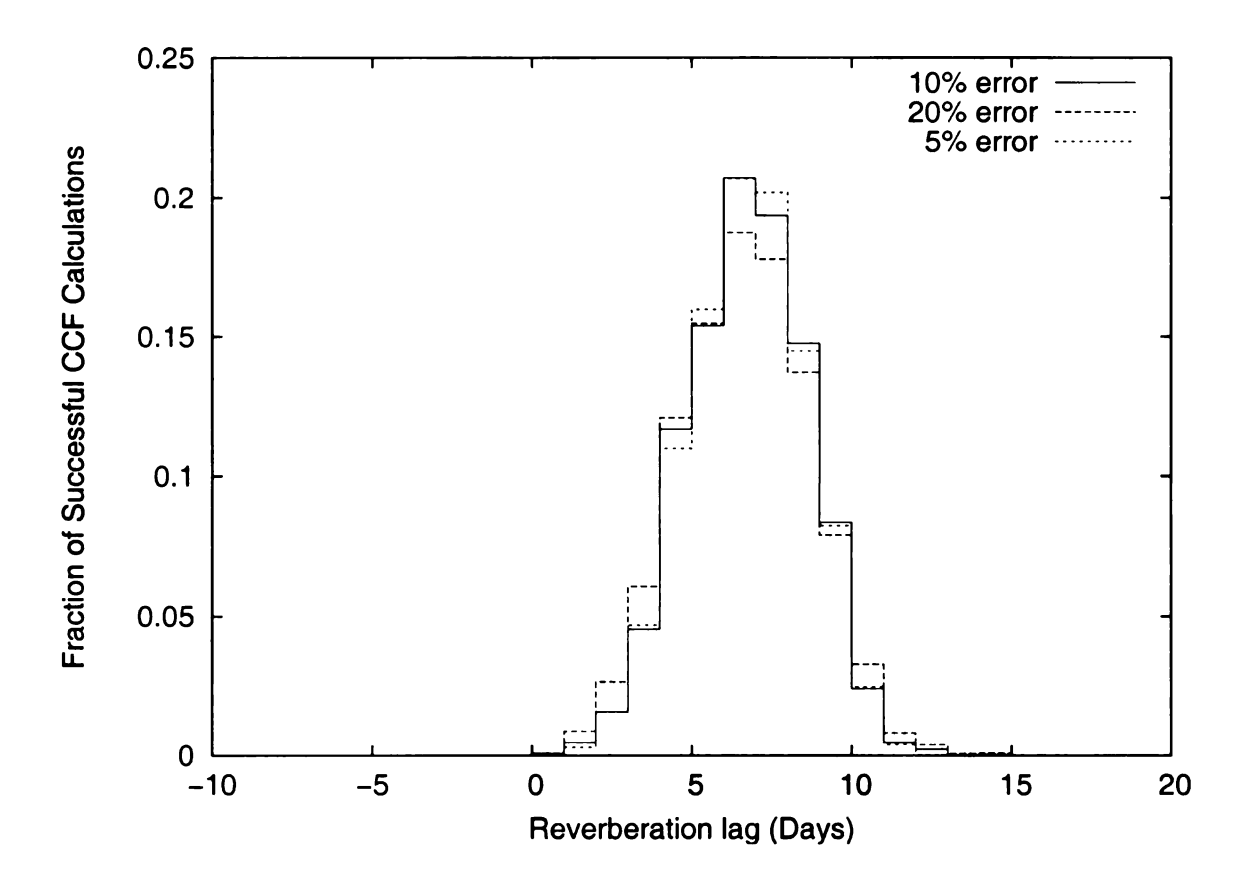


Figure 4.5 He II Error Estimation Test - Three different estimations of the error in the initial UV He II light curve are shown. The qualitative result is the same regardless of the estimated error value.

4.3 Sensitivity to Profile Templates

All of the template profiles used in this work are based on the observed emission line shapes in the object of study, NGC 5548. The two key profiles, the He II λ 4686 BELR profile and the C IV λ 1549 BELR profile were created from the variable component of the emission line seen in the RMS spectra of the optical and UV data respectively. The He II λ 1640 line is more heavily blended but the simplest assumption is that it has the same profile shape as the He II λ 4686 line. This would be true if both lines are formed by recombination and there is no velocity dependent reddening affecting

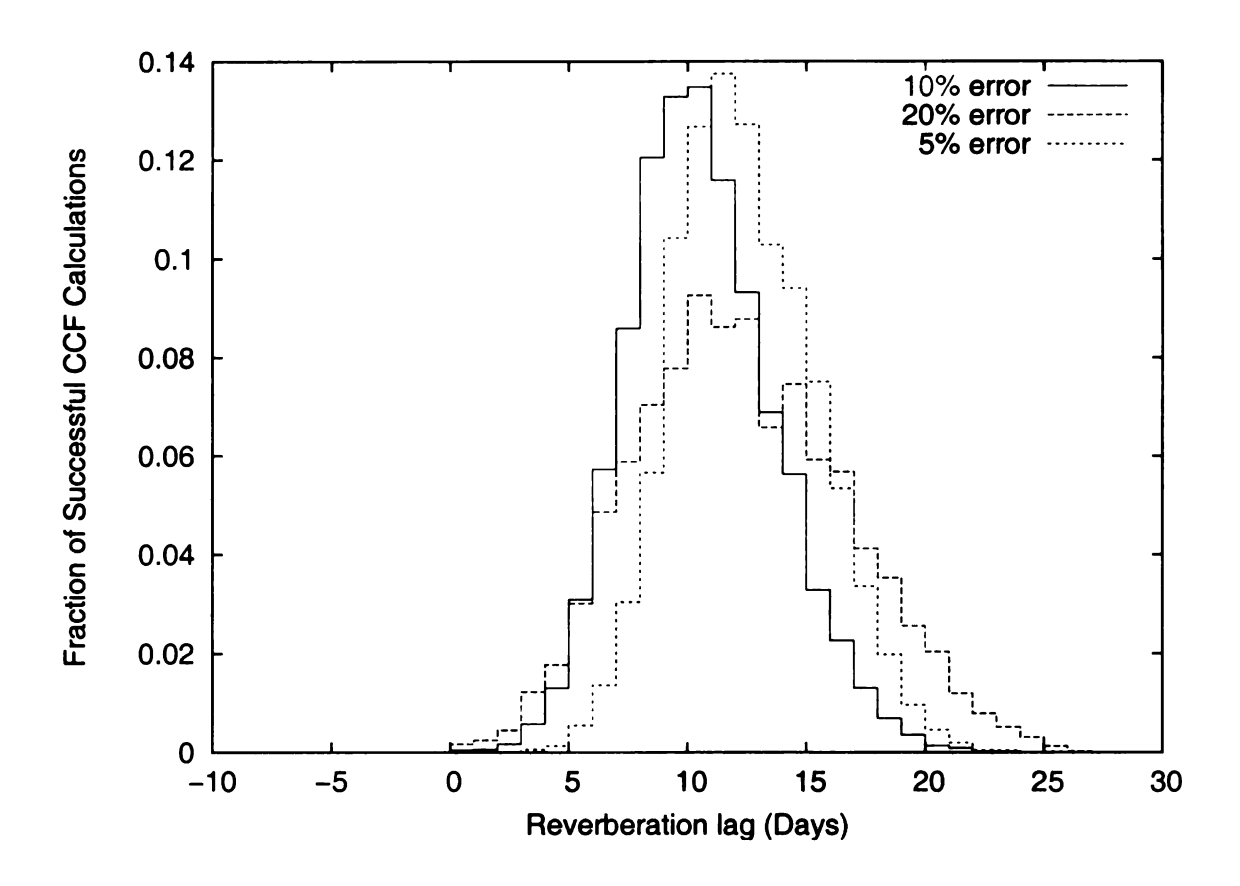


Figure 4.6 C IV Error Estimation Test - Three different estimations of the error in the initial light curve are shown. The qualitative result is the same regardless of the estimated error value.

the $\lambda 1640/\lambda 4686$ intensity ratio after the lines are emitted.

In order to further test the robustness of the assumed template profiles, several different alterations to the template profiles as well as the continuum shape were tested. The results of these permutations can be found in table 4.2.

Table 4.2: Profile Permutations - This table is a summary of the results of several permutations on the profile shapes and components included. Most of these permutations do not make a significant difference in the final result. The details of these permutations are discussed in the text.

Change	He II λ1640	He II λ4686	C IV λ1549
Baseline	6.1 ± 1.5	5.0 ± 2.0	11.8 ± 2.7
$4686~\mathrm{FWHM}+25\%$	6.2 ± 1.4	3.3 ± 5.2	12.0 ± 2.7
$4686~\mathrm{FWHM}$ - 25%	6.3 ± 1.44	1.0 ± 5.2	11.9 ± 2.8
Fe II 9000 km/s	6.23 ± 1.5	4.6 ± 1.7	12.1 ± 2.8
Fe II 3000 km/s	6.4 ± 1.5	4.6 ± 1.8	12.5 ± 2.8
Straight Line	6.3 ± 1.9	5.6 ± 2.4	12.9 ± 3.3
No H β	-	6.1 ± 1.5	-
No C IV	4.4 ± 1.8	3.0 ± 1.8	NA
No O III	6.0 ± 1.5	5.1 ± 2.0	12.6 ± 2.8

The full width at half maximum (FWHM) He II template profile, created from the variable emission in the optical spectrum, was increased and decreased by 25%. While this change had a small effect on the $\lambda 1640$ reverberation lag time, it created a large change in the optical. The reverberation values are misleading however, as the CCCD for the two altered profiles are mostly noise with no well defined peak. This can be seen in figure 4.7. The values presented in table 4.2 are simply the centroid of this relatively featureless CCCD. The UV CCCD did not suffer as severely as the automated fitter was able to compensate by boosting or suppressing all of the blended profiles in the region around $\lambda 1640$. The contamination in the optical $\lambda 4686$ is less severe, and the automated fitter is forced to use mostly the new He II profile to attempt a fit. It is not unexpected, therefore, that the optical fit suffers more when

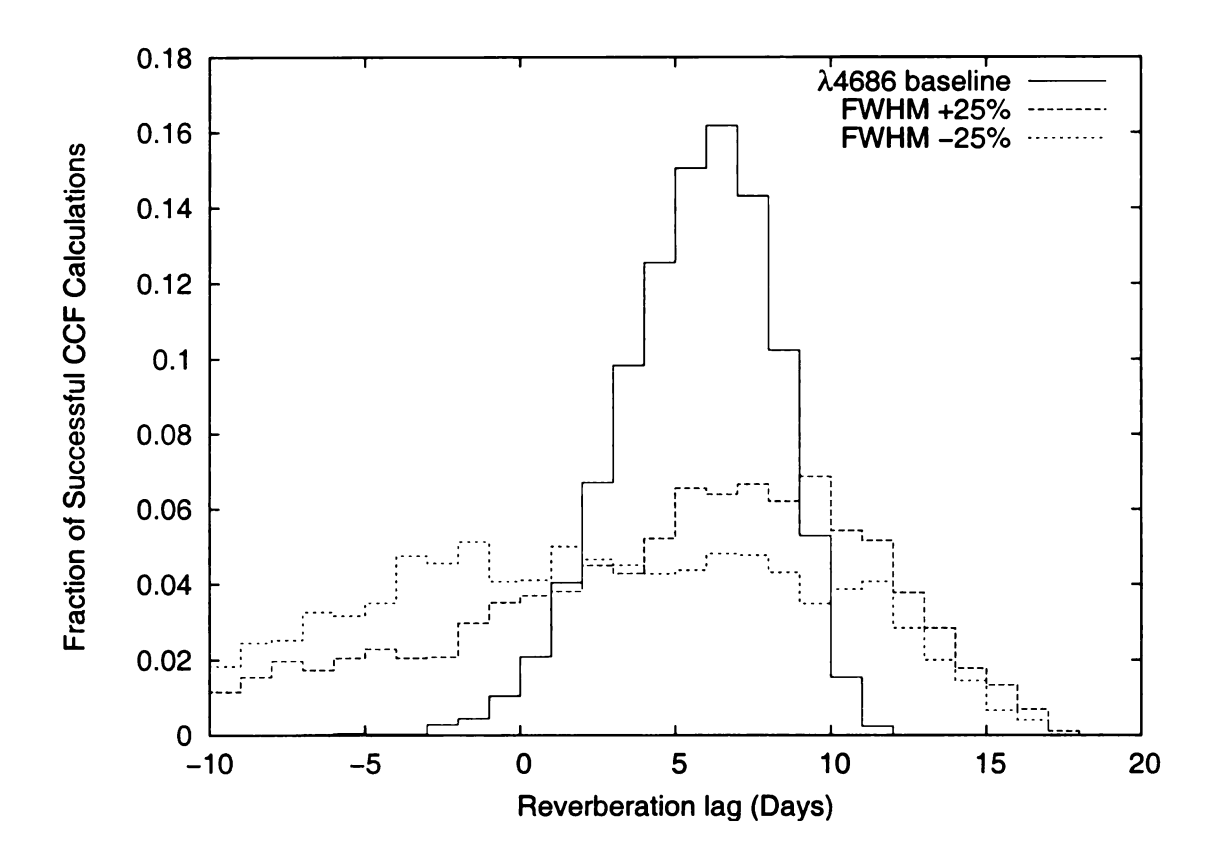


Figure 4.7 He II $\lambda 4686$ Profile Width - The effect of altering the He II $\lambda 4686$ profile FWHM by $\pm 25\%$ is shown. When these altered profiles are used to fit the BELR emission at $\lambda 4686$, the resulting CCCD is mostly featureless with no clear well defined peak. This result is not unexpected as the shape of this variable emission was used to create the original profile. Because the blending in the optical is less severe than in the UV, the automated fitter is forced to "fix" the fit by simply boosting or suppressing the He II emission, leading to a poor fit and therefore a poor CCCD.

The actual value for the broadening of the Fe II multiplet in NCG 5548 is not well constrained. In their detailed analysis of the Fe II emission in NGC 5548, Vestergaard & Peterson (2005) were only able to place the very loose boundaries on the range of broadenings that give acceptable fits to the observed Fe II emission. These values ranged from between 4500 km/s to about 10,000 km/s. While Vestergaard and Peterson found that 6250 km/s yielded the qualitatively best fit for the optical, they preferred a value closer to the higher end of the range for the UV. In this study,

we chose to use a value of 6250 km/s for both the optical and the UV for the sake of simplicity and because the Fe II contamination is fairly small in the regions of interest. Even in AGN that have quite strong Fe II emission, such as Akn 120 studied in detail by Kuehn et al. (2008), the reverberation lag of Fe II is not well constrained. Kuehn et al. found that although the Fe II emission did respond in some way to continuum variations, they were unable to measure a clear reverberation time scale. Because of these loose constraints on the Fe II emission, we decided to try using two different broadenings other than the 6250 km/s that was used as our baseline value. Broadenings of 3000 km/s and 9000 km/s were both substituted into the fit with very little change to the reverberation results for either the He II lines of the C IV line.

Another area where our analysis deviated from previous studies is in our use of a power-law to fit the entire continuum under our regions of interest. In previous studies, a straight line "pseudo-continuum" was drawn under a local region and the emission lines were measured as the flux above this straight line. In order to attempt to simulate this with our automated fitter, we replaced the power law with a straight-line. Because a straight line will do a very poor job of fitting the entire continuum over a large range of wavelengths, the fitting windows were also adjusted to only cover an area near the region of interest (1425 - 1730 Å in the UV, and 4225 - 4275 Å, 4420 - 4676 Å, 4703 - 4838 Å, and 5100 - 5170 Å in the optical.) Six of the optical spectra were rejected due to obviously incorrect fits (57509hx, 57556hx, 57599kx, 57645ix, 57664ma, 57766ix), but the remainder of the optical and the UV fit fairly well. The resultant reverberation lags were similar to the baseline case, with slightly larger errors.

We also consider the possibility that some of our other profiles could be in error. The H β profile, whose wing contaminates the He II λ 4686 emission line could have a shape that is not well characterized by the H α line that was used to create the profile. To test this, the H β emission was removed from the fit, and the window that

included the red wing of He II $\lambda 4686$ was shortened to 4703 - 4760 Å. This likely still includes some contamination from the wing of H β , but still gave enough of the He II region to obtain a good fit. The H β wing of the emission contaminating the He II is likely the cause of the slightly longer lag time that is seen in the cross correlation analysis. The He II $\lambda 1640$ and C IV lines lags remain unchanged.

While the C IV profile in the UV was created from the variable C IV emission, we also attempted to remove the C IV from the fit, with a corresponding adjustment to the fitting window. The ranges 1425 - 1456 Å, 1618 - 1730 Å, 1798 - 1836 Å, 2400 - 2650 Å were used. This loss of range did have an impact on the ability of the fitter to accurately create a blend, and several of the UV spectra were rejected due to obviously incorrect fits (the spectra from dates 57526, 57586, 57606, 57621, 57629, 57649, 57657, 57713, 57737 specifically.) This loss temporal resolution as well as less accurate continuum measurement did have an effect on the He II line lags, although they still agree within error. The C IV lag was obviously not calculated.

The last major profile to be considered was the O III] emission that contaminates the He II $\lambda 1640$. It was removed in a manner similar to that of H β in the optical. The profile was removed from the fit, and the fitting windows were adjusted. The UV was then fit from 1425-1652 Å, 1798 - 1836 Å, and 2400 - 2650 Å. Once again, this had a small effect, but the values for the reverberation lags still agree within error with our baseline values.

Given that the qualitative results are fairly insensitive to these moderate changes in template profile conditions, we take this as an indication that the exact shape of the template profiles. This is true provided that something nearly approximating the correct shape is used. In the case of the changes made to the FWHM of the He II profile, it is clear that when a profile that is obviously wrong is used the results begin to break down. We take this as good evidence in favor of our approach of using template profiles generated from the observed data.

CHAPTER 5: DISCUSSION

In this study, we have carried out a careful reanalysis of an existing set of observations of NGC 5548. In our analysis, we have attempted to fit all of the lines in the complex blended features that include He II $\lambda 1640$ and $\lambda 4686$. While our results for He II are somewhat different from previous studies, they do agree within their error bars. Our technique for fitting these lines was much more refined than in previous studies. Our starting point was to create a template profile from the observed variable component of He II $\lambda 4686$. We then assumed that the He II $\lambda 1640$ emission line had the same profile shape as the He II $\lambda 4686$. This is expected if the lines are formed by recombination and if there are no velocity-dependent reddening effects. Profiles were also created from observed variable and constant profiles in order to attempt to account for the presence of other emission lines that are known to be blended with the optical and UV He II lines. In the special case of the Fe II multiplet feature, a profile from another AGN was used. Each of these profiles was then fit in an automated fashion to each observed spectrum to create light curves for each emission line of interest and finally, an interpolated cross-correlation analysis was performed to formally calculate a characteristic reverberation lag time for each of the studied emission lines. This de-blending of lines that are known to contaminate one another is more sophisticated than has been done in previous studies (e.g. Dietrich et al., 1993; Korista et al., 1995)

We found that the two He II emission lines do have very similar reverberation

lag times, with formal values of 5.0 ± 1.9 days for the optical He II line ($\lambda 4686$) and 6.1 ± 1.5 days UV He II line ($\lambda 1640$.) This result was not unexpected and is in good agreement with predictions from simulations. Unless the two lines are formed in some very different way than the simple recombination processes that are thought to be the case, they should have the same lag times. Our reverberation measurements of the stronger emission line of C IV $\lambda 1549$, with a formal value of 11.8 ± 2.8 , agrees with previous measurements. These results are summarized in table 4.1.

The suprising result here is that both lines are inconsistent with the reverberation lag of C IV. This is surprising because under the simple LOC model, the He II lines should come from the same region that forms C IV (Bottorff et al., 2002). While it is true that He II has a higher ionization potential than C IV, and since previous observations have shown that higher ionization potentials correspond to shorter lag times, it may seem reasonable to find that He II responds more rapidly than C IV. In fact, previous reverberation results also find that C IV has a slightly longer reverberation lag time than the optical He II. However, the simulations of Bottorff et al. (2002) seem to indicate that C IV and He II are emitted most efficiently in similar physical conditions. The question that must be asked, therefore, is if any of the underlying assumptions of the LOC model may be in error.

The LOC model is based on only a few mostly straightforward assumptions.

- 1. The BELR gas covers a wide range in radial distance.
- 2. The BELR gas covers a wide range in density.
- 3. The radial and density distributions can each be described by simple power laws.
- 4. The emitting region can be approximated as a sea of optically thick gas clouds.
- 5. Each cloud sees the same ionizing continuum shape, i.e. they are not in the

shadow of clouds closer in that partially absorb the radiation in a wavelength dependent way.

In the case of NGC 5548, the first assumption is verified by the observed reverberation results. The large range of lag times found for the different emission lines seem to support this basic premise. While C IV has a well determined lagtime of 10-12 days, H β has a 20 day lag and Mg II may be upwards of 70 days (Clavel et al., 1991) in NGC 5548 alone. Similar differences have been found for many other objects.

The second point, that the BELR gas covers a wide density range, is also probably true. The observed spectrum seen in NGC 5548 contains a mix of lines that only radiate efficiently at very different values of the ionization parameter (the ratio of the incident ionizing flux to the gas density.)

However, the assumption that the radial and density distributions can each be described by simple power laws is almost certainly an oversimplification of the true situation. This would at best describe the composite spectrum of many AGN combined together, not that of any one specific object. Many studies of individual objects show emission line profiles that break up into a few major components at different velocities such as that of Q0207-398 (Baldwin et al., 1996) or J1546+5253 (Dhanda et al., 2007). This is almost certainly a demonstration that the radius-density parameter space is not smoothly filled. Looking in more detail at the plots of various LOC plane calculations of Korista et al. (1997) (see figure 5.1), there may be some way to populate the LOC plane with a carefully chosen collection of optically thick clouds that would re-create the observed lag difference between He II and C IV. It is not clear upon first inspection how exactly one could create He II $\lambda 1640$ without also creating C IV $\lambda 1549$ as well. One could, however, simulate this specific collection of gas using a program such as Cloudy (Ferland, 2006) to see if the intensity ratio and reverberation lag ratio might be recovered. This would be fruitful ground for future work.

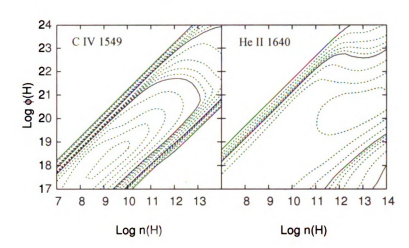


Figure 5.1 Standard LOC Model - The contours in this figure show the standard LOC model (solar chemical abundances and a cloud column density of $10^{23} {\rm cm}^{-2}$) for several emission lines as a function of Hydrogen density, n(H), and incident ionizing continuum, Φ (H). Based on this model, it is difficult to find a place where C IV is produced that does not also produce He II $\lambda 1640$. This figure is from data from Korista et al. (1997)

Regarding the final assumptions, that the gas clouds in the BELR are optically thick and do not filter the continuum "seen" by clouds futher out, there is some evidence that this is not the case with all AGN. Casebeer & Leighly (2003) argue that as least some AGN contain matter-bounded clouds. These clouds would absorb radiation at some wavelengths while passing other wavelengths through. This would certainly violate assumption 5 of the LOC model. It could give rise to a situation wherein a region of highly ionized He⁺⁺ gas could efficiently emit He II through recombination but have carbon ionized to a state higher than C⁺⁺⁺ and therefore having no C IV emission lines. Commonly observed higher-ionization lines such as O VI λ 1034 or the coronal lines such as [Fe X] λ 6374 might also come from such a region.

It is not clear how easily such a system could be constructed with the current model framework. A good starting point would be to run Cloudy with a variety of stopping densities well below the standard value of $N(H) = 10^{23} {\rm cm}^{-2}$. This would be a good follow-up project and a logical next step for future work.

This result, that the He II and C IV are not produced by the same gas, should not necessarily be seen as a large setback for the LOC model. The LOC model does a good job of recreating the spectrum of the average AGN. This does not mean that it can easily predict the behavior of every individual AGN without first carefully crafting a specific set of BELR clouds.

CHAPTER 6: SUMMARY

The goals of this project were to create new techniques and tools to more accurately measure reverberation lag times for heavily blended emission lines. Once that was in place, these tools would be used to measure the reverberation lag of He II, a relatively simple emission line, in both optical and UV spectra. This was done in an attempt to clear up a discrepancy between theoretical models, which predict that the optical and UV He II are produced by the same gas and should therefore have the same reverberation lag time and that these two emission lines should have nearly the same reverberation lag time as C IV, and previous studies, which found that the optical and UV He II lines were in marginal agreement and that the UV He II did not agree with the C IV reverberation lag.

With these goals in mind, this project was quite successful. The optical and UV He II emission were both measured to have reverberation lag times of roughly 5 - 6 days, with far better agreement in the lag-time probability distribution curves for the two lines. Furthermore, the strong C IV line, which is also involved in the heavy blending, was measured to have a lagtime consistent with previous measurements, but the C IV and He II lagtimes do not overlap. This agreement with previous measurements of the strong C IV line helps to validate the technique that was used. Our technique, which required a large software development effort, included using an automated fitting routine to simultaneously fit multiple emission line template profiles that were, themselves, created from observed data.

One rather surprising result was the clear indication that He II and C IV are not created by the same gas within the BELR. This is contrary to what was predicted by the typical model of the BELR but consistent with previous measurements. This is not necessarily a failing of the model, but possibly an indication of oversimplification within the assumptions on which the model was based. The LOC model compared to in this work is a very good predictor for the behavior of the average AGN, but does not necessarily describe any individual AGN without careful crafting of a specific grouping of clouds.

APPENDICES

APPENDIX A: CODE FOR CONTIN.F

This is the FORTRAN code of the optical fitter. It can also be used as a general fitter, as it does not have any hard-coded parameters like the UV fitter does. It calls cfunk f as a subroutine.

```
character*5 plabel(20), junk
double precision ptau(20),pincr(20),puper(20),ploer(20),zero
double precision ftau, err, eplus, eminus, arglis(2)
double precision PI
integer i
integer ip, ierflg, ivarbl, npar, n, nn
double precision x,Y, m, b,yavefile,sdevfile
double precision gauss, chisq, average, stdev, noise
double precision fitout(20),small,chiout(20),errout(20)
real xgauss
integer chistat, card, j, idof
real ran2
external cfunk
character*10 chtest
character*12 glob
integer chlen, IM, IER,xcur,ycur,NAX,IAX(7),IPIX
integer totcount
character chcur
real dxval(5000), dyval(5000), rtest
        real cxval(5000), cyval(5000)
real prix(5000),priy(5000)
real txval(5000), tyval(5000)
real ylim(5000)
real scaley(5000)
real wstart(30), wstop(30), wsig(30), nsmooth(30), woff(30)
integer IMAXD, iof, county, lcount, iof2, wcount, wtest
integer iof3, iof5,iof40
character*26 irafname
real pxmin,pxmax,pymin,pymax,armin,armax
real xbar, sigx, ybar, sigy, yhigh, xhigh
```

```
double precision scale
 common /myscale/ scale
 common /mydata/ dxval, dyval, nnx, wstart, wstop, wcount,
         ncomps, totalo, totcount, wsig, woff, yhigh, xhigh
 common /pridata/ prix,priy,lcount,xbar,sigx,blend
 parameter (nmax=50000)
 common diff(nmax),xinput(nmax,30),shift(nmax),
         oname(30), wold(30), wnew(30), area(30), nxc(30),
         xlamc(30),dlamc(30),totalc(30),nx,xlam0,dlam
 character*50 oname, objfile
 dimension obj(nmax),blend(nmax),ratio(nmax),id(100)
 dimension waves(nmax)
 real crap, wkeep(30), akeep(30)
 character*5 crap2
 real cstart,cstop,left
 double precision conerr, ag(4), ehigh, elow
C *************
 diff(1) = 3.14159
PI = 3.14159
open(71,file='slope.txt')
open(72, file='error.txt')
open(81,file='chi.txt')
open(88,file='offset.txt')
open(89,file='frac.txt')
open(90,file='fracerr.txt')
open(91,file='left.csv')
 32 format(a4,8x,a1,10x,a5,4x,a5,5x,a5)
open(77, file='window.txt')
wcount = 1
read(77,*,IOSTAT=iof5) wstart(wcount),wstop(wcount),nsmooth(wcount)
do while (iof5.eq.0)
   wcount = wcount + 1
   read(77,*,IOSTAT=iof5) wstart(wcount),wstop(wcount),nsmooth(wcount)
enddo
close(77)
c This puts wount back to the correct value. Pointed out by
c Neelam.
wcount = wcount - 1
write (*,*) "wcount = ",wcount
C ************
```

```
c Start setting up our plot. We will output to a
c file called plot.ps and make a 4 x 4 grid of plots
c per page.
        call pgbegin(0,'plot.ps/PS',1,1)
c This opens blends.in and reads in the list of spectra to go get.
c Some of them are put into an array. It should be noted that if a line
c is not properly formatted (i.e. you forget to leave any blank space
c between two numbers) it may not be a fatal error. This routine will
c intrepret the poorly formatted line as the end of the file and the
c program will continue without throwing and error. This can lead to
c it only using a subset of the parameters in your blends.in file.
open(22,file='blends.in',status='old')
read(22,*,IOSTAT=iof3) objfile
write (*,*) objfile
read(22,*,IOSTAT=iof3) const
i=1
read(22,*,IOSTAT=iof3) oname(i),wold(i),wnew(i),area(i)
do while (iof3.eq.0)
   i=i+1
   read(22,*,IOSTAT=iof3) oname(i),wold(i),wnew(i),area(i)
   enddo
ncomps=i-1
c Store the initial values from blends.in in case we need them later
        do n=1,ncomps,1
   wkeep(n) = wnew(n)
   akeep(n) = area(n)
        enddo
C ************
const = 3.20540747E-14
open (21,file='sorted2.in',status='old')
read(21,*,IOSTAT=iof2) objfile
do while (iof2.eq.0)
write (*,*) objfile
```

```
c These are the initial values for the minuit parameters.
c General format is as follows:
c plabel(n) = 'name-of-variable'
c ptau(n) = initial value
c pincr(n) = initial step size
c puper(n) = upper limit (0 for none)
c ploer(n) = lower limit (0 for none)halpha04-a 6562.8 6562.8 0.048
c npar = n (count of how many variables we have for minuit
             to manage)
c The ptau value will be passed to the xval array in your subroutine.
c Minuit will then step around and pass new ptau values to the xval
c array.
c These are the wavelength and area values for each of the input lines
c from blends.in.
npar = 0
do n=1,ncomps,1
   npar = npar + 1
   plabel(npar) = oname(n)
   ptau(npar) = wnew(n)
   pincr(npar)=0.01
   ploer(npar)=wnew(n) - 7.
   puper(npar)=wnew(n) + 7.
   npar = npar + 1
   plabel(npar) = oname(n)
   ptau(npar) = area(n)
   pincr(npar)=0.00001
   ploer(npar) = area(n) * 0.1
   puper(npar)=area(n) * 6.
enddo
c NOTE: For the continuum, we are trying to fit a power law,
c so I am passing it the initial values for a
c continuum = A * (lambda^gamma) fit.
npar = (2*ncomps) + 1
plabel(npar) = 'A'
ptau(npar) = 1.0e-14
pincr(npar)=1.e-15
puper(npar)=1.e-10
ploer(npar)=1.e-15
npar = (2*ncomps) + 2
plabel(npar) = 'gamma'
```

C *************

```
ptau(npar) = -1.8826
pincr(npar)=1.e-4
puper(npar)=1.
ploer(npar)=-2.
c This gives us a total of (2*ncomps) + 2 parameters to
c give to the fitter. This total value is in npar.
C ***********
c Open the iraf file. This is the file we are fitting
c our profile to. Building the fit array should take
c place in the subroutine, since minuit will need to
c tweak parameters.
c It must be a .imh, not a .fits
c read spectrum to be fitted
write(*,*) 'input object file is ',objfile
irafname = objfile
call t6in(objfile,nx,xlam0,dlam,id,obj,nmax)
write(*,*) 'nx, lambda range,dlambda = ',nx,xlam0,xlam0+nx*dlam,dlam
nnx = nx
totalo=0.
yminobj=1.e30
ymaxobj=-1.e30
do i=1,nx
  totalo=totalo+obj(i)
  yminobj=min(yminobj,obj(i))
 ymaxobj=max(ymaxobj,obj(i))
  waves(i)=xlam0-dlam+i*dlam
end do
do i=1,nx
   dxval(i) = waves(i)
  dyval(i) = obj(i)
enddo
C ***********
c SMOOTHING, from Neelam and Baldwin. Even numbers break this. Don't use
       It will make chisq artifically small.
do iwin=1, wcount
   do i=1.nx
if(waves(i).lt.wstart(iwin)) istart=i
if(waves(i).lt.wstop(iwin)) istop=i
   enddo
   istart=min(istart,nx)
   istop=min(istop,nx)
          xsig=0.
```

```
do i=istart, istop
    nsm=min(nsmooth(iwin),2*(nx-i)+1)
            sum=0.
            do j=i-nsm/2, i+nsm/2
            sum=sum+obj(j)
            enddo
           wdiff=obj(i)-sum/nsm
           xsig=xsig+(wdiff*wdiff)
          enddo
           if(istart.lt.istop) then
      wsig(iwin)=sqrt(xsig/(istop-istart))
   else
      wsig(iwin)=sum/nsm
   end if
       enddo
C ************
c read in the blend component spectra
c The continuum (a power law) will be built in the subroutine cfunk.
do i=1,ncomps
  call t6in(oname(i),nxc(i),xlamc(i),dlamc(i),id,xinput(1,i),nmax)
  totalc(i)=0.
    do k=1,nxc(i)
      totalc(i)=totalc(i)+xinput(k,i)
    end do
end do
do i=1.nx
  blend(i)=0.
end do
nb0=nmax
C ************
c Set up minuit to do it's thing.
* Set-up parameters for minuit (aka unit numbers for input, output)
         call mninit(5,6,7)
* Set the initial values of the adjustable parameters (aka the "x")
        in function fcn. Let MINUIT know about those parameters attributes
do ip=1,npar
  zero=0.
   call mnparm(ip,plabel(ip),ptau(ip),pincr(ip),puper(ip),
          ploer(ip),ierflg)
  call mnparm(ip,plabel(ip),ptau(ip),pincr(ip),ploer(ip),
         puper(ip),ierflg)
```

```
if (ierflg.ne.0) write(*,*) 'Par: ',ip,' not entered sucessfully'
end do
* These set the strategies by which Minuit work, higher is more
        "accurate" but more costly in time (see p.24 in MINUIT Ref man
        v94.1). I think this call is optional
arglis(1)=2.
        call mnexcm(cfunk,'SET STR',arglis,1,ierflg,0)
        Stuff for accurate error analysis, see p.22, optional also I think
arglis(1)=1.
call mnexcm(cfunk,'SET ERR',arglis,1,ierflg,0)
        Supress warnings.
arglis(1)=1.
call mnexcm(cfunk, 'SET NOW', arglis, 1, ierflg, 0)
        Sets level of printout detail. -1 is minimum, 3 is highest.
arglis(1)=-1.
call mnexcm(cfunk,'SET PRI',arglis,1,ierflg,0)
        Now use Minimize the minimize the value of the function
       set the max number of iterations with arglis(1) and
        the precision required in arglis(2).
arglis(1)=50000.
arglis(2)=1.e-20
call mnexcm(cfunk,'MIGRAD',arglis,2,ierflg,0)
C ************
       Assuming convergence after <50000 iterations print out
       the current value of the function. Store the values in the
       array fitout.
write(*,*) "-----"
write(*,*) "Results for ",objfile
write(*,*) ""
       do ip=1,npar
   call mnpout(ip, junk,ftau,err,eplus,eminus,ivarbl)
   write(*,*)ip,' ',plabel(ip),' Orig: ',ptau(ip),' Final:',ftau,err
   fitout(ip) = ftau
   errout(ip) = err
       end do
С
       This gets the current status of minimization. Since we are
        'done', this should be the final value of our minimized
С
       function. These parameters are, in order: (1) minimum value
С
       (2) estimated vertical distance to the minimum (3) the value of
С
       parameter uncertainities (4) # of currently variable parameters
       (5) the highest external parameter number defined by the user
С
       (6) that status of the covariance matrix. See page 16 of
       minuit manual.
call mnstat(chiout(1),chiout(2),chiout(3),chiout(4),chiout(5)
```

```
1 ,chistat)
idof = totcount-(ncomps+2)
crap = chiout(1)/idof
write(*,*) "REDUCED CHISQ = ",chiout(1)/idof
write(*,*) "FMIN = ",chiout(1)
write(*,*) "FEDM = ",chiout(2)
write(*,*) "ERRDEF = ",chiout(3)
write(*,*) "NPARI = ",chiout(4)
write(*,*) "NPARX = ",chiout(5)
write(*,*) "ISTAT = ",chiout(6)
write(*,*) "xhigh = ",xhigh
write(*,*) "yhigh = ",yhigh
write(*,*) "-----"
C ***********
       Output the values to a file. In this case, the file is called
       'slope.txt' (for historical reasons) and contains:
glob = objfile
 31 format(a8,1x,E12.6,1x,f8.5,1x,f8.5,1x,f9.5)
write (89,*) glob, chiout(1)/idof, fitout
write (90,*) glob, chiout(1)/idof, errout
write (81,*) glob, chiout(1)/idof
write (88,*) glob, xhigh, yhigh
C ************
20 format(i2,1x,a20,2(0pf9.3),f7.3, 1pe10.2,1x,0pf7.3)
30 format(a20,2(0pf9.3),f7.3, 1pe10.2,1x,0pf7.3)
C ************
c Here, we convert the fractions to flux values for the even parameters
do ip = 1, ncomps
   fitout(2*ip) = fitout(2*ip) * totalo * dlam
   errout(2*ip) = errout(2*ip) * totalo * dlam
end do
c This is where we calculate the flux for the continuum. There is a
c a problem with using this method if your spectra are not all the same
c wavelength range. Trim your spectra or use a different method. I think
c I may put some code here to take the "continuum" between a specific
c wavelength range. It will still use the powerlaw that we fit, but it
c would only keep the flux within a certain range.
c I feel that the correct approach might be to re-evaluate the continuum
c flux from the fitted parameters, integrating over a user specified range
c and then do the calculation again with the parameters slewed to their error
c limits to calculate the error in the flux.
ip = (2*ncomps)+3
c This method assumes that you have no reason to shift the continuum
c using the align routine.
C NOTE: This 'conwin.in' method is no longer used. The continuum
```

```
c is calculated at a specific point.
c Here we open up the input file where the user has specified
c the window to use for the continuum. If the read fails in any
c way (for instance there isn't a file there or it only contains
c one number) we will notice and default to using the whole
c spectral range.
open (40, file='conwin.in', status='unknown')
read (40,*,IOSTAT=iof40) cstart,cstop
if (iof40.ne.0) then
   cstart = xlamc(ncomps+1)
   cstop = xlamc(ncomps+1) + (dlam * nx)
endif
close (40)
c As a test, let's make the starting and ending wavelengths the
c full range for the spectrum.
write (*,*) "Range = ",cstart," - ",cstop
fitout(ip) = 0.
conerr = 0.
ag(1) = 0.
ag(2) = 0.
ag(3) = 0.
ag(4) = 0.
c Find the flux value at 5100.
fitout(ip) = fitout(2*ncomps+1) * (5100./5600.)**(fitout(2*ncomps+2))
c Calculate the four corners
   ag(1) = ag(1) + ((fitout(2*ncomps+1)+errout(2*ncomps+1)) *
     c ((5100./5600.)**(fitout(2*ncomps+2)+errout(2*ncomps+2))))
   ag(2) = ag(2) + ((fitout(2*ncomps+1)-errout(2*ncomps+1)) *
     c ((5100./5600.)**(fitout(2*ncomps+2)+errout(2*ncomps+2))))
   ag(3) = ag(3) + ((fitout(2*ncomps+1)-errout(2*ncomps+1)) *
     c ((5100./5600.)**(fitout(2*ncomps+2)-errout(2*ncomps+2))))
   ag(4) = ag(4) + ((fitout(2*ncomps+1)+errout(2*ncomps+1)) *
     c ((5100./5600.)**(fitout(2*ncomps+2)-errout(2*ncomps+2))))
c Now find the high and low, and subtract them.
elow = 9999.
ehigh = -9999.
do ii=1,4
   if (ag(ii).gt.ehigh) then
      ehigh = ag(ii)
   endif
   if (ag(ii).lt.elow) then
```

```
elow = ag(ii)
   endif
enddo
errout(ip) = dlam * (abs(ehigh - elow)/2.)
write (*,*) "New con = ".fitout(ip)
write(*,*)conerr,fitout(ncomps+1),fitout(ncomps+2)
errout(2*ncomps+4) = 0.
do ip = 1, ncomps
   errout(2*ncomps+4) = (errout(2*ip))**2 + errout(2*ncomps+4)
enddo
errout(2*ncomps+4) = (errout(2*ncomps+3))**2 + errout(2*ncomps+4)
errout(2*ncomps+4) = sqrt(errout(2*ncomps+4))
c Write out the values using fluxes instead of fractions.
write (71,*) glob,chiout(1)/idof,fitout
write (72,*) glob,chiout(1)/idof,errout
C WRITE OUT THE BLENDED SPECTRUM.
call t6out('blends.fit',nx,xlam0,dlam,blend)
left = 0.
do i=1,nx
  diff(i)=obj(i)-blend(i)
  if ((dxval(i).ge.4505.).and.(dxval(i).le.4832.)) then
     left = left + abs(diff(i))
  endif
end do
left = left * dlam
write (91,*) glob, left
call t6out('blends.diff',nx,xlam0,dlam,diff)
C ************
c Let's make a plot of the output.
  pxmin = dxval(1)
   pxmax = dxval(nx)
   pymin = -5.e-14
   pymax = 1.e-13
c This makes it not ask to continue when you end it.
        call pgask(.false.)
c Change window size.
CALL PGENV(pxmin,pxmax,pymin,pymax,0,1)
c Labels for the graph. X, Y, Title. In this case
c I have left the title off and used the Baldwin Plot
c Label System (BPLS).
```

```
CALL PGLAB('wavelength', 'flux','')
c Change font size for BPLS, then label, then change it back.
call pgsch(3.)
call pgtext(pxmin+10.,pymin+0.9*(pymax-pymin),irafname)
call pgsch(1.)
call pgtext(pxmin+10.,pymin, "residual")
c Here we plot the actual graph. # pts, xarray, yarray, symbol
c The first call sets the line style.
call pgsls(1)
call pgline(nx,dxval,dyval)
call pgline(nx,dxval,blend)
call pgline(nx,dxval,diff)
c These make the empty rectangle and the crosshatching in the
c test ranges.
call PGSHS (0., 5., 0.)
CALL PGSFS(3)
wtest = 1
do while (wtest.le.wcount)
   call pgrect(wstart(wtest), wstop(wtest), pymin, pymax)
   wtest = wtest + 1
enddo
CALL PGSFS(2)
wtest = 1
do while (wtest.le.wcount)
   call pgrect(wstart(wtest), wstop(wtest), pymin, pymax)
   wtest = wtest + 1
enddo
C *************
c This will reset out wnew and area back to our inputs from the blends.in.
c If you want your fit to continue to evolve, that is if you want the new
c starting values to be the last ending values, comment this line out.
        do n=1,ncomps,1
           wnew(n) = wkeep(n)
           area(n) = akeep(n)
        enddo
c Grab the next value from our input. The while loop
c will test to see if we are done.
read(21,*,IOSTAT=iof2) objfile
enddo
close(71)
close(72)
close(81)
close(88)
close(89)
close(90)
```

close(91)
 call pgend
end

Appendix B: Code for cfunk.f

This is the cfunk.f subroutine. It is called by the optical fitter, contin.f.

```
subroutine cfunk(npar,grad,fval,xval,iflag,futil)
 double precision fval,xval(*)
 double precision stuff, crap, m, b
 double precision PI, BIGX, SIG, i, x, chi, AMP
 double precision AMP2, BIGX2, SIG2
 double precision grad, futil
 double precision sdev, total, keepme
 real yave, average, stdev, chisq, xgauss
 real armin, armax
 integer count,n,npar,iflag,count1,count2,count3
 integer icomp, ibb
 logical lratio, lprint, slide, wfix
 double precision XX(5000), YY(5000)
real dxval(5000), dyval(5000)
real prix(5000),priy(5000),xbar,sigx
real wstart(30), wstop(30), wsig(30), woff(30)
real ybar, sigy, ydev, yhigh, xhigh
real sdx(5000),spx(5000),sdy(5000),spy(5000)
 integer NNX, lcount, wtest, wcount, ns
 integer totcount
double precision scale
 common /myscale/ scale
 common /mydata/ dxval, dyval, nnx, wstart, wstop, wcount,
c ncomps, totalo, totcount, wsig, woff, yhigh, xhigh
 common /pridata/ prix,priy,lcount,xbar,sigx,blend
parameter (nmax=50000)
common diff(nmax),xinput(nmax,30),shift(nmax),
c oname(30), wold(30), wnew(30), area(30), nxc(30),
c xlamc(30),dlamc(30),totalc(30),nx,xlam0,dlam
character*50 oname, objfile
dimension obj(nmax),blend(nmax),ratio(nmax),id(100)
```

```
open (36, file='gauss.test', status='unknown')
      write(36,*) xval(4),xval(5),xval(6)
do i=1.nx
  blend(i)=0.
end do
c Here we need to hand the values back from the xval array to the
c variables that are used in the blends routines.
c NOTE: This is a dangerous side effect of using the "align" subroutine.
c We are writing over the wnew and area arrays each time. This means that we
c can slowly move the acceptable ranges as we fit more spectra.
c I will take steps to keep this from happening in the main program.
        ibb = 0
        do n=1,ncomps,1
           ibb = ibb + 1
           wnew(n) = xval(ibb)
           ibb = ibb + 1
           area(n) = xval(ibb)
        enddo
c Now for the continuum.
C The y values need to go into the array xinput(XXX,1), I think.
      oname(ncomps+1) = "continuum"
c This is the array size, it is equal to the number of points
c in the wavelength space.
         nxc(ncomps+1) = nnx
c This is the starting wavelength, this is the same as the
c data starting wavelength, xlam0
      xlamc(ncomps+1) = xlam0
c This is the wavelength step, should pass from main program.
      dlamc(ncomps+1) = dlam
c I have no clue what this is. Let's make it 1.
      id(ncomps+1) = ncomps + 1
c These are the y values. Here is where I should calcluate them.
      totalc(ncomps+1) = 0.
      do i=1,nnx
         xinput(i,ncomps+1) = (xval((2*ncomps)+1) *
     c ((dxval(i)/5600.)** xval((2*ncomps)+2)))
         totalc(ncomps+1) = totalc(ncomps+1) + xinput(i,ncomps+1)
         keepme = dxval(i)
c This is the starting wavelength again. You will just have
```

```
c to trust me.
      wold(ncomps+1) = xlam0
c This is the new wavelength to shift to. I suspect we should
c also keep this the same always.
      wnew(ncomps+1) = xlam0
c This is the area, it will be used as a scaling factor.
      area(ncomps+1) = totalc(ncomps+1)/totalo
C Now for the align call.
c Slide should be set to false.
      slide = .false.
do icomp=1,ncomps
  call align(icomp,nout0,noutx,slide)
  scale=area(icomp)*totalo/totalc(icomp)
  do i=1,nx
    blend(i)=blend(i)+shift(i)*scale
  end do
  nb0=min(nb0,nout0)
  nbx=max(nbx,noutx)
fluxc=area(icomp)*totalo*dlam
      enddo
c Adding in the continuum.
      do i=1,nx
         blend(i) = blend(i) + xinput(i,ncomps+1)
      enddo
c Now to calculate the values to minimize
         chi = 0.
         sdev = 0.1
         totcount = 0
         xhigh = 0.
         yhigh = 0.
         wtest = 1
         do while (wtest.le.wcount)
            n = 1
            count1 = 0
            do while (n.le.nnx)
               if (dxval(n).ge.wstart(wtest).and.
                   dxval(n).le.wstop(wtest)) then
     С
                  count1 = count1 + 1
                  sdx(count1) = dxval(n)
                  sdy(count1) = dyval(n)
```

```
spx(count1) = dxval(n)
                  spy(count1) = blend(n)
                  if (dyval(n).gt.yhigh) then
                     xhigh = dxval(n)
                     yhigh = dyval(n)
                  endif
               endif
               n = n + 1
            enddo
      Only do the rest if our spectrum contained this window.
С
            if (count1.gt.0) then
            ydev = wsig(wtest)
            ns = 1
            do while (ns.le.count1)
               chi = chi + chisq(sdy(ns),spy(ns),ydev)
               ns = ns + 1
            totcount = totcount + 1
            enddo
            endif
c Move to the next test region.
            wtest = wtest + 1
         enddo
         close(36)
      fval = chi
      return
      end
```

APPENDIX C: CODE FOR UVCONTIN.F

This is the FORTRAN code of the UV fitter. It calls uvfunk f as a subroutine.

```
character*5 plabel(20), junk
double precision ptau(20),pincr(20),puper(20),ploer(20),zero
double precision ftau, err, eplus, eminus, arglis(2)
double precision PI
integer i
integer ip,ierflg,ivarbl,npar,n,nn
double precision x,Y, m, b,yavefile,sdevfile
double precision gauss, chisq, average, stdev, noise
double precision fitout(20),small,chiout(20),errout(20)
real xgauss
integer chistat, card, j, idof
real ran2
external uvfunk
character*10 chtest
character*12 glob
integer chlen, IM, IER, xcur, ycur, NAX, IAX(7), IPIX
integer totcount
character chcur
real dxval(5000), dyval(5000), rtest
        real cxval(5000), cyval(5000)
real prix(5000),priy(5000)
real txval(5000), tyval(5000)
real ylim(5000)
real scaley(5000)
real wstart(30), wstop(30), wsig(30), nsmooth(30), woff(30)
integer IMAXD, iof, county, lcount, iof2, wcount, wtest
integer iof3, iof5, iof40
character*26 irafname
real pxmin,pxmax,pymin,pymax,armin,armax
real xbar, sigx, ybar, sigy, yhigh, xhigh
double precision scale
common /myscale/ scale
```

```
common /mydata/ dxval,dyval,nnx,wstart,wstop,wcount,
         ncomps, totalo, totcount, wsig, woff, yhigh, xhigh
 common /pridata/ prix,priy,lcount,xbar,sigx,blend
 parameter (nmax=50000)
 common diff(nmax),xinput(nmax,30),shift(nmax),
         oname(30), wold(30), wnew(30), area(30), nxc(30),
         xlamc(30),dlamc(30),totalc(30),nx,xlam0,dlam
 character*50 oname, objfile
 dimension obj(nmax),blend(nmax),ratio(nmax),id(100)
 dimension waves(nmax)
real crap, wkeep(30), akeep(30)
 character*5 crap2
real cstart, cstop
double precision conerr, ag(4), ehigh, elow
C ************
diff(1) = 3.14159
PI = 3.14159
open(71,file='slope.txt')
open(72,file='error.txt')
open(81,file='chi.txt')
open(88,file='offset.txt')
open(89,file='frac.txt')
open(90,file='fracerr.txt')
32 format(a4,8x,a1,10x,a5,4x,a5,5x,a5)
open(77, file='window.txt')
wcount = 1
read(77,*,IOSTAT=iof5) wstart(wcount),wstop(wcount),nsmooth(wcount)
do while (iof5.eq.0)
   wcount = wcount + 1
   read(77,*,IOSTAT=iof5) wstart(wcount),wstop(wcount),nsmooth(wcount)
close(77)
c This puts wount back to the correct value. Pointed out by
c Neelam.
wcount = wcount - 1
write (*,*) "wcount = ",wcount
C *************
c Start setting up our plot. We will output to a
c file called plot.ps.
        call pgbegin(0,'plot.ps/PS',1,1)
```

```
c This opens blends.in and reads in the list of spectra to go get.
c Some of them are put into an array. It should be noted that if a line
c is not properly formatted (i.e. you forget to leave any blank space
c between two numbers) it may not be a fatal error. This routine will
c intrepret the poorly formatted line as the end of the file and the
c program will continue without throwing and error. This can lead to
c it only using a subset of the parameters in your blends.in file.
open(22, file='blends.in', status='old')
read(22,*,IOSTAT=iof3) objfile
write (*,*) objfile
read(22,*,IOSTAT=iof3) const
i=1
read(22,*,IOSTAT=iof3) oname(i),wold(i),wnew(i),area(i)
do while (iof3.eq.0)
   i=i+1
   read(22,*,IOSTAT=iof3) oname(i),wold(i),wnew(i),area(i)
   enddo
ncomps=i-1
c Store the initial values from blends.in in case we need them later
        do n=1,ncomps,1
   wkeep(n) = wnew(n)
   akeep(n) = area(n)
        enddo
C **************
const = 3.20540747E-14
open (21,file='sorted2.in',status='old')
read(21,*,IOSTAT=iof2) objfile
do while (iof2.eq.0)
write (*,*) objfile
C ***********
c These are the initial values for the minuit parameters.
c General format is as follows:
c plabel(n) = 'name-of-variable'
c ptau(n) = initial value
c pincr(n) = initial step size
c puper(n) = upper limit (0 for none)
c ploer(n) = lower limit (0 for none)halpha04-a 6562.8 6562.8 0.048
c npar = n (count of how many variables we have for minuit
             to manage)
c The ptau value will be passed to the xval array in your subroutine.
c Minuit will then step around and pass new ptau values to the xval
c arrav.
c These are the wavelength and area values for each of the input lines
c from blends.in.
npar = 0
```

```
do n=1,ncomps,1
   npar = npar + 1
   plabel(npar) = oname(n)
   ptau(npar) = wnew(n)
   pincr(npar)=0.01
   ploer(npar)=wnew(n) - 5.
   puper(npar)=wnew(n) + 5.
   npar = npar + 1
   plabel(npar) = oname(n)
   ptau(npar) = area(n)
   pincr(npar)=0.0001
   ploer(npar) = area(n) * 0.05
   puper(npar)=area(n) * 5.
enddo
c NOTE: For the continuum, we are trying to fit a power law,
c so I am passing it the initial values for a
c continuum = A * (lambda^gamma) fit.
npar = (2*ncomps) + 1
plabel(npar) = 'A'
ptau(npar) = 1.0e-14
pincr(npar)=1.e-15
puper(npar)=1.e-10
ploer(npar)=1.e-15
npar = (2*ncomps) + 2
plabel(npar) = 'gamma'
ptau(npar) = -1.8826
pincr(npar)=1.e-4
puper(npar)=-0.5
ploer(npar)=-2.
c This gives us a total of (2*ncomps) + 2 parameters to
c give to the fitter. This total value is in npar.
C ************
c Open the iraf file. This is the file we are fitting
c our profile to. Building the fit array should take
c place in the subroutine, since minuit will need to
c tweak parameters.
c It must be a .imh. not a .fits
c read spectrum to be fitted
write(*,*) 'input object file is ',objfile
irafname = objfile
call t6in(objfile,nx,xlam0,dlam,id,obj,nmax)
write(*,*) 'nx, lambda range,dlambda = ',nx,xlam0,xlam0+nx*dlam,dlam
nnx = nx
```

```
totalo=0.
yminobj=1.e30
ymaxobj=-1.e30
do i=1,nx
  totalo=totalo+obi(i)
  yminobj=min(yminobj,obj(i))
  ymaxobj=max(ymaxobj,obj(i))
  waves(i)=xlam0-dlam+i*dlam
end do
do i=1.nx
   dxval(i) = waves(i)
   dyval(i) = obj(i)
c This section is used to hardwire in some parameters that are
c related. There is a corresponding section in the subroutine
c as well as in the code below where we pass the parameters to
c minuit. If you edit one, you may need to edit the others.
c I know the constant flux level of some of the narrow lines.
c Here I convert that flux into a fraction of the total flux
c to be used by the fitter.
c I happen to know that the flux for the narrow_he2.imh line should
c be around 1.4055E-13. With this and the totalo from above, I can
c calculate the actual value for the scale factor for it.
        IUE
ptau(12) = 1.4055e-13 / (totalo*dlam)
ploer(12) = 0.
puper(12) = 0.
c Similarly, the median value for the c4_1549_obs2 should be around
c 5.134e-13.
       IUE
ptau(8) = 5.134e-13 / (totalo*dlam)
ploer(8) = 0.
puper(8) = 0.
c And finally, the median for o3-1665
ptau(10) = 1.04e-13 / (totalo*dlam)
ploer(10) = ptau(10) *0.05
puper(10) = ptau(10) * 5.0
c Now to tie some wavelengths together. You will also need to change some
c things in the subroutine to make this ok.
c C IV BLR
```

```
ptau(5) = ptau(1) - 90.27
ploer(5) = 0.
puper(5) = 0.
c C IV NLR
ptau(7) = ptau(1) - 89.85
ploer(7) = 0.
puper(7) = 0.
c O III 1663 NLR
ptau(9) = ptau(1) + 22.75
ploer(9) = 0.
puper(9) = 0.
c O III 1663 BLR
ptau(13) = ptau(1) + 22.75
ploer(13) = 0.
puper(13) = 0.
c He II NLR
ptau(11) = ptau(1)
ploer(11) = 0.
puper(11) = 0.
C ***********
c SMOOTHING, from Neelam and Baldwin. Even numbers break this. Don't use
c them. It will make chisq artifically small.
do iwin=1,wcount
  do i=1,nx
if(waves(i).lt.wstart(iwin)) istart=i
if(waves(i).lt.wstop(iwin)) istop=i
  enddo
   istart=min(istart,nx)
   istop=min(istop,nx)
          xsig=0.
  do i=istart, istop
   nsm=min(nsmooth(iwin),2*(nx-i)+1)
           do j=i-nsm/2, i+nsm/2
```

```
sum=sum+obj(j)
            enddo
           wdiff=obj(i)-sum/nsm
           xsig=xsig+(wdiff*wdiff)
          enddo
           if(istart.lt.istop) then
      wsig(iwin)=sqrt(xsig/(istop-istart))
   else
      wsig(iwin)=sum/nsm
   end if
   wsig(iwin) = 0.5e-14
        enddo
C **************
c read in the blend component spectra
c The continuum (a power law) will be built in the subroutine uvfunk.
do i=1,ncomps
  call t6in(oname(i),nxc(i),xlamc(i),dlamc(i),id,xinput(1,i),nmax)
  totalc(i)=0.
    do k=1,nxc(i)
      totalc(i)=totalc(i)+xinput(k,i)
end do
do i=1,nx
  blend(i)=0.
end do
nb0=nmax
nbx=0
C ************
c Set up minuit to do it's thing.
* Set-up parameters for minuit (aka unit numbers for input,output)
        call mninit(5,6,7)
* Set the initial values of the adjustable parameters (aka the "x")
        in function fcn. Let MINUIT know about those parameters attributes
 do ip=1,npar
  zero=0.
  call mnparm(ip,plabel(ip),ptau(ip),pincr(ip),ploer(ip),
         puper(ip),ierflg)
  if (ierflg.ne.0) write(*,*) 'Par: ',ip,' not entered sucessfully'
end do
111111111111111111111111111111111111
```

```
c Here is where I set some of the parameters to be constant, so that
c minuit does not adjust them.
arglis(1) = 12
call mnexcm(uvfunk,'FIX',arglis,1,ierflg,0)
arglis(1) = 8
call mnexcm(uvfunk, 'FIX', arglis, 1, ierflg, 0)
arglis(1) = 10
call mnexcm(uvfunk,'FIX',arglis,1,ierflg,0)
arglis(1) = 5
call mnexcm(uvfunk, 'FIX', arglis, 1, ierflg, 0)
arglis(1) = 7
call mnexcm(uvfunk, 'FIX', arglis, 1, ierflg, 0)
arglis(1) = 9
call mnexcm(uvfunk, 'FIX', arglis, 1, ierflg, 0)
arglis(1) = 13
call mnexcm(uvfunk, 'FIX', arglis, 1, ierflg, 0)
arglis(1) = 11
call mnexcm(uvfunk,'FIX',arglis,1,ierflg,0)
* These set the strategies by which Minuit work, higher is more
        "accurate" but more costly in time (see p.24 in MINUIT Ref man
        v94.1). I think this call is optional
arglis(1)=2.
        call mnexcm(uvfunk,'SET STR',arglis,1,ierflg,0)
        Stuff for accurate error analysis, see p.22, optional also I think
arglis(1)=1.
call mnexcm(uvfunk,'SET ERR',arglis,1,ierflg,0)
        Supress warnings.
arglis(1)=1.
call mnexcm(uvfunk,'SET NOW', arglis, 1, ierflg, 0)
        Sets level of printout detail. -1 is minimum, 3 is highest.
arglis(1)=-1.
call mnexcm(uvfunk,'SET PRI',arglis,1,ierflg,0)
        Now use Minimize the minimize the value of the function
        set the max number of iterations with arglis(1) and
С
        the precision required in arglis(2).
```

```
arglis(1)=50000.
arglis(2)=1.e-20
call mnexcm(uvfunk,'MIGRAD',arglis,2,ierflg,0)
C **************
       Assuming convergence after <50000 iterations print out
       the current value of the function. Store the values in the
       array fitout.
write(*,*) "-----"
write(*,*) "Results for ",objfile
write(*,*) ""
       do ip=1,npar
  call mnpout(ip,junk,ftau,err,eplus,eminus,ivarbl)
  write(*,*)ip,' ',plabel(ip),' Orig: ',ptau(ip),' Final:',ftau,err
  fitout(ip) = ftau
  errout(ip) = err
       end do
fitout(5) = fitout(1) - 90.27
fitout(7) = fitout(1) - 89.85
fitout(9) = fitout(1) + 22.76
fitout(13) = fitout(1) + 22.76
fitout(11) = fitout(1)
С
       This gets the current status of minimization. Since we are
       'done', this should be the final value of our minimized
С
C
       function. These parameters are, in order: (1) minimum value
       (2) estimated vertical distance to the minimum (3) the value of
С
       parameter uncertainities (4) # of currently variable parameters
       (5) the highest external parameter number defined by the user
С
       (6) that status of the covariance matrix. See page 16 of
С
       minuit manual.
call mnstat(chiout(1),chiout(2),chiout(3),chiout(4),chiout(5)
    1 ,chistat)
idof = totcount - ((ncomps+2) - 4)
write(*,*) "REDUCED CHISQ = ",chiout(1)/idof
write(*,*) "FMIN = ",chiout(1)
write(*,*) "FEDM = ",chiout(2)
write(*,*) "ERRDEF = ",chiout(3)
write(*,*) "NPARI = ",chiout(4)
write(*,*) "NPARX = ",chiout(5)
write(*,*) "ISTAT = ",chiout(6)
write(*,*) "xhigh = ",xhigh
write(*,*) "yhigh = ",yhigh
```

```
write(*.*) "-----"
C *************
       Output the values to a file. In this case, the file is called
       'slope.txt' (for historical reasons) and contains:
glob = objfile
31 format(a8,1x,E12.6,1x,f8.5,1x,f8.5,1x,f9.5)
write (89,*) glob, chiout(1)/idof, fitout
write (90,*) glob, chiout(1)/idof, errout
write (81,*) glob, chiout(1)/idof
write (88,*) glob, xhigh, yhigh
C ************
20 format(i2,1x,a20,2(0pf9.3),f7.3, 1pe10.2,1x,0pf7.3)
30 format(a20,2(0pf9.3),f7.3, 1pe10.2,1x,0pf7.3)
C *************
c Here, we convert the fractions to flux values for the even parameters
do ip = 1, ncomps
  fitout(2*ip) = fitout(2*ip) * totalo * dlam
  errout(2*ip) = errout(2*ip) * totalo * dlam
end do
c This is where we calculate the flux for the continuum. There is a
c a problem with using this method if your spectra are not all the same
c wavelength range. Trim your spectra or use a different method. I think
c I may put some code here to take the "continuum" between a specific
c wavelength range. It will still use the powerlaw that we fit, but it
c would only keep the flux within a certain range.
c I feel that the correct approach might be to re-evaluate the continuum
c flux from the fitted parameters, integrating over a user specified range
c and then do the calculation again with the parameters slewed to their error
c limits to calculate the error in the flux.
ip = (2*ncomps)+3
c Here we open up the input file where the user has specified
c the window to use for the continuum. If the read fails in any
c way (for instance there isn't a file there or it only contains
c one number) we will notice and default to using the whole
c spectral range.
c NOTE: This 'conwin.in' part is no longer used. We calculate
c the continuum at a specific point.
```

```
open (40,file='conwin.in',status='unknown')
read (40,*,IOSTAT=iof40) cstart,cstop
if (iof40.ne.0) then
   cstart = xlamc(ncomps+1)
   cstop = xlamc(ncomps+1) + (dlam * nx)
endif
close (40)
c As a test, let's make the starting and ending wavelengths the
c full range for the spectrum.
write (*,*) "Range = ",cstart," - ",cstop
fitout(ip) = 0.
conerr = 0.
ag(1) = 0.
ag(2) = 0.
ag(3) = 0.
ag(4) = 0.
c Find the flux value at 1337.
fitout(ip) = fitout(2*ncomps+1) * (1337./5600.)**(fitout(2*ncomps+2))
c Calculate the four corners
   ag(1) = ag(1) + ((fitout(2*ncomps+1)+errout(2*ncomps+1)) *
     c ((1840./5600.)**(fitout(2*ncomps+2)+errout(2*ncomps+2))))
   ag(2) = ag(2) + ((fitout(2*ncomps+1)-errout(2*ncomps+1)) *
     c ((1840./5600.)**(fitout(2*ncomps+2)+errout(2*ncomps+2))))
   ag(3) = ag(3) + ((fitout(2*ncomps+1)-errout(2*ncomps+1)) *
     c ((1840./5600.)**(fitout(2*ncomps+2)-errout(2*ncomps+2))))
   ag(4) = ag(4) + ((fitout(2*ncomps+1)+errout(2*ncomps+1)) *
     c ((1840./5600.)**(fitout(2*ncomps+2)-errout(2*ncomps+2))))
c Now find the high and low, and subtract them.
elow = 9999.
ehigh = -9999.
do ii=1,4
   if (ag(ii).gt.ehigh) then
      ehigh = ag(ii)
   if (ag(ii).lt.elow) then
```

```
elow = ag(ii)
   endif
enddo
errout(ip) = dlam * abs(ehigh - elow)
write (*,*) "New con = ",fitout(ip)
write(*,*)conerr,fitout(ncomps+1),fitout(ncomps+2)
c Write out the values using fluxes instead of fractions.
write (71,*) glob,chiout(1)/idof,fitout
write (72,*) glob,chiout(1)/idof,errout
C WRITE OUT THE BLENDED SPECTRUM.
call t6out('blends.fit',nx,xlam0,dlam,blend)
do i=1,nx
  diff(i)=obj(i)-blend(i)
end do
call t6out('blends.diff',nx,xlam0,dlam,diff)
C ***********
c Let's make a plot of the output.
   pxmin = 1443.
  pxmax = 1750.
  pymin = -5.e-14
  pymax = 1.e-13
c This makes it not ask to continue when you end it.
        call pgask(.false.)
c Change window size.
CALL PGENV(pxmin,pxmax,pymin,pymax,0,1)
c Labels for the graph. X, Y, Title. In this case
c I have left the title off and used the Baldwin Plot
c Label System (BPLS).
CALL PGLAB('wavelength', 'flux','')
c Change font size for BPLS, then label, then change it back.
call pgsch(3.)
call pgtext(pxmin+10.,pymin+0.9*(pymax-pymin),irafname)
call pgsch(1.)
call pgtext(pxmin+10.,pymin,"residual")
c Here we plot the actual graph. # pts, xarray, yarray, symbol
c The first call sets the line style.
```

```
call pgsls(1)
call pgline(nx,dxval,dyval)
call pgline(nx,dxval,blend)
call pgline(nx,dxval,diff)
c These make the empty rectangle and the crosshatching in the
c test ranges.
call PGSHS (0., 5., 0.)
CALL PGSFS(3)
wtest = 1
do while (wtest.le.wcount)
   call pgrect(wstart(wtest), wstop(wtest), pymin, pymax)
   wtest = wtest + 1
enddo
CALL PGSFS(2)
wtest = 1
do while (wtest.le.wcount)
   call pgrect(wstart(wtest), wstop(wtest), pymin, pymax)
   wtest = wtest + 1
enddo
C *************
c This will reset out wnew and area back to our inputs from the blends.in.
c If you want your fit to continue to evolve, that is if you want the new
c starting values to be the last ending values, comment this line out.
        do n=1,ncomps,1
           wnew(n) = wkeep(n)
           area(n) = akeep(n)
        enddo
c Grab the next value from our input. The while loop
c will test to see if we are done.
read(21,*,IOSTAT=iof2) objfile
enddo
close(71)
close(72)
close(81)
close(88)
close(89)
close(90)
   call pgend
end
```

APPENDIX D: CODE FOR UVFUNK.F

This is the uvfunk.f subroutine. It is called by the UV fitter, uvcontin.f.

```
subroutine uvfunk(npar,grad,fval,xval,iflag,futil)
 double precision fval,xval(*)
 double precision stuff, crap, m, b
 double precision PI, BIGX, SIG, i, x, chi, AMP
 double precision AMP2, BIGX2, SIG2
 double precision grad, futil
 double precision sdev, total, keepme
 real yave, average, stdev, chisq, xgauss
 real armin, armax
 integer count, n, npar, if lag, count1, count2, count3
 integer icomp, ibb
 logical lratio, lprint, slide, wfix
 double precision XX(5000), YY(5000)
 real dxval(5000), dyval(5000)
 real prix(5000),priy(5000),xbar,sigx
 real wstart(30), wstop(30), wsig(30), woff(30)
 real ybar, sigy, ydev, yhigh, xhigh
 real sdx(5000),spx(5000),sdy(5000),spy(5000)
 integer NNX, lcount, wtest, wcount, ns
 integer totcount
 double precision scale
 common /myscale/ scale
 common /mydata/ dxval,dyval,nnx,wstart,wstop,wcount,
c ncomps, totalo, totcount, wsig, woff, yhigh, xhigh
 common /pridata/ prix,priy,lcount,xbar,sigx,blend
parameter (nmax=50000)
 common diff(nmax), xinput(nmax, 30), shift(nmax),
c oname(30), wold(30), wnew(30), area(30), nxc(30),
c xlamc(30),dlamc(30),totalc(30),nx,xlam0,dlam
 character*50 oname, objfile
 dimension obj(nmax),blend(nmax),ratio(nmax),id(100)
```

```
open (36, file='gauss.test', status='unknown')
      write(36.*) xval(4).xval(5).xval(6)
do i=1.nx
  blend(i)=0.
end do
c Here we need to hand the values back from the xval array to the
c variables that are used in the blends routines.
c NOTE: This is a dangerous side effect of using the "align" subroutine.
c We are writing over the wnew and area arrays each time. This means that we
c can slowly move the acceptable ranges as we fit more spectra.
c I will take steps to keep this from happening in the main program.
        ibb = 0
        do n=1,ncomps,1
           ibb = ibb + 1
           wnew(n) = xval(ibb)
           ibb = ibb + 1
           area(n) = xval(ibb)
        enddo
!!!!!!!!!!!!!!!!!!!!!!!!!!!!!!!!!!!!!
        wnew(5) = wnew(1) - 90.27
        wnew(7) = wnew(1) - 89.85
        wnew(9) = wnew(1) + 22.76
        wnew(13) = wnew(1) + 22.76
        wnew(11) = wnew(1)
1111111111111111111111111111111111
c Now for the continuum.
C The y values need to go into the array xinput(XXX,1), I think.
      oname(ncomps+1) = "continuum"
c This is the array size, it is equal to the number of points
c in the wavelength space.
         nxc(ncomps+1) = nnx
c This is the starting wavelength, this is the same as the
c data starting wavelength, xlam0
      xlamc(ncomps+1) = xlam0
c This is the wavelength step, should pass from main program.
      dlamc(ncomps+1) = dlam
c I have no clue what this is. Let's make it 1.
      id(ncomps+1) = ncomps + 1
c These are the y values. Here is where I should calcluate them.
      totalc(ncomps+1) = 0.
      do i=1,nnx
```

```
xinput(i,ncomps+1) = (xval((2*ncomps)+1) *
     c ((dxval(i)/5600.)** xval((2*ncomps)+2)))
         totalc(ncomps+1) = totalc(ncomps+1) + xinput(i,ncomps+1)
         keepme = dxval(i)
      enddo
c This is the starting wavelength again. You will just have
c to trust me.
      wold(ncomps+1) = xlam0
c This is the new wavelength to shift to. I suspect we should
c also keep this the same always.
      wnew(ncomps+1) = xlam0
c This is the area, it will be used as a scaling factor.
       area(ncomps+1) = xval((2*ncomps)+3)
      area(ncomps+1) = totalc(ncomps+1)/totalo
C Now for the align call.
c Slide should be set to false.
      slide = .false.
do icomp=1,ncomps
  call align(icomp,nout0,noutx,slide)
  scale=area(icomp)*totalo/totalc(icomp)
 do i=1,nx
    blend(i)=blend(i)+shift(i)*scale
  end do
 nb0=min(nb0,nout0)
 nbx=max(nbx,noutx)
 fluxc=area(icomp)*totalo*dlam
      enddo
c Adding in the continuum.
      do i=1,nx
         blend(i) = blend(i) + xinput(i,ncomps+1)
      enddo
c Now to calculate the values to minimize
         chi = 0.
         sdev = 0.1
         totcount = 0
         xhigh = 0.
         yhigh = 0.
         wtest = 1
```

```
do while (wtest.le.wcount)
            n = 1
            count1 = 0
            do while (n.le.nnx)
               if (dxval(n).ge.wstart(wtest).and.
                   dxval(n).le.wstop(wtest)) then
     С
                  count1 = count1 + 1
                  sdx(count1) = dxval(n)
                  sdy(count1) = dyval(n)
                  spx(count1) = dxval(n)
                  spy(count1) = blend(n)
                  if (dyval(n).gt.yhigh) then
                     xhigh = dxval(n)
                     yhigh = dyval(n)
                  endif
               endif
               n = n + 1
            enddo
      Only do the rest if our spectrum contained this window.
С
            if (count1.gt.0) then
            ydev = wsig(wtest)
            ns = 1
            do while (ns.le.count1)
               chi = chi + chisq(sdy(ns),spy(ns),ydev)
               ns = ns + 1
            totcount = totcount + 1
            enddo
            endif
c Move to the next test region.
            wtest = wtest + 1
         enddo
         close(36)
      fval = chi
      return
      end
```

APPENDIX E: CODE FOR FUNCTIONS.F

The following are some useful function that are called by the fitting code.

```
c -----
c Function to calculate a value in a gaussian.
c I will make this more generic later.
double precision function xgauss(AMP,BIGX,SIG,x)
c real function xgauss(AMP,BIGX,SIG,x)
implicit none
double precision AMP, BIGX, SIG
real X
c real AMP, BIGX, SIG, X
c gauss = AMP * \exp(-((x - BIGX)**2)/(2.*(SIG**2)))
       xval(4) * exp(-((dxval(i) - xval(5))**2)/(2.*(xval(6)**2)))
        xgauss = SIG
        xgauss = (2.*(SIG**2))
С
        xgauss = (((x - BIGX)**2)/(2.*(SIG**2)))
       xgauss = AMP * exp(-((x - BIGX)**2)/(2.*(SIG**2)))
c write (*,*) xgauss
return
end
c Function to calculate the current part of the chi^2
c sum. This is NOT the entire chi^2, although I may make one
c that handles an array. In this case, B is the value
c you have more confidence it (you divide by B).
c double precision function chisq(A,B,sdev)
real function chisq(A,B,sdev)
implicit none
c double precision A,B,sdev
real A,B,sdev
c chisq = ((dabs(A - B))**2.) / (sdev**2.)
```

```
chisq = ((abs(A - B))**2.) / (sdev**2.)
return
end
C -----
c Function to calculate the average value in an
c array. Pass it the array and the length of the
c array.
c double precision function average(YY,n)
real function average(YY,n)
implicit none
c double precision YY(*),total
real YY(*),total
integer n, i
total = 0.0
do 10 i = 1, n
   total = total + YY(i)
 10 continue
average = total / (dble(float(n)))
return
end
c Function to calculate the stdev value in an
c array. Pass it the array, the length of the
c array, and the average value of the array.
c NOTE TO SELF: REWRITE SO THAT IT WILL CALL
C FOR THE AVERAGE USING THE ABOVE FUNCTION?
c double precision function stdev(YY,n,ave)
real function stdev(YY,n,ave)
implicit none
c double precision YY(*),total,ave
real YY(*),total,ave
integer n, i
total = 0.0
```

```
do 10 i = 1,n
  total = total + ((YY(n) - ave)**2)
 10 continue
stdev = dsqrt((1.0/(dble(float(n))-1.0)) * total)
return
end
c ------
c Function to find the minium of an array.
c Pass it the array and the length of the array.
real function armin(YY,n)
implicit none
real YY(*),min
integer n,i
min = YY(1)
do 10 i=2,n
  if (YY(i).lt.min) then
     min = YY(i)
     endif
10 continue
  armin = min
  return
  end
C -----
c Function to find the maximum of an array.
c Pass it the array and the length of the array.
real function armax(YY,n)
implicit none
real YY(*),max
integer n,i
max = YY(1)
do 10 i=2,n
  if (YY(i).gt.max) then
     max = YY(i)
     endif
```

```
10
      continue
   armax = max
   return
   end
C -----
c Function to make a not-so-random number
c This routine is not really random. Use the next
c one instead.
real function random(seed,randx)
integer seed
real randx
seed = 2045 * seed + 1
seed = seed - (seed/1048576)*1048576
randx = real(seed+1)/1048577.0
return
end
C-----
c This one actually makes a decent random number.
c You need to initialize it with a seed. Thereafer
c call it with the same value (1) to get a random
c number. This is taken from Numerical Recipies in
c FORTRAN, 2nd edition, page 272
     FUNCTION ran2(idum)
     INTEGER idum, IM1, IM2, IMM1, IA1, IA2, IQ1, IQ2, IR1, IR2, NTAB, NDIV, idum3
     REAL ran2, AM, EPS, RNMX
     PARAMETER (IM1=2147483563, IM2=2147483399, AM=1./IM1, IMM1=IM1-1,
          IA1=40014, IA2=40692, IQ1=53668, IQ2=52774, IR1=12211,
    С
          IR2=3791, NTAB=32, NDIV=1+IMM1/NTAB, EPS=1.2e-7, RNMX=1.-EPS)
     INTEGER idum2,j,k,iv(NTAB),iy
     SAVE iv, iy, idum2
     DATA idum2/123456789/,iv/NTAB*0/,iy/0/
     idum3=idum
     if (idum3.le.0) then
        idum3=max(-idum3,1)
        idum2=idum3
        do 11 j=NTAB+8,1,-1
           k=idum3/IQ1
```

```
idum3=IA1*(idum3-k*IQ1)-k*IR1
            if(idum3.lt.0) idum3=idum3+IM1
            if (j.le.NTAB) iv(j)=idum3
 11
         enddo
         iy=iv(1)
      endif
      k=idum3/IQ1
      idum3=IA1*(idum3-k*IQ1)-k*IR1
      if (idum3.lt.0) idum3=idum3+IM1
      k=idum2/I02
      idum2=IA2*(idum2-k*IQ2)-k*IR2
      if (idum2.lt.0) idum2=idum2+IM2
      j=1+iy/NDIV
      iy=iv(j)-idum2
      iv(j)=idum3
      if (iy.lt.1) iy=iy+IMM1
      ran2=min(AM*iy,RNMX)
      return
      END
c The following are functions that were developed by
c Dr. Jack Baldwin. (And possibly Dr. Brian Sharpee.)
subroutine align(icomp,nout0,noutx)
c sets up call to XPAND subroutine.
parameter (nmax=50000)
common diff(nmax), xinput(nmax, 30), shift(nmax),
          oname(30), wold(30), wnew(30), area(30), nxc(30),
     x
          xlamc(30),dlamc(30),totalc(30),nx,xlam0,dlam
character*50 oname
do i=1,nx
shift(i)=0.
end do
ilenb=nmax
xlamj=xlam0
dlamj=dlam
xlami=xlamc(icomp)
dlami=dlamc(icomp)
i=icomp
```

```
c IF (SLIDE) THEN
c DX=DLAMJ/DLAMI
c CXJ=(XLAMI-XLAMJ+WNEW(I)-WOLD(I)+.5*(dlamj-dlami))/DLAMJ
c ELSE
c write(*.*)" "
c write(*,*)"WOLD(I), DLAMJ, WNEW(I), DLAMI"
c write(*,*) WOLD(I),DLAMJ,WNEW(I),DLAMI
c write(*,*) " "
DX=WOLD(I)*DLAMJ/(WNEW(I)*DLAMI)
c write (*,*) "dx = ",DX
CXJ=((XLAMI-.5*dlami)*WNEW(I)/WOLD(I)-XLAMJ)/DLAMJ+1.5
c write (*,*) "CXJ = ",CXJ
        CXI=1.
        NCI=nxc(i)
        IF (CXJ.GE.1.) GOTO 7300
        CXI=1.-(CXJ-1.)*DX
        CXJ=1.
        NCI=NCI-CXI+1
7300 IF (CXI+NCI.LT.ILENB-1.) GOTO 7800
       NCI=ILENB-1.-CXI
7800
       continue
c write (*,*) "CXJ = ",CXJ
c write (*,*) " "
c write (*,*) xinput(1,icomp),ilenb,CXJ,CXI,NCI,DX,noutx
CALL XPAND(xinput(1,icomp),shift,ilenb,CXJ,CXI,NCI,DX,noutx)
c write (*,*) "shift(1) = ",shift(1)
c write(*,*) 'cxj,cxi,nci,dx,noutx,xlami,xlamj',
           cxj,cxi,nci,dx,noutx,xlami,xlamj
nout0=cxj
return
end
       SUBROUTINE XPAND(bufi, bufj, ilenb, CXJ, CXI, NCI, DX, jstop)
C LINEAR SCRUNCH FROM bufi TO bufj.
c also returns jstop=last pixel filled in output buffer
c NOTE TO SELF: I THINK THAT THIS ROUTINE IS STILL RETURNING
C ODD VALUES, NEED TO DIG DEEPER.
```

```
dimension bufi(1), bufj(1)
c write(*,*) 'XPAND cxj,cxi,nci,dx',cxj,cxi,nci,dx
        NCIX=NCI
        IF (CXI+NCI.GE.ILENB) NCIX=ILENB-.1-CXI
        JCH=CXJ+1
        IF (AINT(CXJ).EQ.CXJ) JCH=CXJ
        JSTOP=CXJ+NCIX/DX-1.
        IF (JSTOP.GT.ILENB-1) JSTOP=ILENB-1
        CX2=CXI+(JCH-CXJ)*DX
        IX2=CX2
        REM=(1.-AMOD(CX2,1.))*bufi(IX2)
3000
        CX1=CX2
        CX2=CX1+DX
        ICX1=IFIX(CX1)+1
        ICX2=CX2
        SUM=REM
        IF (ICX2-ICX1) 3800,3600,3600
3600
        I=ICX1
3700
        SUM=SUM+bufi(I)
        I=I+1
        IF (I-ICX2) 3700,3700,3800
        REM=(FLOAT(ICX2+1)-CX2)*bufi(ICX2)
3800
c write (*,*) 'Prepare to die.'
        bufj(JCH)=(SUM-REM)
        JCH=JCH+1
        IF (JCH-JSTOP) 3000,3000,4000
4000
        RETURN
      END
```

APPENDIX F: TEMPLATE PROFILES

This chapter contains table formatted versions of the template profiles that were used in this study

Table F.1: C IV BELR Template - c4_blr_smooth

Wavelength	Flux
1486.46997070313	9.555542E-16
1488.43620073796	7.878893E-16
1490.40243077279	1.085533E-15
1492.36866080761	1.811270E-15
1494.33489084244	2.411968E-15
1496.30112087727	2.109406E-15
1498.2673509121	1.793699E-15
1500.23358094693	1.600550E-15
1502.19981098176	1.742496E-15
1504.16604101658	1.455960E-15
1506.13227105141	1.755119E-15
1508.09850108624	2.651444E-15
1510.06473112107	3.796852E-15
1512.0309611559	4.689520E-15
1513.99719119072	5.576753E-15
1515.96342122555	5.796336E-15
1517.92965126038	5.428699E-15
1519.89588129521	4.965610E-15
1521.86211133004	5.013607E-15
1523.82834136487	6.108739E-15
1525.79457139969	8.075923E-15
1527.76080143452	9.815303E-15
1529.72703146935	1.116838E-14
1531.69326150418	1.146565E-14
1533.65949153901	1.277366E-14
1535.62572157383	1.491611E-14
1537.59195160866	1.740484E-14
1539.55818164349	1.939291E-14
1541.52441167832	2.040391E-14

Table F.1: C IV BELR Template (continued)

Wavelength	Flux
1543.49064171315	2.098864E-14
1545.45687174798	2.120340E-14
1547.4231017828	2.249443E-14
1549.38933181763	2.318910E-14
1551.35556185246	2.252947E-14
1553.32179188729	2.163747E-14
1555.28802192212	2.057907E-14
1557.25425195694	1.949838E-14
1559.22048199177	1.773638E-14
1561.1867120266	1.557651E-14
1563.15294206143	1.452734E-14
1565.11917209626	1.234087E-14
1567.08540213109	1.079152E-14
1569.05163216591	9.238349E-15
1571.01786220074	8.286056E-15
1572.98409223557	7.320719E-15
1574.9503222704	6.000376E-15
1576.91655230523	4.954878E-15
1578.88278234005	3.547751E-15
1580.84901237488	2.745185E-15
1582.81524240971	2.272479E-15
1584.78147244454	2.485506E-15
1586.74770247937	2.795652E-15
1588.7139325142	2.071041E-15
1590.68016254902	1.329357E-15
1592.64639258385	7.451243E-16
1594.61262261868	1.399852E-15

Table F.2: He II BELR Template - smooth_4686

Wavelength	Flux
4474.65771484375	-2.226108E-20
4476.62394487858	4.524233E-18
4478.59017491341	1.649479E-17
4480.55640494823	2.093099E-17
4482.52263498306	2.183218E-17
4484.48886501789	1.529701E-17
4486.45509505272	1.689205E-17
4488.42132508755	1.888768E-17
4490.38755512238	1.936672E-17
4492.3537851572	1.720526E-17
4494.32001519203	1.499648E-17

Table F.2: He II BELR Template (continued)

Wavelength	Flux
4496.28624522686	1.495106E-17
4498.25247526169	1.766637E-17
4500.21870529652	2.027571E-17
4502.18493533134	2.271065E-17
4504.15116536617	2.647071E-17
4506.117395401	3.023264E-17
4508.08362543583	3.306995E-17
4510.04985547066	3.657374E-17
4512.01608550549	4.009806E-17
4513.98231554031	4.391710E-17
4515.94854557514	4.984802E-17
4517.91477560997	5.583877E-17
4519.8810056448	6.007345E-17
4521.84723567963	6.353339E-17
4523.81346571446	6.812777E-17
4525.77969574928	7.329635E-17
4527.74592578411	7.865452E-17
4529.71215581894	8.631378E-17
4531.67838585377	9.506347E-17
4533.6446158886	1.046404E-16
4535.61084592342	1.153526E-16
4537.57707595825	1.233549E-16
4539.54330599308	1.299636E-16
4541.50953602791	1.371751E-16
4543.47576606274	1.438533E-16
4545.44199609756	1.487064E-16
4547.40822613239	1.518830E-16
4549.37445616722	1.548249E-16
4551.34068620205	1.561565E-16
4553.30691623688	1.561655E-16
4555.27314627171	1.557713E-16
4557.23937630653	1.554378E-16
4559.20560634136	1.561853E-16
4561.17183637619	1.574520E-16
4563.13806641102	1.597001E-16
4565.10429644585	1.625481E-16
4567.07052648068	1.676775E-16
4569.0367565155	1.755404E-16
4571.00298655033	1.840473E-16
4572.96921658516	1.918970E-16
4574.93544661999	1.988599E-16
4576.90167665482	2.063728E-16
4578.86790668964	2.157849E-16 2.239470E-16
4580.83413672447	
4582.8003667593	2.312843E-16

Table F.2: He II BELR Template (continued)

Wavelength	Flux
4584.76659679413	2.384045E-16
4586.73282682896	2.459172E-16
4588.69905686378	2.521743E-16
4590.66528689861	2.573554E-16
4592.63151693344	2.610859E-16
4594.59774696827	2.646214E-16
4596.5639770031	2.690273E-16
4598.53020703793	2.717301E-16
4600.49643707275	2.728816E-16
4602.46266710758	2.787224E-16
4604.42889714241	2.867272E-16
4606.39512717724	2.935437E-16
4608.36135721207	2.989477E-16
4610.32758724689	3.032740E-16
4612.29381728172	3.077107E-16
4614.26004731655	3.143824E-16
4616.22627735138	3.227494E-16
4618.19250738621	
	3.289767E-16
4620.15873742104	3.334984E-16
4622.12496745586	3.372909E-16 3.379981E-16
4624.09119749069	
4626.05742752552	3.371117E-16
4628.02365756035	3.371088E-16
4629.98988759518	3.377916E-16
4631.95611763001	3.391300E-16
4633.92234766483	3.405739E-16
4635.88857769966	3.409171E-16
4637.85480773449	3.391662E-16
4639.82103776932	3.396290E-16
4641.78726780415	3.419186E-16
4643.75349783897	3.428730E-16
4645.7197278738	3.439865E-16
4647.68595790863	3.459071E-16
4649.65218794346	3.469655E-16
4651.61841797829	3.483239E-16
4653.58464801311	3.522086E-16
4655.55087804794	3.545163E-16
4657.51710808277	3.554608E-16
4659.4833381176	3.582956E-16
4661.44956815243	3.596801E-16
4663.41579818726	3.600871E-16
4665.38202822208	3.604621E-16
4667.34825825691	3.590709E-16
4669.31448829174	3.560959E-16
4671.28071832657	3.531387E-16

Table F.2: He II BELR Template (continued)

Wavelength	Flux
4673.2469483614	3.479621E-16
4675.21317839623	3.395000E-16
4677.17940843105	3.321598E-16
4679.14563846588	3.261837E-16
4681.11186850071	3.217771E-16
4683.07809853554	3.182733E-16
4685.04432857037	3.149227E-16
4687.01055860519	3.122995E-16
4688.97678864002	3.091749E-16
4690.94301867485	3.057804E-16
4692.90924870968	3.031961E-16
4694.87547874451	3.018968E-16
4696.84170877934	2.990091E-16
4698.80793881416	2.948490E-16
4700.77416884899	2.903954E-16
4702.74039888382	2.823232E-16
4704.70662891865	2.745228E-16
4706.67285895348	2.686461E-16
4708.6390889883	2.626774E-16
4710.60531902313	2.583398E-16
4712.57154905796	2.558496E-16
4714.53777909279	2.513373E-16
4716.50400912762	2.452573E-16
4718.47023916245	2.418306E-16
4720.43646919727	2.419612E-16
4722.4026992321	2.429396E-16
4724.36892926693	2.432827E-16
4726.33515930176	2.414252E-16
4728.30138933659	2.359441E-16
4730.26761937141	2.305466E-16
4732.23384940624	2.258931E-16
4734.20007944107	2.217075E-16
4736.1663094759	2.184997E-16
4738.13253951073	2.162233E-16
4740.09876954556	2.150377E-16
4742.06499958038	2.115558E-16
4744.03122961521	2.063860E-16
4745.99745965004	2.011232E-16
4747.96368968487	1.970393E-16
4749.9299197197	1.968767E-16
4751.89614975452	1.978460E-16
4753.86237978935	1.979965E-16
4755.82860982418	1.982249E-16
4757.79483985901	1.994668E-16
4759.76106989384	2.002487E-16

Table F.2: He II BELR Template (continued)

227. 24.4	
Wavelength	Flux
4761.72729992867	1.989347E-16
4763.69352996349	1.986144E-16
4765.65975999832	1.986824E-16
4767.62599003315	2.007840E-16
4769.59222006798	2.038013E-16
4771.55845010281	2.055911E-16
4773.52468013764	2.079819E-16
4775.49091017246	2.109205E-16
4777.45714020729	2.125124E-16
4779.42337024212	2.124999E-16
4781.38960027695	2.129367E-16
4783.35583031178	2.137377E-16
4785.3220603466	2.133939E-16
4787.28829038143	2.120735E-16
4789.25452041626	2.087943E-16
4791.22075045109	2.045651E-16
4793.18698048592	2.007191E-16
4795.15321052075	1.936779E-16
4797.11944055557	1.851315E-16
4799.0856705904	1.760814E-16
4801.05190062523	1.662250E-16
4803.01813066006	1.559882E-16
4804.98436069489	1.443273E-16
4806.95059072971	1.314655E-16
4808.91682076454	1.200364E-16
4810.88305079937	1.107629E-16
4812.8492808342	1.035315E-16
4814.81551086903	9.607090E-17
4816.78174090386	8.986784E-17
4818.74797093868	8.399395E-17
4820.71420097351	7.803100E-17
4822.68043100834	7.272366E-17
4824.64666104317	6.623011E-17
4826.612891078	6.150891E-17
4828.57912111282	5.820838E-17
4830.54535114765	5.501518E-17
4832.51158118248	5.234666E-17
4834.47781121731	5.102761E-17
4836.44404125214	5.060465E-17
4838.41027128696	4.909309E-17
4840.37650132179	4.514991E-17
4842.34273135662	4.132433E-17
4844.30896139145	4.860989E-17
4846.27519142628	5.703022E-17
4848.24142146111	5.280361E-17

Table F.2: He II BELR Template (continued)

Wavelength	Flux
4850.20765149593	3.763022E-17
4852.17388153076	1.218048E-17
4854.14011156559	-1.475658E-17

Table F.3: He I BELR Template - $smooth_5876$

Wavelength	Flux
5711.41650390625	1.798370E-17
5713.38273394108	2.056418E-17
5715.34896397591	2.450033E-17
5717.31519401074	1.889557E-17
5719.28142404556	1.191293E-17
5721.24765408039	3.978324E-18
5723.21388411522	4.286419E-18
5725.18011415005	4.278359E-18
5727.14634418488	2.730118E-18
5729.1125742197	1.735316E-18
5731.07880425453	2.635988E-18
5733.04503428936	3.759410E-18
5735.01126432419	4.240993E-18
5736.97749435902	6.857291E-18
5738.94372439385	1.196061E-17
5740.90995442867	1.663132E-17
5742.8761844635	1.859282E-17
5744.84241449833	1.743692E-17
5746.80864453316	1.718315E-17
5748.77487456799	2.017405E-17
5750.74110460282	2.308250E-17
5752.70733463764	2.502209E-17
5754.67356467247	2.959958E-17
5756.6397947073	3.541167E-17
5758.60602474213	3.843989E-17
5760.57225477695	3.954854E-17
5762.53848481178	4.035626E-17
5764.50471484661	4.345871E-17
5766.47094488144	5.037816E-17
5768.43717491627	5.675592E-17
5770.4034049511	6.044200E-17
5772.36963498592	6.356995E-17
5774.33586502075	6.524549E-17
5776.30209505558	7.057997E-17
5778.26832509041	8.411846E-17

Table F.3: He I BELR Template (continued)

Wavelength Flux 5780.23455512524 9.817483E-17 5782.20078516006 1.122901E-16 5784.16701519489 1.328877E-16 5786.13324522972 1.492696E-16 5788.09947526455 1.549276E-16 5790.06570529938 1.610768E-16 5792.03193533421 1.662751E-16 5793.99816536903 1.705157E-16 5795.96439540386 1.813911E-16 5797.93062543869 1.895944E-16 5799.89685547352 1.874678E-16 5801.86308550835 1.852574E-16 5803.82931554317 1.837783E-16 5805.795545578 1.775525E-16 5807.76177561283 1.768070E-16 5809.72800564766 1.868581E-16 5811.69423568249 1.987073E-16 5813.66046571732 2.133718E-16 5817.59292578697 2.395498E-16 5821.52538585663 2.617535E-16 5823.49161589146 2.770660E-16 5827.42407596111 3.062284E-16 5831.35653603077 3.259849E-16 5835.28899610043 3.428737E-16<		
5782.20078516006 1.122901E-16 5784.16701519489 1.328877E-16 5786.13324522972 1.492696E-16 5788.09947526455 1.549276E-16 5790.06570529938 1.610768E-16 5792.03193533421 1.662751E-16 5793.99816536903 1.705157E-16 5795.96439540386 1.813911E-16 5797.93062543869 1.895944E-16 5799.89685547352 1.874678E-16 5801.86308550835 1.852574E-16 5803.82931554317 1.837783E-16 5807.76177561283 1.768070E-16 5809.72800564766 1.868581E-16 5811.69423568249 1.987073E-16 5813.66046571732 2.133718E-16 5817.59292578697 2.395498E-16 5821.52538585663 2.617535E-16 5823.49161589146 2.770660E-16 5825.45784592629 2.922752E-16 5827.42407596111 3.062284E-16 5831.35653603077 3.259849E-16 5835.28899610043 3.428737E-16 5837.25522613525 3.498115E-16 5841.18768620491 <	Wavelength	Flux
5784.167015194891.328877E-165786.133245229721.492696E-165788.099475264551.549276E-165790.065705299381.610768E-165792.031935334211.662751E-165793.998165369031.705157E-165795.964395403861.813911E-165797.930625438691.895944E-165799.896855473521.874678E-165801.863085508351.852574E-165805.7955455781.775525E-165807.761775612831.768070E-165809.728005647661.868581E-165811.694235682491.987073E-165813.660465717322.133718E-165817.592925786972.395498E-165823.491615891462.770660E-165823.491615891462.770660E-165825.457845926292.922752E-165827.424075961113.062284E-165831.356536030773.259849E-165833.32276606563.343572E-165835.288996100433.428737E-165837.255226135253.498115E-165839.221456170083.584567E-165841.187686204913.678721E-165843.153916239743.746906E-16	5780.23455512524	9.817483E-17
5786.133245229721.492696E-165788.099475264551.549276E-165790.065705299381.610768E-165792.031935334211.662751E-165793.998165369031.705157E-165795.964395403861.813911E-165797.930625438691.895944E-165799.896855473521.874678E-165801.863085508351.852574E-165803.829315543171.837783E-165805.7955455781.775525E-165807.761775612831.768070E-165811.694235682491.987073E-165813.660465717322.133718E-165815.626695752142.293091E-165819.55915582182.488080E-165821.525385856632.617535E-165823.491615891462.770660E-165825.457845926292.922752E-165827.424075961113.062284E-165831.356536030773.259849E-165833.32276606563.343572E-165835.288996100433.428737E-165837.255226135253.498115E-165839.221456170083.584567E-165841.187686204913.678721E-165843.153916239743.746906E-16	5782.20078516006	1.122901E-16
5788.099475264551.549276E-165790.065705299381.610768E-165792.031935334211.662751E-165793.998165369031.705157E-165795.964395403861.813911E-165797.930625438691.895944E-165799.896855473521.874678E-165801.863085508351.852574E-165805.7955455781.775525E-165807.761775612831.768070E-165809.728005647661.868581E-165811.694235682491.987073E-165813.660465717322.133718E-165817.592925786972.395498E-165819.55915582182.488080E-165823.491615891462.770660E-165827.424075961113.062284E-165831.356536030773.259849E-165833.32276606563.343572E-165837.255226135253.498115E-165839.221456170083.584567E-165841.187686204913.678721E-165843.153916239743.746906E-16	5784.16701519489	1.328877E-16
5790.065705299381.610768E-165792.031935334211.662751E-165793.998165369031.705157E-165795.964395403861.813911E-165797.930625438691.895944E-165799.896855473521.874678E-165801.863085508351.852574E-165803.829315543171.837783E-165805.7955455781.775525E-165807.761775612831.768070E-165809.728005647661.868581E-165811.694235682491.987073E-165813.660465717322.133718E-165817.592925786972.395498E-165819.55915582182.488080E-165823.491615891462.770660E-165825.457845926292.9922752E-165827.424075961113.062284E-165831.356536030773.259849E-165833.32276606563.343572E-165835.288996100433.428737E-165837.255226135253.498115E-165839.221456170083.584567E-165841.187686204913.678721E-165843.153916239743.746906E-16	5786.13324522972	1.492696E-16
5792.031935334211.662751E-165793.998165369031.705157E-165795.964395403861.813911E-165797.930625438691.895944E-165799.896855473521.874678E-165801.863085508351.852574E-165803.829315543171.837783E-165805.7955455781.775525E-165807.761775612831.768070E-165809.728005647661.868581E-165811.694235682491.987073E-165813.660465717322.133718E-165817.592925786972.395498E-165819.55915582182.488080E-165823.491615891462.770660E-165825.457845926292.922752E-165827.424075961113.062284E-165833.32276606563.343572E-165835.288996100433.428737E-165837.255226135253.498115E-165839.221456170083.584567E-165841.187686204913.678721E-165843.153916239743.746906E-16	5788.09947526455	1.549276E-16
5793.998165369031.705157E-165795.964395403861.813911E-165797.930625438691.895944E-165799.896855473521.874678E-165801.863085508351.852574E-165803.829315543171.837783E-165807.761775612831.768070E-165809.728005647661.868581E-165811.694235682491.987073E-165813.660465717322.133718E-165817.592925786972.395498E-165819.55915582182.488080E-165823.491615891462.770660E-165825.457845926292.922752E-165827.424075961113.062284E-165833.32276606563.343572E-165835.288996100433.428737E-165837.255226135253.498115E-165841.187686204913.678721E-165843.153916239743.746906E-16	5790.06570529938	1.610768E-16
5795.964395403861.813911E-165797.930625438691.895944E-165799.896855473521.874678E-165801.863085508351.852574E-165803.829315543171.837783E-165805.7955455781.775525E-165807.761775612831.768070E-165809.728005647661.868581E-165811.694235682491.987073E-165813.660465717322.133718E-165815.626695752142.293091E-165817.592925786972.395498E-165821.525385856632.617535E-165823.491615891462.770660E-165825.457845926292.922752E-165827.424075961113.062284E-165831.356536030773.259849E-165833.32276606563.343572E-165835.288996100433.428737E-165837.255226135253.498115E-165839.221456170083.584567E-165841.187686204913.678721E-165843.153916239743.746906E-16	5792.03193533421	1.662751E-16
5797.930625438691.895944E-165799.896855473521.874678E-165801.863085508351.852574E-165803.829315543171.837783E-165805.7955455781.775525E-165807.761775612831.768070E-165809.728005647661.868581E-165811.694235682491.987073E-165813.660465717322.133718E-165815.626695752142.293091E-165817.592925786972.395498E-165821.525385856632.617535E-165823.491615891462.770660E-165825.457845926292.922752E-165827.424075961113.062284E-165831.356536030773.259849E-165833.32276606563.343572E-165837.255226135253.498115E-165837.255226135253.498115E-165841.187686204913.678721E-165843.153916239743.746906E-16	5793.99816536903	1.705157E-16
5799.896855473521.874678E-165801.863085508351.852574E-165803.829315543171.837783E-165805.7955455781.775525E-165807.761775612831.768070E-165809.728005647661.868581E-165811.694235682491.987073E-165813.660465717322.133718E-165815.626695752142.293091E-165819.55915582182.488080E-165821.525385856632.617535E-165823.491615891462.770660E-165827.424075961113.062284E-165829.390305995943.176406E-165831.356536030773.259849E-165833.32276606563.343572E-165837.255226135253.498115E-165839.221456170083.584567E-165841.187686204913.678721E-165843.153916239743.746906E-16	5795.96439540386	1.813911E-16
5801.86308550835 1.852574E-16 5803.82931554317 1.837783E-16 5805.795545578 1.775525E-16 5807.76177561283 1.768070E-16 5809.72800564766 1.868581E-16 5811.69423568249 1.987073E-16 5813.66046571732 2.133718E-16 5815.62669575214 2.293091E-16 5817.59292578697 2.395498E-16 5821.52538585663 2.617535E-16 5823.49161589146 2.770660E-16 5825.45784592629 2.922752E-16 5827.42407596111 3.062284E-16 5831.35653603077 3.259849E-16 5833.3227660656 3.343572E-16 5837.25522613525 3.498115E-16 5839.22145617008 3.584567E-16 5841.18768620491 3.678721E-16 5843.15391623974 3.746906E-16	5797.93062543869	1.895944E-16
5803.82931554317 1.837783E-16 5805.795545578 1.775525E-16 5807.76177561283 1.768070E-16 5809.72800564766 1.868581E-16 5811.69423568249 1.987073E-16 5813.66046571732 2.133718E-16 5815.62669575214 2.293091E-16 5817.59292578697 2.395498E-16 5819.5591558218 2.488080E-16 5823.49161589146 2.770660E-16 5825.45784592629 2.922752E-16 5827.42407596111 3.062284E-16 5831.35653603077 3.259849E-16 5833.3227660656 3.343572E-16 5835.28899610043 3.428737E-16 5837.25522613525 3.498115E-16 5841.18768620491 3.678721E-16 5843.15391623974 3.746906E-16	5799.89685547352	1.874678E-16
5805.795545578 1.775525E-16 5807.76177561283 1.768070E-16 5809.72800564766 1.868581E-16 5811.69423568249 1.987073E-16 5813.66046571732 2.133718E-16 5815.62669575214 2.293091E-16 5817.59292578697 2.395498E-16 5819.5591558218 2.488080E-16 5823.49161589146 2.770660E-16 5825.45784592629 2.922752E-16 5827.42407596111 3.062284E-16 5831.35653603077 3.259849E-16 5833.3227660656 3.343572E-16 5837.25522613525 3.498115E-16 5839.22145617008 3.584567E-16 5841.18768620491 3.678721E-16 5843.15391623974 3.746906E-16	5801.86308550835	1.852574E-16
5807.76177561283 1.768070E-16 5809.72800564766 1.868581E-16 5811.69423568249 1.987073E-16 5813.66046571732 2.133718E-16 5815.62669575214 2.293091E-16 5817.59292578697 2.395498E-16 5819.5591558218 2.488080E-16 5821.52538585663 2.617535E-16 5823.49161589146 2.770660E-16 5827.42407596111 3.062284E-16 5829.39030599594 3.176406E-16 5831.35653603077 3.259849E-16 5833.3227660656 3.343572E-16 5837.25522613525 3.498115E-16 5839.22145617008 3.584567E-16 5841.18768620491 3.678721E-16 5843.15391623974 3.746906E-16	5803.82931554317	1.837783E-16
5809.72800564766 1.868581E-16 5811.69423568249 1.987073E-16 5813.66046571732 2.133718E-16 5815.62669575214 2.293091E-16 5817.59292578697 2.395498E-16 5819.5591558218 2.488080E-16 5821.52538585663 2.617535E-16 5823.49161589146 2.770660E-16 5827.42407596111 3.062284E-16 5829.39030599594 3.176406E-16 5831.35653603077 3.259849E-16 5835.28899610043 3.428737E-16 5837.25522613525 3.498115E-16 5841.18768620491 3.678721E-16 5843.15391623974 3.746906E-16	5805.795545578	1.775525E-16
5811.69423568249 1.987073E-16 5813.66046571732 2.133718E-16 5815.62669575214 2.293091E-16 5817.59292578697 2.395498E-16 5819.5591558218 2.488080E-16 5821.52538585663 2.617535E-16 5823.49161589146 2.770660E-16 5827.42407596111 3.062284E-16 5829.39030599594 3.176406E-16 5831.35653603077 3.259849E-16 5835.28899610043 3.428737E-16 5837.25522613525 3.498115E-16 5841.18768620491 3.678721E-16 5843.15391623974 3.746906E-16	5807.76177561283	1.768070E-16
5813.66046571732 2.133718E-16 5815.62669575214 2.293091E-16 5817.59292578697 2.395498E-16 5819.5591558218 2.488080E-16 5821.52538585663 2.617535E-16 5823.49161589146 2.770660E-16 5825.45784592629 2.922752E-16 5827.42407596111 3.062284E-16 5829.39030599594 3.176406E-16 5831.35653603077 3.259849E-16 5835.28899610043 3.428737E-16 5837.25522613525 3.498115E-16 5839.22145617008 3.584567E-16 5841.18768620491 3.678721E-16 5843.15391623974 3.746906E-16	5809.72800564766	1.868581E-16
5815.62669575214 2.293091E-16 5817.59292578697 2.395498E-16 5819.5591558218 2.488080E-16 5821.52538585663 2.617535E-16 5823.49161589146 2.770660E-16 5825.45784592629 2.922752E-16 5827.42407596111 3.062284E-16 5829.39030599594 3.176406E-16 5831.35653603077 3.259849E-16 5835.28899610043 3.428737E-16 5837.25522613525 3.498115E-16 5841.18768620491 3.678721E-16 5843.15391623974 3.746906E-16	5811.69423568249	1.987073E-16
5817.59292578697 2.395498E-16 5819.5591558218 2.488080E-16 5821.52538585663 2.617535E-16 5823.49161589146 2.770660E-16 5825.45784592629 2.922752E-16 5827.42407596111 3.062284E-16 5829.39030599594 3.176406E-16 5831.35653603077 3.259849E-16 5833.3227660656 3.343572E-16 5837.25522613525 3.498115E-16 5839.22145617008 3.584567E-16 5841.18768620491 3.678721E-16 5843.15391623974 3.746906E-16	5813.66046571732	2.133718E-16
5819.5591558218 2.488080E-16 5821.52538585663 2.617535E-16 5823.49161589146 2.770660E-16 5825.45784592629 2.922752E-16 5827.42407596111 3.062284E-16 5829.39030599594 3.176406E-16 5831.35653603077 3.259849E-16 5833.3227660656 3.343572E-16 5837.25522613525 3.498115E-16 5839.22145617008 3.584567E-16 5841.18768620491 3.678721E-16 5843.15391623974 3.746906E-16	5815.62669575214	2.293091E-16
5821.52538585663 2.617535E-16 5823.49161589146 2.770660E-16 5825.45784592629 2.922752E-16 5827.42407596111 3.062284E-16 5829.39030599594 3.176406E-16 5831.35653603077 3.259849E-16 5833.3227660656 3.343572E-16 5837.25522613525 3.498115E-16 5839.22145617008 3.584567E-16 5841.18768620491 3.678721E-16 5843.15391623974 3.746906E-16	5817.59292578697	2.395498E-16
5823.49161589146 2.770660E-16 5825.45784592629 2.922752E-16 5827.42407596111 3.062284E-16 5829.39030599594 3.176406E-16 5831.35653603077 3.259849E-16 5833.3227660656 3.343572E-16 5835.28899610043 3.428737E-16 5837.25522613525 3.498115E-16 5839.22145617008 3.584567E-16 5841.18768620491 3.678721E-16 5843.15391623974 3.746906E-16	5819.5591558218	2.488080E-16
5825.45784592629 2.922752E-16 5827.42407596111 3.062284E-16 5829.39030599594 3.176406E-16 5831.35653603077 3.259849E-16 5833.3227660656 3.343572E-16 5835.28899610043 3.428737E-16 5837.25522613525 3.498115E-16 5839.22145617008 3.584567E-16 5841.18768620491 3.678721E-16 5843.15391623974 3.746906E-16	5821.52538585663	2.617535E-16
5827.42407596111 3.062284E-16 5829.39030599594 3.176406E-16 5831.35653603077 3.259849E-16 5833.3227660656 3.343572E-16 5835.28899610043 3.428737E-16 5837.25522613525 3.498115E-16 5839.22145617008 3.584567E-16 5841.18768620491 3.678721E-16 5843.15391623974 3.746906E-16	5823.49161589146	2.770660E-16
5829.39030599594 3.176406E-16 5831.35653603077 3.259849E-16 5833.3227660656 3.343572E-16 5835.28899610043 3.428737E-16 5837.25522613525 3.498115E-16 5839.22145617008 3.584567E-16 5841.18768620491 3.678721E-16 5843.15391623974 3.746906E-16	5825.45784592629	2.922752E-16
5831.35653603077 3.259849E-16 5833.3227660656 3.343572E-16 5835.28899610043 3.428737E-16 5837.25522613525 3.498115E-16 5839.22145617008 3.584567E-16 5841.18768620491 3.678721E-16 5843.15391623974 3.746906E-16	5827.42407596111	3.062284E-16
5833.3227660656 3.343572E-16 5835.28899610043 3.428737E-16 5837.25522613525 3.498115E-16 5839.22145617008 3.584567E-16 5841.18768620491 3.678721E-16 5843.15391623974 3.746906E-16	5829.39030599594	3.176406E-16
5835.28899610043 3.428737E-16 5837.25522613525 3.498115E-16 5839.22145617008 3.584567E-16 5841.18768620491 3.678721E-16 5843.15391623974 3.746906E-16	5831.35653603077	3.259849E-16
5837.25522613525 3.498115E-16 5839.22145617008 3.584567E-16 5841.18768620491 3.678721E-16 5843.15391623974 3.746906E-16	5833.3227660656	3.343572E-16
5839.22145617008 3.584567E-16 5841.18768620491 3.678721E-16 5843.15391623974 3.746906E-16	5835.28899610043	3.428737E-16
5841.18768620491 3.678721E-16 5843.15391623974 3.746906E-16	5837.25522613525	3.498115E-16
5843.15391623974 3.746906E-16	5839.22145617008	3.584567E-16
	5841.18768620491	3.678721E-16
5845.12014627457 3.792348E-16	5843.15391623974	3.746906E-16
	5845.12014627457	3.792348E-16
5847.0863763094 3.841199E-16	5847.0863763094	3.841199E-16
5849.05260634422 3.890883E-16	5849.05260634422	3.890883E-16
5851.01883637905 3.933548E-16	5851.01883637905	3.933548E-16
5852.98506641388 3.984716E-16	5852.98506641388	3.984716E-16
5854.95129644871 4.010937E-16	5854.95129644871	4.010937E-16
5856.91752648354 4.016112E-16	5856.91752648354	4.016112E-16
5858.88375651837 4.034503E-16	5858.88375651837	4.034503E-16
5860.84998655319 4.037147E-16	5860.84998655319	4.037147E-16
5862.81621658802 4.019326E-16	5862.81621658802	4.019326E-16
5864.78244662285 4.016117E-16	5864.78244662285	4.016117E-16
5866.74867665768 4.005899E-16	5866.74867665768	4.005899E-16

Table F.3: He I BELR Template (continued)

Wavelength Flux 5868.71490669251 3.962944E-16 5870.68113672733 3.907658E-16 5872.64736676216 3.861842E-16 5874.61359679699 3.794923E-16 5876.57982683182 3.717947E-16 5878.54605686665 3.644897E-16 5880.51228690147 3.579477E-16 5882.4785169363 3.524358E-16 5884.44474697113 3.486686E-16 5886.41097700596 3.450174E-16 5888.37720704079 3.437430E-16 5892.30966711044 3.522810E-16 5894.27589714527 3.554158E-16 5898.20835721493 3.650251E-16 5902.14081728459 3.727435E-16 5902.14081728459 3.727435E-16 5904.10704731941 3.754703E-16 5908.03950738907 3.757477E-16 5910.0057374239 3.731654E-16 5911.97196745873 3.607532E-16 5915.90442752838 3.548780E-16 5917.87065756321 3.493588E-16 5919.83688759804 3.425913E-16 5925.73557770252 3.171068E-16<		
5870.68113672733 3.907658E-16 5872.64736676216 3.861842E-16 5874.61359679699 3.794923E-16 5876.57982683182 3.717947E-16 5878.54605686665 3.644897E-16 5880.51228690147 3.579477E-16 5882.4785169363 3.524358E-16 5884.44474697113 3.486686E-16 5886.41097700596 3.450174E-16 5889.334343707562 3.472859E-16 5892.30966711044 3.522810E-16 5894.27589714527 3.554158E-16 5896.2421271801 3.594253E-16 5898.20835721493 3.650251E-16 5902.14081728459 3.727435E-16 5906.07327735424 3.764105E-16 5908.03950738907 3.757477E-16 5913.93819749355 3.607532E-16 5915.90442752838 3.548780E-16 5917.87065756321 3.49358E-16 5923.76934766769 3.266659E-16 5925.73557770252 3.171068E-16 5933.60049784184 2.861237E-16 5935.56672787666 2.773342E-16 5939.49918794632 <td< th=""><th>Wavelength</th><th></th></td<>	Wavelength	
5872.64736676216 3.861842E-16 5874.61359679699 3.794923E-16 5876.57982683182 3.717947E-16 5878.54605686665 3.644897E-16 5880.51228690147 3.579477E-16 5882.4785169363 3.524358E-16 5884.44474697113 3.486686E-16 5886.41097700596 3.450174E-16 5888.37720704079 3.437430E-16 5890.34343707562 3.472859E-16 5892.30966711044 3.522810E-16 5894.27589714527 3.554158E-16 5898.20835721493 3.650251E-16 5990.17458724976 3.698083E-16 5902.14081728459 3.727435E-16 5906.07327735424 3.764105E-16 5908.03950738907 3.757477E-16 5910.0057374239 3.731654E-16 5913.93819749355 3.607532E-16 5915.90442752838 3.548780E-16 5919.83688759804 3.425913E-16 5923.76934766769 3.266659E-16 5925.73557770252 3.171068E-16 5933.60049784184 2.861237E-16 5935.56672787666 <td< td=""><td>5868.71490669251</td><td>3.962944E-16</td></td<>	5868.71490669251	3.962944E-16
5874.61359679699 3.794923E-16 5876.57982683182 3.717947E-16 5878.54605686665 3.644897E-16 5880.51228690147 3.579477E-16 5882.4785169363 3.524358E-16 5884.44474697113 3.486686E-16 5886.41097700596 3.450174E-16 5888.37720704079 3.437430E-16 5890.34343707562 3.472859E-16 5892.30966711044 3.522810E-16 5894.27589714527 3.554158E-16 5898.20835721493 3.650251E-16 5900.17458724976 3.698083E-16 5902.14081728459 3.727435E-16 5906.07327735424 3.764105E-16 5908.03950738907 3.757477E-16 5910.0057374239 3.731654E-16 5913.93819749355 3.607532E-16 5915.90442752838 3.548780E-16 5917.87065756321 3.493588E-16 5919.83688759804 3.425913E-16 5923.76934766769 3.266659E-16 5925.73557770252 3.171068E-16 5937.53295791149 2.661563E-16 5935.56672787666 <td< td=""><td>5870.68113672733</td><td>3.907658E-16</td></td<>	5870.68113672733	3.907658E-16
5876.57982683182 3.717947E-16 5878.54605686665 3.644897E-16 5880.51228690147 3.579477E-16 5882.4785169363 3.524358E-16 5884.44474697113 3.486686E-16 5886.41097700596 3.450174E-16 5888.37720704079 3.437430E-16 5890.34343707562 3.472859E-16 5892.30966711044 3.522810E-16 5894.27589714527 3.554158E-16 5898.20835721493 3.650251E-16 5900.17458724976 3.698083E-16 5902.14081728459 3.727435E-16 5906.07327735424 3.764105E-16 5908.03950738907 3.757477E-16 5910.0057374239 3.731654E-16 5913.93819749355 3.607532E-16 5915.90442752838 3.548780E-16 5917.87065756321 3.493588E-16 5919.83688759804 3.425913E-16 5927.70180773735 3.085326E-16 5927.70180773735 3.085326E-16 5927.70180773735 3.085326E-16 5933.60049784184 2.861237E-16 5935.56672787666 <td< td=""><td>5872.64736676216</td><td>3.861842E-16</td></td<>	5872.64736676216	3.861842E-16
5878.54605686665 3.644897E-16 5880.51228690147 3.579477E-16 5882.4785169363 3.524358E-16 5884.44474697113 3.486686E-16 5886.41097700596 3.450174E-16 5888.37720704079 3.437430E-16 5890.34343707562 3.472859E-16 5892.30966711044 3.522810E-16 5896.2421271801 3.594253E-16 5898.20835721493 3.650251E-16 5900.17458724976 3.698083E-16 5902.14081728459 3.727435E-16 5906.07327735424 3.764105E-16 5908.03950738907 3.757477E-16 5910.0057374239 3.731654E-16 5913.93819749355 3.607532E-16 5915.90442752838 3.548780E-16 5917.87065756321 3.493588E-16 5919.83688759804 3.425913E-16 5923.76934766769 3.266659E-16 5927.70180773735 3.085326E-16 5929.66803777218 3.014570E-16 5933.60049784184 2.861237E-16 5935.56672787666 2.773342E-16 5937.53295791149	5874.61359679699	3.794923E-16
5880.51228690147 3.579477E-16 5882.4785169363 3.524358E-16 5884.44474697113 3.486686E-16 5886.41097700596 3.450174E-16 5888.37720704079 3.437430E-16 5890.34343707562 3.472859E-16 5892.30966711044 3.522810E-16 5894.27589714527 3.554158E-16 5896.2421271801 3.594253E-16 5898.20835721493 3.650251E-16 5900.17458724976 3.698083E-16 5902.14081728459 3.727435E-16 5904.10704731941 3.754703E-16 5908.03950738907 3.757477E-16 5910.0057374239 3.731654E-16 5913.93819749355 3.607532E-16 5915.90442752838 3.548780E-16 5919.83688759804 3.425913E-16 5921.80311763287 3.266659E-16 5925.73557770252 3.171068E-16 5927.70180773735 3.085326E-16 5929.66803777218 3.014570E-16 5933.60049784184 2.861237E-16 5937.53295791149 2.661563E-16 5943.43164801598	5876.57982683182	3.717947E-16
5882.4785169363 3.524358E-16 5884.44474697113 3.486686E-16 5886.41097700596 3.450174E-16 5888.37720704079 3.437430E-16 5890.34343707562 3.472859E-16 5892.30966711044 3.522810E-16 5894.27589714527 3.554158E-16 5896.2421271801 3.594253E-16 5898.20835721493 3.650251E-16 5900.17458724976 3.698083E-16 5902.14081728459 3.727435E-16 5904.10704731941 3.754703E-16 5908.03950738907 3.757477E-16 5910.0057374239 3.731654E-16 5913.93819749355 3.607532E-16 5915.90442752838 3.548780E-16 5917.87065756321 3.493588E-16 5919.83688759804 3.425913E-16 5923.76934766769 3.266659E-16 5925.73557770252 3.171068E-16 5931.63426780701 2.941019E-16 5933.60049784184 2.861237E-16 5937.53295791149 2.661563E-16 5943.43164801598 2.303582E-16 5945.39787805081 2.201736E-16 5947.36410808563 2.092005E-1	5878.54605686665	3.644897E-16
5884.44474697113 3.486686E-16 5886.41097700596 3.450174E-16 5888.37720704079 3.437430E-16 5890.34343707562 3.472859E-16 5892.30966711044 3.522810E-16 5894.27589714527 3.554158E-16 5898.20835721493 3.650251E-16 5900.17458724976 3.698083E-16 5902.14081728459 3.727435E-16 5904.10704731941 3.754703E-16 5908.03950738907 3.757477E-16 5910.0057374239 3.731654E-16 5913.93819749355 3.607532E-16 5915.90442752838 3.548780E-16 5917.87065756321 3.493588E-16 5919.83688759804 3.425913E-16 5923.76934766769 3.266659E-16 5927.70180773735 3.085326E-16 5929.66803777218 3.014570E-16 5933.60049784184 2.861237E-16 5937.53295791149 2.661563E-16 5939.49918794632 2.536590E-16 5947.36410808563 2.092005E-16 5947.36410808563 2.092005E-16 5947.36410808563 2.092005E-16 5949.33033812046 1.959612E	5880.51228690147	3.579477E-16
5886.41097700596 3.450174E-16 5888.37720704079 3.437430E-16 5890.34343707562 3.472859E-16 5892.30966711044 3.522810E-16 5894.27589714527 3.554158E-16 5896.2421271801 3.594253E-16 5898.20835721493 3.650251E-16 5900.17458724976 3.698083E-16 5902.14081728459 3.727435E-16 5904.10704731941 3.754703E-16 5908.03950738907 3.757477E-16 5910.0057374239 3.731654E-16 5913.93819749355 3.607532E-16 5915.90442752838 3.548780E-16 5917.87065756321 3.493588E-16 5921.80311763287 3.349542E-16 5923.76934766769 3.266659E-16 5927.70180773735 3.085326E-16 5927.70180773735 3.085326E-16 5933.60049784184 2.861237E-16 5937.53295791149 2.661563E-16 5939.49918794632 2.536590E-16 5943.43164801598 2.303582E-16 5945.39787805081 2.201736E-16 5949.33033812046 <td< td=""><td>5882.4785169363</td><td>3.524358E-16</td></td<>	5882.4785169363	3.524358E-16
5888.37720704079 3.437430E-16 5890.34343707562 3.472859E-16 5892.30966711044 3.522810E-16 5894.27589714527 3.554158E-16 5896.2421271801 3.594253E-16 5898.20835721493 3.650251E-16 5900.17458724976 3.698083E-16 5902.14081728459 3.727435E-16 5904.10704731941 3.754703E-16 5908.03950738907 3.757477E-16 5910.0057374239 3.731654E-16 5913.93819749355 3.607532E-16 5915.90442752838 3.548780E-16 5917.87065756321 3.493588E-16 5919.83688759804 3.425913E-16 5923.76934766769 3.266659E-16 5925.73557770252 3.171068E-16 5931.63426780701 2.941019E-16 5935.56672787666 2.773342E-16 5939.49918794632 2.536590E-16 5941.46541798115 2.416549E-16 5943.3033812046 1.959612E-16 5949.33033812046 1.959612E-16 5953.26279819012 1.702803E-16	5884.44474697113	3.486686E-16
5890.34343707562 3.472859E-16 5892.30966711044 3.522810E-16 5894.27589714527 3.554158E-16 5896.2421271801 3.594253E-16 5898.20835721493 3.650251E-16 5900.17458724976 3.698083E-16 5902.14081728459 3.727435E-16 5904.10704731941 3.754703E-16 5908.03950738907 3.757477E-16 5910.0057374239 3.731654E-16 5913.93819749355 3.607532E-16 5915.90442752838 3.548780E-16 5917.87065756321 3.493588E-16 5919.83688759804 3.425913E-16 5923.76934766769 3.266659E-16 5925.73557770252 3.171068E-16 5929.66803777218 3.014570E-16 5933.60049784184 2.861237E-16 5937.53295791149 2.661563E-16 5937.53295791149 2.661563E-16 5943.43164801598 2.303582E-16 5945.39787805081 2.201736E-16 5947.36410808563 2.092005E-16 5949.33033812046 1.959612E-16 5953.26279819012 1.702803E-16	5886.41097700596	3.450174E-16
5892.30966711044 3.522810E-16 5894.27589714527 3.554158E-16 5896.2421271801 3.594253E-16 5898.20835721493 3.650251E-16 5900.17458724976 3.698083E-16 5902.14081728459 3.727435E-16 5904.10704731941 3.754703E-16 5908.03950738907 3.757477E-16 5910.0057374239 3.731654E-16 5913.93819749355 3.607532E-16 5915.90442752838 3.548780E-16 5917.87065756321 3.493588E-16 5918.83688759804 3.425913E-16 5923.76934766769 3.266659E-16 5925.73557770252 3.171068E-16 5927.70180773735 3.085326E-16 5929.66803777218 3.014570E-16 5933.60049784184 2.861237E-16 5937.53295791149 2.661563E-16 5939.49918794632 2.536590E-16 5943.43164801598 2.303582E-16 5947.36410808563 2.092005E-16 5949.33033812046 1.959612E-16 5953.26279819012 1.702803E-16	5888.37720704079	3.437430E-16
5894.275897145273.554158E-165896.24212718013.594253E-165898.208357214933.650251E-165900.174587249763.698083E-165902.140817284593.727435E-165904.107047319413.754703E-165908.039507389073.757477E-165910.00573742393.731654E-165911.971967458733.6675422E-165913.938197493553.607532E-165915.904427528383.548780E-165919.836887598043.425913E-165921.803117632873.266659E-165923.769347667693.266659E-165925.735577702523.171068E-165927.701807737353.085326E-165929.668037772183.014570E-165931.634267807012.941019E-165933.600497841842.861237E-165935.566727876662.773342E-165939.499187946322.536590E-165941.465417981152.416549E-165943.431648015982.303582E-165945.397878050812.201736E-165947.364108085632.092005E-165949.330338120461.959612E-165951.296568155291.824040E-165953.262798190121.702803E-16	5890.34343707562	3.472859E-16
5896.24212718013.594253E-165898.208357214933.650251E-165900.174587249763.698083E-165902.140817284593.727435E-165904.107047319413.754703E-165908.039507389073.757477E-165910.00573742393.731654E-165913.938197493553.607532E-165915.904427528383.548780E-165917.870657563213.493588E-165919.836887598043.425913E-165923.769347667693.266659E-165925.735577702523.171068E-165927.701807737353.085326E-165929.668037772183.014570E-165931.634267807012.941019E-165933.600497841842.861237E-165937.532957911492.661563E-165937.532957911492.661563E-165943.431648015982.303582E-165945.397878050812.201736E-165947.364108085632.092005E-165949.330338120461.959612E-165951.296568155291.824040E-165953.262798190121.702803E-16	5892.30966711044	3.522810E-16
5898.20835721493 3.650251E-16 5900.17458724976 3.698083E-16 5902.14081728459 3.727435E-16 5904.10704731941 3.754703E-16 5906.07327735424 3.764105E-16 5908.03950738907 3.757477E-16 5910.0057374239 3.731654E-16 5913.93819749355 3.607532E-16 5915.90442752838 3.548780E-16 5917.87065756321 3.493588E-16 5919.83688759804 3.425913E-16 5921.80311763287 3.266659E-16 5925.73557770252 3.171068E-16 5927.70180773735 3.085326E-16 5929.66803777218 3.014570E-16 5933.60049784184 2.861237E-16 5937.53295791149 2.661563E-16 5939.49918794632 2.536590E-16 5943.43164801598 2.303582E-16 5945.39787805081 2.201736E-16 5947.36410808563 2.092005E-16 5949.33033812046 1.959612E-16 5953.26279819012 1.702803E-16	5894.27589714527	3.554158E-16
5900.17458724976 3.698083E-16 5902.14081728459 3.727435E-16 5904.10704731941 3.754703E-16 5906.07327735424 3.764105E-16 5908.03950738907 3.757477E-16 5910.0057374239 3.731654E-16 5911.97196745873 3.675422E-16 5913.93819749355 3.607532E-16 5915.90442752838 3.548780E-16 5917.87065756321 3.493588E-16 5919.83688759804 3.425913E-16 5923.76934766769 3.266659E-16 5925.73557770252 3.171068E-16 5929.66803777218 3.014570E-16 5931.63426780701 2.941019E-16 5933.60049784184 2.861237E-16 5937.53295791149 2.661563E-16 5939.49918794632 2.536590E-16 5941.46541798115 2.416549E-16 5945.39787805081 2.201736E-16 5947.36410808563 2.092005E-16 5949.33033812046 1.959612E-16 5953.26279819012 1.702803E-16	5896.2421271801	3.594253E-16
5902.14081728459 3.727435E-16 5904.10704731941 3.754703E-16 5906.07327735424 3.764105E-16 5908.03950738907 3.757477E-16 5910.0057374239 3.731654E-16 5911.97196745873 3.675422E-16 5913.93819749355 3.607532E-16 5915.90442752838 3.548780E-16 5917.87065756321 3.493588E-16 5919.83688759804 3.425913E-16 5923.76934766769 3.266659E-16 5923.76934766769 3.266659E-16 5927.70180773735 3.085326E-16 5929.66803777218 3.014570E-16 5931.63426780701 2.941019E-16 5933.60049784184 2.861237E-16 5937.53295791149 2.661563E-16 5939.49918794632 2.536590E-16 5941.46541798115 2.416549E-16 5945.39787805081 2.201736E-16 5949.33033812046 1.959612E-16 5949.33033812046 1.959612E-16 5953.26279819012 1.702803E-16	5898.20835721493	3.650251E-16
5904.10704731941 3.754703E-16 5906.07327735424 3.764105E-16 5908.03950738907 3.757477E-16 5910.0057374239 3.731654E-16 5911.97196745873 3.675422E-16 5913.93819749355 3.607532E-16 5915.90442752838 3.548780E-16 5917.87065756321 3.493588E-16 5919.83688759804 3.425913E-16 5921.80311763287 3.349542E-16 5923.76934766769 3.266659E-16 5925.73557770252 3.171068E-16 5927.70180773735 3.085326E-16 5929.66803777218 3.014570E-16 5931.63426780701 2.941019E-16 5933.60049784184 2.861237E-16 5937.53295791149 2.661563E-16 5939.49918794632 2.536590E-16 5943.43164801598 2.303582E-16 5945.39787805081 2.201736E-16 5949.33033812046 1.959612E-16 5951.29656815529 1.824040E-16 5953.26279819012 1.702803E-16	5900.17458724976	3.698083E-16
5906.073277354243.764105E-165908.039507389073.757477E-165910.00573742393.731654E-165911.971967458733.675422E-165913.938197493553.607532E-165915.904427528383.548780E-165917.870657563213.493588E-165919.836887598043.425913E-165921.803117632873.266659E-165923.769347667693.266659E-165925.735577702523.171068E-165929.668037772183.014570E-165931.634267807012.941019E-165933.600497841842.861237E-165937.532957911492.661563E-165939.499187946322.536590E-165943.431648015982.303582E-165947.364108085632.092005E-165949.330338120461.959612E-165951.296568155291.824040E-165953.262798190121.702803E-16	5902.14081728459	3.727435E-16
5908.03950738907 3.757477E-16 5910.0057374239 3.731654E-16 5911.97196745873 3.675422E-16 5913.93819749355 3.607532E-16 5915.90442752838 3.548780E-16 5917.87065756321 3.493588E-16 5919.83688759804 3.425913E-16 5921.80311763287 3.349542E-16 5923.76934766769 3.266659E-16 5925.73557770252 3.171068E-16 5929.66803777218 3.014570E-16 5931.63426780701 2.941019E-16 5933.60049784184 2.861237E-16 5937.53295791149 2.661563E-16 5939.49918794632 2.536590E-16 5941.46541798115 2.416549E-16 5945.39787805081 2.201736E-16 5949.33033812046 1.959612E-16 5951.29656815529 1.824040E-16 5953.26279819012 1.702803E-16	5904.10704731941	3.754703E-16
5910.00573742393.731654E-165911.971967458733.675422E-165913.938197493553.607532E-165915.904427528383.548780E-165917.870657563213.493588E-165919.836887598043.425913E-165921.803117632873.349542E-165923.769347667693.266659E-165925.735577702523.171068E-165927.701807737353.085326E-165929.668037772183.014570E-165931.634267807012.941019E-165933.600497841842.861237E-165937.532957911492.661563E-165939.499187946322.536590E-165941.465417981152.416549E-165943.431648015982.303582E-165947.364108085632.092005E-165949.330338120461.959612E-165951.296568155291.824040E-165953.262798190121.702803E-16	5906.07327735424	3.764105E-16
5911.97196745873 3.675422E-16 5913.93819749355 3.607532E-16 5915.90442752838 3.548780E-16 5917.87065756321 3.493588E-16 5919.83688759804 3.425913E-16 5921.80311763287 3.349542E-16 5923.76934766769 3.266659E-16 5925.73557770252 3.171068E-16 5927.70180773735 3.085326E-16 5929.66803777218 3.014570E-16 5931.63426780701 2.941019E-16 5933.60049784184 2.861237E-16 5937.53295791149 2.661563E-16 5939.49918794632 2.536590E-16 5943.43164801598 2.303582E-16 5945.39787805081 2.201736E-16 5949.33033812046 1.959612E-16 5951.29656815529 1.824040E-16 5953.26279819012 1.702803E-16	5908.03950738907	3.757477E-16
5913.93819749355 3.607532E-16 5915.90442752838 3.548780E-16 5917.87065756321 3.493588E-16 5919.83688759804 3.425913E-16 5921.80311763287 3.266659E-16 5923.76934766769 3.266659E-16 5925.73557770252 3.171068E-16 5929.66803777218 3.014570E-16 5931.63426780701 2.941019E-16 5933.60049784184 2.861237E-16 5937.53295791149 2.661563E-16 5939.49918794632 2.536590E-16 5941.46541798115 2.416549E-16 5945.39787805081 2.201736E-16 5947.36410808563 2.092005E-16 5949.33033812046 1.959612E-16 5951.29656815529 1.824040E-16 5953.26279819012 1.702803E-16	5910.0057374239	3.731654E-16
5915.90442752838 3.548780E-16 5917.87065756321 3.493588E-16 5919.83688759804 3.425913E-16 5921.80311763287 3.349542E-16 5923.76934766769 3.266659E-16 5925.73557770252 3.171068E-16 5927.70180773735 3.085326E-16 5929.66803777218 3.014570E-16 5931.63426780701 2.941019E-16 5933.60049784184 2.861237E-16 5937.53295791149 2.661563E-16 5939.49918794632 2.536590E-16 5941.46541798115 2.416549E-16 5945.39787805081 2.201736E-16 5947.36410808563 2.092005E-16 5949.33033812046 1.959612E-16 5951.29656815529 1.824040E-16 5953.26279819012 1.702803E-16	5911.97196745873	3.675422E-16
5917.87065756321 3.493588E-16 5919.83688759804 3.425913E-16 5921.80311763287 3.349542E-16 5923.76934766769 3.266659E-16 5925.73557770252 3.171068E-16 5927.70180773735 3.085326E-16 5929.66803777218 3.014570E-16 5931.63426780701 2.941019E-16 5933.60049784184 2.861237E-16 5937.53295791149 2.661563E-16 5939.49918794632 2.536590E-16 5943.43164801598 2.303582E-16 5945.39787805081 2.201736E-16 5947.36410808563 2.092005E-16 5949.33033812046 1.959612E-16 5953.26279819012 1.702803E-16	5913.93819749355	3.607532E-16
5919.83688759804 3.425913E-16 5921.80311763287 3.349542E-16 5923.76934766769 3.266659E-16 5925.73557770252 3.171068E-16 5927.70180773735 3.085326E-16 5929.66803777218 3.014570E-16 5931.63426780701 2.941019E-16 5933.60049784184 2.861237E-16 5935.56672787666 2.773342E-16 5937.53295791149 2.661563E-16 5939.49918794632 2.536590E-16 5943.43164801598 2.303582E-16 5945.39787805081 2.201736E-16 5947.36410808563 2.092005E-16 5949.33033812046 1.959612E-16 5953.26279819012 1.702803E-16	5915.90442752838	3.548780E-16
5921.80311763287 3.349542E-16 5923.76934766769 3.266659E-16 5925.73557770252 3.171068E-16 5927.70180773735 3.085326E-16 5929.66803777218 3.014570E-16 5931.63426780701 2.941019E-16 5933.60049784184 2.861237E-16 5937.53295791149 2.661563E-16 5939.49918794632 2.536590E-16 5941.46541798115 2.416549E-16 5943.43164801598 2.303582E-16 5947.36410808563 2.092005E-16 5949.33033812046 1.959612E-16 5951.29656815529 1.824040E-16 5953.26279819012 1.702803E-16	5917.87065756321	3.493588E-16
5923.76934766769 3.266659E-16 5925.73557770252 3.171068E-16 5927.70180773735 3.085326E-16 5929.66803777218 3.014570E-16 5931.63426780701 2.941019E-16 5933.60049784184 2.861237E-16 5935.56672787666 2.773342E-16 5937.53295791149 2.661563E-16 5939.49918794632 2.536590E-16 5941.46541798115 2.416549E-16 5943.43164801598 2.303582E-16 5947.36410808563 2.092005E-16 5949.33033812046 1.959612E-16 5951.29656815529 1.824040E-16 5953.26279819012 1.702803E-16	5919.83688759804	3.425913E-16
5925.73557770252 3.171068E-16 5927.70180773735 3.085326E-16 5929.66803777218 3.014570E-16 5931.63426780701 2.941019E-16 5933.60049784184 2.861237E-16 5935.56672787666 2.773342E-16 5937.53295791149 2.661563E-16 5939.49918794632 2.536590E-16 5941.46541798115 2.416549E-16 5945.39787805081 2.201736E-16 5947.36410808563 2.092005E-16 5949.33033812046 1.959612E-16 5951.29656815529 1.824040E-16 5953.26279819012 1.702803E-16	5921.80311763287	3.349542E-16
5927.70180773735 3.085326E-16 5929.66803777218 3.014570E-16 5931.63426780701 2.941019E-16 5933.60049784184 2.861237E-16 5935.56672787666 2.773342E-16 5937.53295791149 2.661563E-16 5939.49918794632 2.536590E-16 5941.46541798115 2.416549E-16 5943.43164801598 2.303582E-16 5945.39787805081 2.201736E-16 5947.36410808563 2.092005E-16 5949.33033812046 1.959612E-16 5953.26279819012 1.702803E-16	5923.76934766769	3.266659E-16
5929.66803777218 3.014570E-16 5931.63426780701 2.941019E-16 5933.60049784184 2.861237E-16 5935.56672787666 2.773342E-16 5937.53295791149 2.661563E-16 5939.49918794632 2.536590E-16 5941.46541798115 2.416549E-16 5943.43164801598 2.303582E-16 5945.39787805081 2.201736E-16 5947.36410808563 2.092005E-16 5949.33033812046 1.959612E-16 5951.29656815529 1.824040E-16 5953.26279819012 1.702803E-16	5925.73557770252	3.171068E-16
5931.63426780701 2.941019E-16 5933.60049784184 2.861237E-16 5935.56672787666 2.773342E-16 5937.53295791149 2.661563E-16 5939.49918794632 2.536590E-16 5941.46541798115 2.416549E-16 5943.43164801598 2.303582E-16 5945.39787805081 2.201736E-16 5947.36410808563 2.092005E-16 5949.33033812046 1.959612E-16 5951.29656815529 1.824040E-16 5953.26279819012 1.702803E-16	5927.70180773735	3.085326E-16
5933.60049784184 2.861237E-16 5935.56672787666 2.773342E-16 5937.53295791149 2.661563E-16 5939.49918794632 2.536590E-16 5941.46541798115 2.416549E-16 5943.43164801598 2.303582E-16 5945.39787805081 2.201736E-16 5947.36410808563 2.092005E-16 5949.33033812046 1.959612E-16 5953.26279819012 1.702803E-16	5929.66803777218	3.014570E-16
5935.56672787666 2.773342E-16 5937.53295791149 2.661563E-16 5939.49918794632 2.536590E-16 5941.46541798115 2.416549E-16 5943.43164801598 2.303582E-16 5945.39787805081 2.201736E-16 5947.36410808563 2.092005E-16 5949.33033812046 1.959612E-16 5951.29656815529 1.824040E-16 5953.26279819012 1.702803E-16	5931.63426780701	2.941019E-16
5937.53295791149 2.661563E-16 5939.49918794632 2.536590E-16 5941.46541798115 2.416549E-16 5943.43164801598 2.303582E-16 5945.39787805081 2.201736E-16 5947.36410808563 2.092005E-16 5949.33033812046 1.959612E-16 5951.29656815529 1.824040E-16 5953.26279819012 1.702803E-16	5933.60049784184	2.861237E-16
5939.49918794632 2.536590E-16 5941.46541798115 2.416549E-16 5943.43164801598 2.303582E-16 5945.39787805081 2.201736E-16 5947.36410808563 2.092005E-16 5949.33033812046 1.959612E-16 5951.29656815529 1.824040E-16 5953.26279819012 1.702803E-16	5935.56672787666	2.773342E-16
5941.46541798115 2.416549E-16 5943.43164801598 2.303582E-16 5945.39787805081 2.201736E-16 5947.36410808563 2.092005E-16 5949.33033812046 1.959612E-16 5951.29656815529 1.824040E-16 5953.26279819012 1.702803E-16	5937.53295791149	2.661563E-16
5943.43164801598 2.303582E-16 5945.39787805081 2.201736E-16 5947.36410808563 2.092005E-16 5949.33033812046 1.959612E-16 5951.29656815529 1.824040E-16 5953.26279819012 1.702803E-16	5939.49918794632	2.536590E-16
5945.39787805081 2.201736E-16 5947.36410808563 2.092005E-16 5949.33033812046 1.959612E-16 5951.29656815529 1.824040E-16 5953.26279819012 1.702803E-16	5941.46541798115	2.416549E-16
5947.36410808563 2.092005E-16 5949.33033812046 1.959612E-16 5951.29656815529 1.824040E-16 5953.26279819012 1.702803E-16	5943.43164801598	2.303582E-16
5949.33033812046 1.959612E-16 5951.29656815529 1.824040E-16 5953.26279819012 1.702803E-16	5945.39787805081	2.201736E-16
5951.29656815529 1.824040E-16 5953.26279819012 1.702803E-16	5947.36410808563	2.092005E-16
5953.26279819012 1.702803E-16	5949.33033812046	1.959612E-16
	5951.29656815529	1.824040E-16
	5953.26279819012	1.702803E-16
	5955.22902822495	1.585227E-16

Table F.3: He I BELR Template (continued)

Wavelength	Flux
5957.19525825977	1.471449E-16
5959.1614882946	1.381627E-16
5961.12771832943	1.314515E-16
5963.09394836426	1.253538E-16
5965.06017839909	1.200129E-16
5967.02640843392	1.152927E-16
5968.99263846874	1.107399E-16
5970.95886850357	1.066755E-16
5972.9250985384	1.040117E-16
5974.89132857323	1.014354E-16
5976.85755860806	9.888097E-17
5978.82378864288	9.666658E-17
5980.79001867771	9.494531E-17
5982.75624871254	9.200690E-17
5984.72247874737	8.800691E-17
5986.6887087822	8.428245E-17
5988.65493881703	7.998856E-17
5990.62116885185	7.538843E-17
5992.58739888668	7.284490E-17
5994.55362892151	7.045000E-17
5996.51985895634	6.797649E-17
5998.48608899117	6.547438E-17
6000.45231902599	6.343528E-17
6002.41854906082	6.232525E-17
6004.38477909565	6.358009E-17
6006.35100913048	6.536425E-17
6008.31723916531	6.596458E-17
6010.28346920014	6.644891E-17
6012.24969923496	6.712898E-17
6014.21592926979	6.645418E-17
6016.18215930462	6.365165E-17
6018.14838933945	6.001508E-17
6020.11461937428	5.845642E-17
6022.08084940911	5.806977E-17
6024.04707944393	5.404528E-17
6026.01330947876	4.717112E-17
6027.97953951359	4.317035E-17
6029.94576954842	4.084554E-17
6031.91199958325	3.927451E-17
6033.87822961807	3.848322E-17
6035.8444596529	3.831944E-17
6037.81068968773	3.959378E-17
6039.77691972256	4.082546E-17
6041.74314975739	3.978679E-17
6043.70937979222	3.692428E-17
	U.UULTLULF11

Table F.3: He I BELR Template (continued)

Wavelength	\mathbf{Flux}
6045.67560982704	3.552637E-17
6047.64183986187	3.460570E-17
6049.6080698967	3.144946E-17
6051.57429993153	2.699929E-17
6053.54052996636	2.147413E-17
6055.50676000118	1.502911E-17
6057.47299003601	1.036778E-17
6059.43922007084	6.606877E-18
6061.40545010567	2.603421E-18
6063.3716801405	-1.727231E-18
6065.33791017532	-5.237146E-18
6067.30414021015	-8.889238E-18
6069.27037024498	-9.563139E-18
6071.23660027981	-6.476895E-18
6073.20283031464	-8.658044E-18
6075.16906034947	-5.760093E-18
6077.13529038429	5.545684E-18

Table F.4: H β BELR Template - smooth_halpha

Wavelength	Flux
6204.93994140625	2.470912E-17
6206.90617144108	3.138737E-17
6208.87240147591	3.393811E-17
6210.83863151074	3.531292E-17
6212.80486154556	3.479353E-17
6214.77109158039	3.344160E-17
6216.73732161522	3.429950E-17
6218.70355165005	3.524041E-17
6220.66978168488	3.535926E-17
6222.6360117197	3.462812E-17
6224.60224175453	3.301380E-17
6226.56847178936	3.197182E-17
6228.53470182419	3.341499E-17
6230.50093185902	3.459055E-17
6232.46716189384	3.406275E-17
6234.43339192867	3.462393E-17
6236.3996219635	3.578811E-17
6238.36585199833	3.744813E-17
6240.33208203316	3.920526E-17
6242.29831206799	4.114707E-17
6244.26454210281	4.410804E-17

Table F.4: $H\beta$ BELR Template (continued)

Wavelength	Flux
6246.23077213764	4.627474E-17
6248.19700217247	4.685538E-17
6250.1632322073	4.688901E-17
6252.12946224213	4.781967E-17
6254.09569227695	4.979140E-17
6256.06192231178	5.158497E-17
6258.02815234661	5.360073E-17
6259.99438238144	5.437622E-17
6261.96061241627	5.426348E-17
6263.9268424511	5.494872E-17
6265.89307248592	5.661864E-17
6267.85930252075	6.035104E-17 6.403553E-17
6269.82553255558 6271.79176259041	6.592892E-17
6273.75799262524	6.802436E-17
6275.72422266007	7.185032E-17
6277.69045269489	7.480487E-17
6279.65668272972	7.511221E-17
6281.62291276455	7.520856E-17
6283.58914279938	7.597098E-17
6285.55537283421	7.802443E-17
6287.52160286903	8.163739E-17
6289.48783290386	8.707652E-17
6291.45406293869	9.544873E-17
6293.42029297352	1.050273E-16
6295.38652300835	1.113931E-16
6297.35275304318	1.146173E-16
6299.318983078	1.169401E-16
6301.28521311283	1.194395E-16
6303.25144314766	1.229063E-16
6305.21767318249	1.250254E-16
6307.18390321732	1.239049E-16
6309.15013325214	1.219971E-16
6311.11636328697	1.199884E-16
6313.0825933218	1.166322E-16
6315.04882335663	1.132347E-16
6317.01505339146	1.135615E-16
6318.98128342629	1.153381E-16
6320.94751346111	1.173775E-16
6322.91374349594	1.208985E-16
6324.87997353077	1.237250E-16
6326.8462035656	1.274813E-16
6328.81243360043	1.335145E-16
6330.77866363525	1.394530E-16
6332.74489367008	1.437759E-16

Table F.4: $H\beta$ BELR Template (continued)

Wavelength	Flux
6334.71112370491	1.470713E-16
6336.67735373974	1.516006E-16
6338.64358377457	1.556169E-16
6340.6098138094	1.592275E-16
6342.57604384422	1.629258E-16
6344.54227387905	1.656886E-16
6346.50850391388	1.680657E-16
6348.47473394871	1.700208E-16
6350.44096398354	1.717445E-16
6352.40719401836	1.737646E-16
6354.37342405319	1.756099E-16
6356.33965408802	1.768902E-16
6358.30588412285	1.764521E-16
6360.27211415768	1.752646E-16
6362.23834419251	1.753727E-16
6364.20457422733	1.774204E-16
6366.17080426216	1.810469E-16
6368.13703429699	1.856733E-16
6370.10326433182	1.905573E-16
6372.06949436665	1.955774E-16
6374.03572440148	1.985264E-16
6376.0019544363	2.008650E-16
6377.96818447113	2.035754E-16
6379.93441450596	2.053441E-16
6381.90064454079	2.055454E-16
6383.86687457561	2.026673E-16
6385.83310461044	1.997591E-16
6387.79933464527	1.963774E-16
6389.7655646801	1.922151E-16
6391.73179471493	1.881551E-16
6393.69802474976	1.830282E-16
6395.66425478458	1.770930E-16
6397.63048481941	1.721010E-16
6399.59671485424	1.687625E-16
6401.56294488907	1.669813E-16
6403.5291749239	1.658638E-16
6405.49540495873	1.661034E-16
6407.46163499355	1.653334E-16
6409.42786502838	1.640935E-16
6411.39409506321	1.631261E-16
6413.36032509804	1.625696E-16
6415.32655513287	1.631119E-16
6417.29278516769	1.660541E-16
6419.25901520252	1.693939E-16
6421.22524523735	1.727282E-16

Table F.4: $H\beta$ BELR Template (continued)

Wavelength	Flux
6423.19147527218	1.774323E-16
6425.15770530701	1.821949E-16
6427.12393534184	1.885894E-16
6429.09016537666	1.985706E-16
6431.05639541149	2.115752E-16
6433.02262544632	2.284933E-16
6434.98885548115	2.494287E-16
6436.95508551598	2.716319E-16
6438.92131555081	2.933112E-16
6440.88754558563	3.166915E-16
6442.85377562046	3.419889E-16
6444.82000565529	3.677062E-16
6446.78623569012	3.968587E-16
6448.75246572495	4.288621E-16
6450.71869575977	4.609749E-16
6452.6849257946	4.935644E-16
6454.65115582943	5.264588E-16
6456.61738586426	5.606630E-16
6458.58361589909	5.994395E-16
6460.54984593391	6.408052E-16
6462.51607596874	6.827488E-16
6464.48230600357	7.268004E-16
6466.4485360384	7.755210E-16
6468.41476607323	8.310800E-16
6470.38099610806	8.951710E-16
6472.34722614288	9.685033E-16
6474.31345617771	1.052640E-15
6476.27968621254	1.148176E-15
6478.24591624737	1.251438E-15
6480.2121462822	1.361126E-15
6482.17837631703	1.482315E-15
6484.14460635185	1.614353E-15
6486.11083638668	1.752979E-15
6488.07706642151	1.895414E-15
6490.04329645634	2.040084E-15
6492.00952649117	2.187079E-15
6493.975756526	2.334599E-15
6495.94198656082	2.480961E-15
6497.90821659565	2.626958E-15
6499.87444663048	2.773383E-15
6501.84067666531	2.918876E-15
6503.80690670014	3.061826E-15
6505.77313673496	3.197480E-15
6507.73936676979	3.327646E-15
6509.70559680462	3.453143E-15

Table F.4: $H\beta$ BELR Template (continued)

Wavelength	Flux
6511.67182683945	3.572533E-15
6513.63805687428	3.680501E-15
6515.60428690911	3.780276E-15
6517.57051694393	3.873117E-15
6519.53674697876	3.955677E-15
6521.50297701359	4.027324E-15
6523.46920704842	4.090613E-15
6525.43543708325	4.142525E-15
6527.40166711807	4.186529E-15
6529.3678971529	4.225201E-15
6531.33412718773	4.256342E-15
6533.30035722256	4.278422E-15
6535.26658725739	4.291480E-15
6537.23281729221	4.293124E-15
6539.19904732704	4.282466E-15
6541.16527736187	4.260930E-15
6543.1315073967	4.228644E-15
6545.09773743153	4.189292E-15
6547.06396746635	4.153377E-15
6549.03019750118	4.121228E-15
6550.99642753601	4.092857E-15
6552.96265757084	4.074641E-15
6554.92888760567	4.060103E-15
6556.8951176405	4.043423E-15
6558.86134767532	4.020488E-15
6560.82757771015	3.989100E-15
6562.79380774498	3.958606E-15
6564.76003777981	3.942636E-15
6566.72626781464	3.942782E-15
6568.69249784947	3.958823E-15
6570.65872788429	3.997225E-15
6572.62495791912	4.057596E-15
6574.59118795395	4.133325E-15
6576.55741798878	4.220459E-15
6578.52364802361	4.310659E-15
6580.48987805844	4.401957E-15
6582.45610809326	4.499583E-15
6584.42233812809	4.603118E-15
6586.38856816292	4.700990E-15
6588.35479819775	4.785036E-15
6590.32102823258	4.848201E-15
6592.2872582674	4.881145E-15
6594.25348830223	4.879714E-15
6596.21971833706	4.846394E-15
6598.18594837189	4.791387E-15

Table F.4: $H\beta$ BELR Template (continued)

Wavelength	Flux
6600.15217840672	4.727138E-15
6602.11840844155	4.657593E-15
6604.08463847637	4.578283E-15
6606.0508685112	4.478202E-15
6608.01709854603	4.353729E-15
6609.98332858086	4.206287E-15
6611.94955861569	4.038476E-15
6613.91578865051	3.857809E-15
6615.88201868534	3.667759E-15
6617.84824872017	3.472053E-15
6619.814478755	3.274302E-15
6621.78070878983	3.077654E-15
6623.74693882465	2.886332E-15
6625.71316885948	2.702906E-15
6627.67939889431	2.529920E-15
6629.64562892914	2.370161E-15
6631.61185896397	2.224352E-15
6633.57808899879	2.090458E-15
6635.54431903362	1.965545E-15
6637.51054906845	1.848374E-15
6639.47677910328	1.736192E-15
6641.44300913811	1.627123E-15
6643.40923917294	1.522360E-15
6645.37546920776	1.424175E-15
6647.34169924259	1.332424E-15
6649.30792927742	1.245603E-15
6651.27415931225	1.164588E-15
6653.24038934708	1.089870E-15
6655.20661938191	1.021842E-15
6657.17284941673	9.610996E-16
6659.13907945156	9.062608E-16
6661.10530948639	8.564242E-16
6663.07153952122	8.133149E-16
6665.03776955605	7.761119E-16
6667.00399959088	7.408232E-16
6668.9702296257	7.063557E-16
6670.93645966053	6.757995E-16
6672.90268969536	6.474701E-16
6674.86891973019	6.191346E-16
6676.83514976502	5.920317E-16
6678.80137979985	5.664707E-16
6680.76760983467	5.436521E-16
6682.7338398695	5.243954E-16
6684.70006990433	5.064624E-16
6686.66629993916	4.905786E-16

Table F.4: $H\beta$ BELR Template (continued)

Wavelength	Flux
6688.63252997399	4.774609E-16
6690.59876000881	4.657864E-16
6692.56499004364	4.544573E-16
6694.53122007847	4.447459E-16
6696.4974501133	4.377419E-16
6698.46368014813	4.319426E-16
6700.42991018296	4.267059E-16
6702.39614021778	4.233484E-16
6704.36237025261	4.221168E-16
6706.32860028744	4.228176E-16
6708.29483032227	4.235020E-16
6710.2610603571	4.212616E-16
6712.22729039192	4.139987E-16
6714.19352042675	4.023766E-16
6716.15975046158	3.904572E-16
6718.12598049641	3.839514E-16
6720.09221053124	3.829168E-16
6722.05844056606	3.834688E-16
6724.02467060089	3.819233E-16
6725.99090063572	3.740112E-16
6727.95713067055	3.585939E-16
6729.92336070538	3.391528E-16
6731.8895907402	3.216520E-16
6733.85582077503	3.109380E-16
6735.82205080986	3.055293E-16
6737.78828084469	3.008265E-16
6739.75451087952	2.899299E-16
6741.72074091435	2.712330E-16
6743.68697094917	2.502973E-16
6745.653200984	2.305991E-16
6747.61943101883	2.166122E-16
6749.58566105366	2.106724E-16
6751.55189108849	2.086952E-16
6753.51812112332	2.077926E-16
6755.48435115814	2.072439E-16
6757.45058119297	2.051172E-16
6759.4168112278	2.029035E-16
6761.38304126263	2.019390E-16
6763.34927129746	2.021970E-16
6765.31550133228	2.013463E-16
6767.28173136711	2.005507E-16
6769.24796140194	1.974665E-16
6771.21419143677	1.928130E-16
6773.1804214716	1.890513E-16
6775.14665150643	1.847589E-16
0110:14000100040	1.04100315-10

Table F.4: H\beta BELR Template (continued)

Wavelength Flux 6777.11288154125 1.805759E-16 6779.07911157608 1.783198E-16 6781.04534161091 1.757076E-16 6783.01157164574 1.737771E-16 6784.97780168057 1.732217E-16 6786.9440317154 1.733951E-16 6788.91026175022 1.727604E-16 6790.87649178505 1.721449E-16 6792.84272181988 1.719640E-16 6794.80895185471 1.723211E-16 6796.77518188954 1.724544E-16 6798.74141192436 1.708294E-16 6800.70764195919 1.664712E-16 6804.64010202885 1.583783E-16 6806.60633206368 1.544931E-16 6810.53879213333 1.469733E-16 6812.50502216816 1.428561E-16 6814.47125220299 1.397207E-16 6816.43748223782 1.359377E-16 6820.36994230747 1.292932E-16 6822.3361723423 1.285335E-16 6826.26863241196 1.243141E-16 6832.16732251644 1.209083E-16 6834.13355255127 1.208359E-16<
6779.07911157608 1.783198E-16 6781.04534161091 1.757076E-16 6783.01157164574 1.737771E-16 6784.97780168057 1.732217E-16 6786.9440317154 1.733951E-16 6798.891026175022 1.727604E-16 6790.87649178505 1.721449E-16 6794.80895185471 1.723211E-16 6796.77518188954 1.724544E-16 6798.74141192436 1.708294E-16 6800.70764195919 1.664712E-16 6802.67387199402 1.621107E-16 6804.64010202885 1.583783E-16 6806.60633206368 1.544931E-16 6810.53879213333 1.469733E-16 6814.4712520299 1.397207E-16 6814.4712520299 1.397207E-16 6816.43748223782 1.359377E-16 6816.43748223782 1.359377E-16 6820.36994230747 1.292932E-16 6820.36994230747 1.292932E-16 6823.361723423 1.285335E-16 6826.26863241196 1.243141E-16 6828.23486244679 1.226796E-16 6830.20109248161 1.213784E-16 6832.16732251644 1.209083E-16 6834.13355255127 1.208359E-16 6836.0997825861 1.188904E-16 6838.06601262093 1.167562E-16 6840.03224265576 1.165240E-16
6781.04534161091 1.757076E-16 6783.01157164574 1.737771E-16 6784.97780168057 1.732217E-16 6786.9440317154 1.733951E-16 6798.891026175022 1.727604E-16 6790.87649178505 1.721449E-16 6792.84272181988 1.719640E-16 6794.80895185471 1.723211E-16 6796.77518188954 1.724544E-16 6798.74141192436 1.708294E-16 6800.70764195919 1.664712E-16 6804.64010202885 1.583783E-16 6806.60633206368 1.544931E-16 6808.57256209851 1.512843E-16 6810.53879213333 1.469733E-16 6814.47125220299 1.397207E-16 6816.43748223782 1.359377E-16 6818.40371227265 1.321583E-16 6820.36994230747 1.292932E-16 6820.36994230747 1.292932E-16 6822.3361723423 1.267035E-16 6826.26863241196 1.243141E-16 6828.23486244679 1.226796E-16 6830.20109248161 1.213784E-16 6832.16732251644 1.209083E-16 6834.13355255127 1.208359E-16 6836.0997825861 1.188904E-16 6838.06601262093 1.167562E-16 6838.06601262093 1.167562E-16
6783.011571645741.737771E-166784.977801680571.732217E-166786.94403171541.733951E-166788.910261750221.727604E-166790.876491785051.721449E-166792.842721819881.719640E-166794.808951854711.723211E-166796.775181889541.724544E-166798.741411924361.708294E-166800.707641959191.664712E-166804.640102028851.583783E-166806.606332063681.544931E-166810.538792133331.469733E-166812.505022168161.428561E-166814.471252202991.397207E-166816.437482237821.359377E-166820.369942307471.292932E-166822.33617234231.267035E-166824.302402377131.267035E-166826.268632411961.243141E-166828.234862446791.226796E-166830.201092481611.213784E-166832.167322516441.209083E-166834.133552551271.208359E-166836.09978258611.188904E-166838.066012620931.167562E-166840.032242655761.165240E-16
6784.977801680571.732217E-166786.94403171541.733951E-166788.910261750221.727604E-166790.876491785051.721449E-166792.842721819881.719640E-166794.808951854711.723211E-166796.775181889541.724544E-166798.741411924361.708294E-166800.707641959191.664712E-166802.673871994021.621107E-166804.640102028851.583783E-166805.572562098511.512843E-166810.538792133331.469733E-166812.505022168161.428561E-166814.471252202991.397207E-166816.437482237821.359377E-166820.369942307471.292932E-166822.33617234231.285335E-166826.268632411961.243141E-166828.234862446791.226796E-166830.201092481611.213784E-166832.167322516441.209083E-166834.133552551271.208359E-166836.09978258611.188904E-166838.066012620931.167562E-166840.032242655761.165240E-16
6786.94403171541.733951E-166788.910261750221.727604E-166790.876491785051.721449E-166792.842721819881.719640E-166794.808951854711.723211E-166796.775181889541.724544E-166798.741411924361.708294E-166800.707641959191.664712E-166804.640102028851.583783E-166806.606332063681.544931E-166810.538792133331.469733E-166812.505022168161.428561E-166814.471252202991.397207E-166816.437482237821.359377E-166820.369942307471.292932E-166822.33617234231.285335E-166826.268632411961.243141E-166828.234862446791.226796E-166830.201092481611.213784E-166832.167322516441.209083E-166836.09978258611.188904E-166838.066012620931.167562E-166840.032242655761.165240E-16
6788.910261750221.727604E-166790.876491785051.721449E-166792.842721819881.719640E-166794.808951854711.723211E-166796.775181889541.724544E-166798.741411924361.708294E-166800.707641959191.664712E-166804.640102028851.583783E-166806.606332063681.544931E-166810.538792133331.469733E-166812.505022168161.428561E-166814.471252202991.397207E-166816.437482237821.359377E-166818.403712272651.321583E-166820.369942307471.292932E-166824.302402377131.267035E-166826.268632411961.243141E-166828.234862446791.226796E-166830.201092481611.213784E-166832.167322516441.209083E-166836.09978258611.188904E-166838.066012620931.167562E-166840.032242655761.165240E-16
6790.87649178505 1.721449E-16 6792.84272181988 1.719640E-16 6794.80895185471 1.723211E-16 6796.77518188954 1.724544E-16 6798.74141192436 1.708294E-16 6800.70764195919 1.664712E-16 6802.67387199402 1.621107E-16 6804.64010202885 1.583783E-16 6806.60633206368 1.544931E-16 6810.53879213333 1.469733E-16 6812.50502216816 1.428561E-16 6814.47125220299 1.397207E-16 6816.43748223782 1.359377E-16 6820.36994230747 1.292932E-16 6822.3361723423 1.267035E-16 6824.30240237713 1.267035E-16 6826.26863241196 1.243141E-16 6832.16732251644 1.209083E-16 6834.13355255127 1.208359E-16 6836.0997825861 1.188904E-16 6838.06601262093 1.167562E-16 6840.03224265576 1.165240E-16
6792.842721819881.719640E-166794.808951854711.723211E-166796.775181889541.724544E-166798.741411924361.708294E-166800.707641959191.664712E-166802.673871994021.621107E-166804.640102028851.583783E-166808.572562098511.512843E-166810.538792133331.469733E-166812.505022168161.428561E-166814.471252202991.397207E-166816.437482237821.359377E-166820.369942307471.292932E-166822.33617234231.285335E-166824.302402377131.267035E-166826.268632411961.243141E-166828.234862446791.226796E-166830.201092481611.213784E-166832.167322516441.209083E-166834.133552551271.208359E-166836.09978258611.188904E-166838.066012620931.167562E-166840.032242655761.165240E-16
6794.80895185471 1.723211E-16 6796.77518188954 1.724544E-16 6798.74141192436 1.708294E-16 6800.70764195919 1.664712E-16 6802.67387199402 1.621107E-16 6804.64010202885 1.583783E-16 6806.60633206368 1.544931E-16 6808.57256209851 1.512843E-16 6810.53879213333 1.469733E-16 6812.50502216816 1.428561E-16 6814.47125220299 1.397207E-16 6816.43748223782 1.359377E-16 6820.36994230747 1.292932E-16 6822.3361723423 1.285335E-16 6826.26863241196 1.243141E-16 6828.23486244679 1.226796E-16 6830.20109248161 1.213784E-16 6832.16732251644 1.209083E-16 6834.13355255127 1.208359E-16 6836.0997825861 1.188904E-16 6838.06601262093 1.167562E-16 6840.03224265576 1.165240E-16
6796.775181889541.724544E-166798.741411924361.708294E-166800.707641959191.664712E-166802.673871994021.621107E-166804.640102028851.583783E-166806.606332063681.544931E-166810.538792133331.469733E-166812.505022168161.428561E-166814.471252202991.397207E-166816.437482237821.359377E-166818.403712272651.321583E-166820.369942307471.292932E-166824.302402377131.267035E-166826.268632411961.243141E-166832.167322516441.213784E-166832.167322516441.209083E-166836.09978258611.188904E-166838.066012620931.167562E-166840.032242655761.165240E-16
6798.741411924361.708294E-166800.707641959191.664712E-166802.673871994021.621107E-166804.640102028851.583783E-166806.606332063681.544931E-166808.572562098511.512843E-166810.538792133331.469733E-166812.505022168161.428561E-166814.471252202991.397207E-166816.437482237821.359377E-166820.369942307471.292932E-166822.33617234231.285335E-166824.302402377131.267035E-166826.268632411961.243141E-166832.234862446791.226796E-166830.201092481611.213784E-166832.167322516441.209083E-166836.09978258611.188904E-166838.066012620931.167562E-166840.032242655761.165240E-16
6800.70764195919 1.664712E-16 6802.67387199402 1.621107E-16 6804.64010202885 1.583783E-16 6806.60633206368 1.544931E-16 6808.57256209851 1.512843E-16 6810.53879213333 1.469733E-16 6812.50502216816 1.428561E-16 6814.47125220299 1.397207E-16 6816.43748223782 1.359377E-16 6818.40371227265 1.321583E-16 6820.36994230747 1.292932E-16 6822.3361723423 1.285335E-16 6824.30240237713 1.267035E-16 6826.26863241196 1.243141E-16 6828.23486244679 1.226796E-16 6830.20109248161 1.213784E-16 6832.16732251644 1.209083E-16 6834.13355255127 1.208359E-16 6836.0997825861 1.188904E-16 6838.06601262093 1.167562E-16 6840.03224265576 1.165240E-16
6802.67387199402 1.621107E-16 6804.64010202885 1.583783E-16 6806.60633206368 1.544931E-16 6808.57256209851 1.512843E-16 6810.53879213333 1.469733E-16 6812.50502216816 1.428561E-16 6814.47125220299 1.397207E-16 6816.43748223782 1.359377E-16 6818.40371227265 1.321583E-16 6820.36994230747 1.292932E-16 6822.3361723423 1.285335E-16 6824.30240237713 1.267035E-16 6826.26863241196 1.243141E-16 6828.23486244679 1.226796E-16 6830.20109248161 1.213784E-16 6832.16732251644 1.209083E-16 6834.13355255127 1.208359E-16 6836.0997825861 1.188904E-16 6838.06601262093 1.167562E-16 6840.03224265576 1.165240E-16
6804.64010202885 1.583783E-16 6806.60633206368 1.544931E-16 6808.57256209851 1.512843E-16 6810.53879213333 1.469733E-16 6812.50502216816 1.428561E-16 6814.47125220299 1.397207E-16 6816.43748223782 1.359377E-16 6818.40371227265 1.321583E-16 6820.36994230747 1.292932E-16 6822.3361723423 1.285335E-16 6824.30240237713 1.267035E-16 6826.26863241196 1.243141E-16 6828.23486244679 1.226796E-16 6830.20109248161 1.213784E-16 6832.16732251644 1.209083E-16 6834.13355255127 1.208359E-16 6836.0997825861 1.188904E-16 6838.06601262093 1.167562E-16 6840.03224265576 1.165240E-16
6806.60633206368 1.544931E-16 6808.57256209851 1.512843E-16 6810.53879213333 1.469733E-16 6812.50502216816 1.428561E-16 6814.47125220299 1.397207E-16 6816.43748223782 1.359377E-16 6818.40371227265 1.321583E-16 6820.36994230747 1.292932E-16 6822.3361723423 1.285335E-16 6824.30240237713 1.267035E-16 6826.26863241196 1.243141E-16 6828.23486244679 1.226796E-16 6830.20109248161 1.213784E-16 6832.16732251644 1.209083E-16 6834.13355255127 1.208359E-16 6836.0997825861 1.188904E-16 6838.06601262093 1.167562E-16 6840.03224265576 1.165240E-16
6808.57256209851 1.512843E-16 6810.53879213333 1.469733E-16 6812.50502216816 1.428561E-16 6814.47125220299 1.397207E-16 6816.43748223782 1.359377E-16 6818.40371227265 1.321583E-16 6820.36994230747 1.292932E-16 6822.3361723423 1.285335E-16 6824.30240237713 1.267035E-16 6826.26863241196 1.243141E-16 6828.23486244679 1.226796E-16 6830.20109248161 1.213784E-16 6832.16732251644 1.209083E-16 6834.13355255127 1.208359E-16 6836.0997825861 1.188904E-16 6838.06601262093 1.167562E-16 6840.03224265576 1.165240E-16
6810.53879213333 1.469733E-16 6812.50502216816 1.428561E-16 6814.47125220299 1.397207E-16 6816.43748223782 1.359377E-16 6818.40371227265 1.321583E-16 6820.36994230747 1.292932E-16 6822.3361723423 1.285335E-16 6824.30240237713 1.267035E-16 6826.26863241196 1.243141E-16 6828.23486244679 1.226796E-16 6830.20109248161 1.213784E-16 6832.16732251644 1.209083E-16 6834.13355255127 1.208359E-16 6836.0997825861 1.188904E-16 6838.06601262093 1.167562E-16 6840.03224265576 1.165240E-16
6812.50502216816 1.428561E-16 6814.47125220299 1.397207E-16 6816.43748223782 1.359377E-16 6818.40371227265 1.321583E-16 6820.36994230747 1.292932E-16 6822.3361723423 1.285335E-16 6824.30240237713 1.267035E-16 6826.26863241196 1.243141E-16 6828.23486244679 1.226796E-16 6830.20109248161 1.213784E-16 6832.16732251644 1.209083E-16 6834.13355255127 1.208359E-16 6836.0997825861 1.188904E-16 6838.06601262093 1.167562E-16 6840.03224265576 1.165240E-16
6814.47125220299 1.397207E-16 6816.43748223782 1.359377E-16 6818.40371227265 1.321583E-16 6820.36994230747 1.292932E-16 6822.3361723423 1.285335E-16 6824.30240237713 1.267035E-16 6826.26863241196 1.243141E-16 6828.23486244679 1.226796E-16 6830.20109248161 1.213784E-16 6832.16732251644 1.209083E-16 6834.13355255127 1.208359E-16 6836.0997825861 1.188904E-16 6838.06601262093 1.167562E-16 6840.03224265576 1.165240E-16
6816.43748223782 1.359377E-16 6818.40371227265 1.321583E-16 6820.36994230747 1.292932E-16 6822.3361723423 1.285335E-16 6824.30240237713 1.267035E-16 6826.26863241196 1.243141E-16 6828.23486244679 1.226796E-16 6830.20109248161 1.213784E-16 6832.16732251644 1.209083E-16 6834.13355255127 1.208359E-16 6836.0997825861 1.188904E-16 6838.06601262093 1.167562E-16 6840.03224265576 1.165240E-16
6818.40371227265 1.321583E-16 6820.36994230747 1.292932E-16 6822.3361723423 1.285335E-16 6824.30240237713 1.267035E-16 6826.26863241196 1.243141E-16 6828.23486244679 1.226796E-16 6830.20109248161 1.213784E-16 6832.16732251644 1.209083E-16 6834.13355255127 1.208359E-16 6836.0997825861 1.188904E-16 6838.06601262093 1.167562E-16 6840.03224265576 1.165240E-16
6820.36994230747 1.292932E-16 6822.3361723423 1.285335E-16 6824.30240237713 1.267035E-16 6826.26863241196 1.243141E-16 6828.23486244679 1.226796E-16 6830.20109248161 1.213784E-16 6832.16732251644 1.209083E-16 6834.13355255127 1.208359E-16 6836.0997825861 1.188904E-16 6838.06601262093 1.167562E-16 6840.03224265576 1.165240E-16
6822.3361723423 1.285335E-16 6824.30240237713 1.267035E-16 6826.26863241196 1.243141E-16 6828.23486244679 1.226796E-16 6830.20109248161 1.213784E-16 6832.16732251644 1.209083E-16 6834.13355255127 1.208359E-16 6836.0997825861 1.188904E-16 6838.06601262093 1.167562E-16 6840.03224265576 1.165240E-16
6824.30240237713 1.267035E-16 6826.26863241196 1.243141E-16 6828.23486244679 1.226796E-16 6830.20109248161 1.213784E-16 6832.16732251644 1.209083E-16 6834.13355255127 1.208359E-16 6836.0997825861 1.188904E-16 6838.06601262093 1.167562E-16 6840.03224265576 1.165240E-16
6826.26863241196 1.243141E-16 6828.23486244679 1.226796E-16 6830.20109248161 1.213784E-16 6832.16732251644 1.209083E-16 6834.13355255127 1.208359E-16 6836.0997825861 1.188904E-16 6838.06601262093 1.167562E-16 6840.03224265576 1.165240E-16
6828.23486244679 1.226796E-16 6830.20109248161 1.213784E-16 6832.16732251644 1.209083E-16 6834.13355255127 1.208359E-16 6836.0997825861 1.188904E-16 6838.06601262093 1.167562E-16 6840.03224265576 1.165240E-16
6830.20109248161 1.213784E-16 6832.16732251644 1.209083E-16 6834.13355255127 1.208359E-16 6836.0997825861 1.188904E-16 6838.06601262093 1.167562E-16 6840.03224265576 1.165240E-16
6832.16732251644 1.209083E-16 6834.13355255127 1.208359E-16 6836.0997825861 1.188904E-16 6838.06601262093 1.167562E-16 6840.03224265576 1.165240E-16
6834.13355255127 1.208359E-16 6836.0997825861 1.188904E-16 6838.06601262093 1.167562E-16 6840.03224265576 1.165240E-16
6836.0997825861 1.188904E-16 6838.06601262093 1.167562E-16 6840.03224265576 1.165240E-16
6838.06601262093 1.167562E-16 6840.03224265576 1.165240E-16
6840.03224265576 1.165240E-16
CO 41 000 470 COOF 0 1 1 COCF 4T3 1 C
6841.99847269058 1.162654E-16
6843.96470272541 1.153029E-16
6845.93093276024 1.156900E-16
6847.89716279507 1.146683E-16
6849.8633928299 1.129787E-16
6851.82962286473 1.125464E-16
6853.79585289955 1.118631E-16
6855.76208293438 1.097402E-16
6857.72831296921 1.076880E-16
6859.69454300404 1.065333E-16
6861.66077303887 1.036240E-16
6863.62700307369 1.008830E-16

Table F.4: $H\beta$ BELR Template (continued)

Wavelength	Flux
6865.59323310852	9.941723E-17
6867.55946314335	9.836731E-17
6869.52569317818	9.899505E-17
6871.49192321301	9.989987E-17
6873.45815324784	9.872328E-17
6875.42438328266	9.805009E-17
6877.39061331749	9.991049E-17
6879.35684335232	1.025136E-16
6881.32307338715	1.042061E-16
6883.28930342198	1.059879E-16
6885.2555334568	1.067030E-16
6887.22176349163	1.069361E-16
6889.18799352646	1.071202E-16
6891.15422356129	1.059941E-16
6893.12045359612	1.039432E-16
6895.08668363095	1.018756E-16
6897.05291366577	1.000824E-16
6899.0191437006	9.843286E-17
6900.98537373543	9.745626E-17
6902.95160377026	9.550489E-17
6904.91783380509	9.395984E-17
6906.88406383991	9.255356E-17
6908.85029387474	8.976951E-17
6910.81652390957	8.790642E-17
6912.7827539444	8.705714E-17
6914.74898397923	8.640128E-17
6916.71521401405	8.620677E-17
6918.68144404888	8.564016E-17
6920.64767408371	8.375203E-17
6922.61390411854	8.051756E-17
6924.58013415337	8.026651E-17
6926.5463641882	8.030790E-17
6928.51259422302	8.059127E-17
6930.47882425785	8.205407E-17
6932.44505429268	8.242054E-17
6934.41128432751	8.276763E-17
6936.37751436234	8.359578E-17
6938.34374439716	8.405809E-17
6940.30997443199	8.503781E-17
6942.27620446682	8.780586E-17
6944.24243450165	9.121252E-17
6946.20866453648	9.120476E-17
6948.17489457131	8.936094E-17
6950.14112460613	8.877355E-17
6952.10735464096	9.040408E-17

Table F.4: $H\beta$ BELR Template (continued)

Wavelength	Flux
6954.07358467579	9.342787E-17
6956.03981471062	9.619375E-17
6958.00604474545	9.685842E-17
6959.97227478028	9.223746E-17
6961.9385048151	9.675278E-17
6963.90473484993	1.106353E-16
6965.87096488476	9.989899E-17
6967.83719491959	6.706839E-17

Table F.5: C IV NELR Template - $c4_1549_{obs2}$

Wavelength	\mathbf{Flux}
1545.45678710937	7.499969E-17
1547.4230171442	1.941433E-14
1549.38924717903	5.025726E-14
1551.35547721385	6.703341E-14
1553.32170724868	4.388938E-14
1555.28793728351	2.777132E-14
1557.25416731834	1.335886E-14
1559.22039735317	4.519212E-15

Table FIELEN Template]O III] 1663 NELR Template - o3-1663

Wavelength	Flux	
1653.59942114353	0.	
1655.56565117836	3.818165E-15	
1657.53188121319	1.653593E-14	
1659.49811124802	7.897442E-14	
1661.46434128284	1.120051E-13	
1663.43057131767	8.360156E-14	
1665.3968013525	1.998717E-13	
1667.36303138733	1.659833E-13	
1669.32926142216	2.908810E-14	
1671.29549145698	3.295298E-15	
1673.26172149181	0.	

Table F.7: He II NELR Template - $narrow_he2$

Wavelength	Flux
1624.10595703125	-5.407848E-16
1626.07218706608	3.087130E-16
1628.03841710091	2.028263E-15
1630.00464713573	3.025209E-15
1631.97087717056	6.918567E-15
1633.93710720539	9.955625E-15
1635.90333724022	1.507005E-14
1637.86956727505	1.842422E-14
1639.83579730988	1.869978E-14
1641.8020273447	1.393788E-14
1643.76825737953	1.094051E-14
1645.73448741436	3.784189E-15
1647.70071744919	2.362817E-15
1649.66694748402	-1.916310E-16

Table F.8: O III 1663 BELR Template - o3-blr7

Wavelength	Flux
1645.	3.998061E-14
1647.	4.024494E-14
1649.	4.194744E-14
1651.	4.336624E-14
1653.	4.381397E-14
1655.	4.454867E-14
1657.	4.517564E-14
1659.	4.559542E-14
1661.	4.551842E-14
1663.	4.531951E-14
1665.	4.480633E-14
1667.	4.485704E-14
1669.	4.383002E-14
1671.	4.299172E-14
1673.	4.151335E-14
1675.	3.996005E-14
1677.	3.996005E-14

BIBLIOGRAPHY

REFERENCES

- Baldwin, J., Ferland, G., Korista, K., & Verner, D. 1995, ApJ, 455, L119+
- Baldwin, J. A., Ferland, G. J., Korista, K. T., Carswell, R. F., Hamann, F., Phillips, M. M., Verner, D., Wilkes, B. J., & Williams, R. E. 1996, ApJ, 461, 664
- Blandford, R. D. & McKee, C. F. 1982, ApJ, 255, 419
- Bohlin, R. C., Harris, A. W., Holm, A. V., & Gry, C. 1990, ApJS, 73, 413
- Bottorff, M. C., Baldwin, J. A., Ferland, G. J., Ferguson, J. W., & Korista, K. T. 2002, ApJ, 581, 932
- Casebeer, D. & Leighly, K. M. 2003, in Astronomical Society of the Pacific Conference Series, Vol. 290, Active Galactic Nuclei: From Central Engine to Host Galaxy, ed. S. Collin, F. Combes, & I. Shlosman, 81-+
- Clavel, J., Reichert, G. A., Alloin, D., Crenshaw, D. M., Kriss, G., Krolik, J. H., Malkan, M. A., Netzer, H., Peterson, B. M., Wamsteker, W., Altamore, A., Baribaud, T., Barr, P., Beck, S., Binette, L., Bromage, G. E., Brosch, N., Diaz, A. I., Filippenko, A. V., Fricke, K., Gaskell, C. M., Giommi, P., Glass, I. S., Gondhalekar, P., Hackney, R. L., Halpern, J. P., Hutter, D. J., Joersaeter, S., Kinney, A. L., Kollatschny, W., Koratkar, A., Korista, K. T., Laor, A., Lasota, J.-P., Leibowitz, E., Maoz, D., Martin, P. G., Mazeh, T., Meurs, E. J. A., Nair, A. D., O'Brien, P., Pelat, D., Perez, E., Perola, G. C., Ptak, R. L., Rodriguez-Pascual, P., Rosenblatt, E. I., Sadun, A. C., Santos-Lleo, M., Shaw, R. A., Smith, P. S., Stirpe, G. M., Stoner, R., Sun, W. H., Ulrich, M.-H., van Groningen, E., & Zheng, W. 1991, ApJ, 366, 64
- de La Pena, M. D., Nichols-Bohlin, J., Levay, K. L., & Michalitsianos, A. 1994, in ASP Conf. Ser. 61: Astronomical Data Analysis Software and Systems III, 127-+
- de Vaucouleurs, G., de Vaucouleurs, A., Corwin, H. G., Buta, R. J., Paturel, G., & Fouque, P. 1991, Third Reference Catalogue of Bright Galaxies (Volume 1-3, XII, 2069 pp. 7 figs.. Springer-Verlag Berlin Heidelberg New York)
- Dhanda, N., Baldwin, J. A., Bentz, M. C., & Osmer, P. S. 2007, ApJ, 658, 804
- Dietrich, M., Kollatschny, W., Peterson, B. M., Bechtold, J., Bertram, R., Bochkarev, N. G., Boroson, T. A., Carone, T. E., Elvis, M., Filippenko, A. V., Gaskell, C. M., Huchra, J. P., Hutchings, J. B., Koratkar, A. P., Korista, K. T., Lame, N. J., Laor, A., MacAlpine, G. M., Malkan, M. A., Mendes de Oliveira, C., Netzer, H., Penfold, J., Penston, M. V., Perez, E., Pogge, R. W., Richmond, M. W., Rosenblatt, E. I., Shapovalova, A. I., Shields, J. C., Smith, H. A., Smith, P. S., Sun, W.-H., Thiele, U., Veilleux, S., Wagner, R. M., Wilkes, B. J., Wills, B. J., & Wills, D. 1993, ApJ, 408, 416

Ferland, G. J. 1999, PASP, 111, 1524

—. 2006, Hazy, A Brief Introduction to Cloudy 06.02 (University of Kentucky Internal Report, 565 pages)

Gaskell, C. M. 2008, in Revista Mexicana de Astronomia y Astrofisica Conference Series, Vol. 32, Revista Mexicana de Astronomia y Astrofisica Conference Series, 1–11

Greenstein, J. L. & Schmidt, M. 1964, ApJ, 140, 1

Hamann, F. & Ferland, G. 1999, ARA&A, 37, 487

Hamann, F., Korista, K. T., Ferland, G. J., Warner, C., & Baldwin, J. 2002, ApJ, 564, 592

Kaspi, S. 2007, in Astronomical Society of the Pacific Conference Series, Vol. 373, The Central Engine of Active Galactic Nuclei, ed. L. C. Ho & J.-W. Wang, 13-+

Koratkar, A., Evans, I., Pesto, S., & Taylor, C. 1997, ApJ, 491, 536

Korista, K., Baldwin, J., Ferland, G., & Verner, D. 1997, ApJS, 108, 401

Korista, K. T., Alloin, D., Barr, P., Clavel, J., Cohen, R. D., Crenshaw, D. M., Evans, I. N., Horne, K., Koratkar, A. P., Kriss, G. A., Krolik, J. H., Malkan, M. A., Morris, S. L., Netzer, H., O'Brien, P. T., Peterson, B. M., Reichert, G. A., Rodriguez-Pascual, P. M., Wamsteker, W., Anderson, K. S. J., Axon, D. J., Benitez, E., Berlind, P., Bertram, R., Blackwell, Jr., J. H., Bochkarev, N. G., Boisson, C., Carini, M., Carrillo, R., Carone, T. E., Cheng, F.-Z., Christensen, J. A., Chuvaev, K. K., Dietrich, M., Dokter, J. J., Doroshenko, V., Dultzin-Hacyan, D., England, M. N., Espey, B. R., Filippenko, A. V., Gaskell, C. M., Goad, M. R., Ho, L. C., Huchra, J. P., Jiang, X. J., Kaspi, S., Kollatschny, W., Laor, A., Luminet, J.-P., MacAlpine, G. M., MacKenty, J. W., Malkov, Y. F., Maoz, D., Martin, P. G., Matheson, T., McCollum, B., Merkulova, N., Metik, L., Mignoli, M., Miller, H. R., Pastoriza, M. G., Pelat, D., Penfold, J., Perez, M., Perola, G. C., Persaud, J. L., Peters, J., Pitts, R., Pogge, R. W., Pronik, I., Pronik, V. I., Ptak, R. L., Rawley, L., Recondo-Gonzalez, M. C., Rodriguez-Espinosa, J. M., Romanishin, W., Sadun, A. C., Salamanca, I., Santos-Lleo, M., Sekiguchi, K., Sergeev, S. G., Shapovalova, A. I., Shields, J. C., Shrader, C., Shull, J. M., Silbermann, N. A., Sitko, M. L., Skillman, D. R., Smith, H. A., Smith, S. M., Snijders, M. A. J., Sparke, L. S., Stirpe, G. M., Stoner, R. E., Sun, W.-H., Thiele, U., Tokarz, S., Tsvetanov, Z. I., Turnshek, D. A., Veilleux, S., Wagner, R. M., Wagner, S. J., Wanders, I., Wang, T., Welsh, W. F., Weymann, R. J., White, R. J., Wilkes, B. J., Wills, B. J., Winge, C., Wu, H., & Zou, Z. L. 1995, ApJS, 97, 285

Kuehn, C. A., Baldwin, J. A., Peterson, B. M., & Korista, K. T. 2008, ApJ, 673, 69MacAlpine, G. M. 1981, ApJ, 251, 465

- O'Brien, P. T., Dietrich, M., Leighly, K., Alloin, D., Clavel, J., Crenshaw, D. M., Horne, K., Kriss, G. A., Krolik, J. H., Malkan, M. A., Netzer, H., Peterson, B. M., Reichert, G. A., Rodríguez-Pascual, P. M., Wamsteker, W., Anderson, K. S. J., Bochkarev, N. G., Cheng, F.-Z., Filippenko, A. V., Gaskell, C. M., George, I. M., Goad, M. R., Ho, L. C., Kaspi, S., Kollatschny, W., Korista, K. T., MacAlpine, G., Marlow, D., Martin, P. G., Morris, S. L., Pogge, R. W., Qian, B.-C., Recondo-Gonzalez, M. C., Espinosa, J. M. R., Santos-Lleó, M., Shapovalova, A. I., Shull, J. M., Stirpe, G. M., Sun, W.-H., Turner, T. J., Vio, R., Wagner, S., Wanders, I., Wills, K. A., Wu, H., Xue, S.-J., & Zou, Z.-L. 1998, ApJ, 509, 163
- Oke, J. B. & Schmidt, M. 1963, AJ, 68, 288
- Osterbrock, D. E. 1989, Astrophysics of gaseous nebulae and active galactic nuclei (Research supported by the University of California, John Simon Guggenheim Memorial Foundation, University of Minnesota, et al. Mill Valley, CA, University Science Books, 1989, 422 p.)
- Peterson, B. M. 1993, PASP, 105, 247
- Peterson, B. M. 2006, in Lecture Notes in Physics, Berlin Springer Verlag, Vol. 693, Physics of Active Galactic Nuclei at all Scales, ed. D. Alloin, 77-+
- Peterson, B. M., Alloin, D., Axon, D., Balonek, T. J., Bertram, R., Boroson, T. A., Christensen, J. A., Clements, S. D., Dietrich, M., Elvis, M., Filippenko, A. V., Gaskell, C. M., Haswell, C. A., Huchra, J. P., Jackson, N., Kollatschny, W., Korista, K. T., Lame, N. J., Leacock, R. J., Lin, S.-N., Malkan, M. A., Monk, A. S., Penston, M. V., Pogge, R. W., Robinson, A., Rosenblatt, E. I., Shields, J. C., Smith, A. G., Stirpe, G. M., Sun, W.-H., Turner, T. J., Wagner, R. M., Wilkes, B. J., & Wills, B. J. 1992, ApJ, 392, 470
- Peterson, B. M., Balonek, T. J., Barker, E. S., Bechtold, J., Bertram, R., Bochkarev, N. G., Bolte, M. J., Bond, D., Boroson, T. A., Carini, M. T., Carone, T. E., Christensen, J. A., Clements, S. D., Cochran, A. L., Cohen, R. D., Crampton, D., Dietrich, M., Elvis, M., Ferguson, A., Filippenko, A. V., Fricke, K. J., Gaskell, C. M., Halpern, J. P., Huchra, J. P., Hutchings, J. B., Kollatschny, W., Koratkar, A. P., Korista, K. T., Krolik, J. H., Lame, N. J., Laor, A., Leacock, R. J., MacAlpine, G. M., Malkan, M. A., Maoz, D., Miller, H. R., Morris, S. L., Netzer, H., Oliveira, C. L. M., Penfold, J., Penston, M. V., Perez, E., Pogge, R. W., Richmond, M. W., Romanishin, W., Rosenblatt, E. I., Saddlemyer, L., Sadun, A., Sawyer, S. R., Shields, J. C., Shapovalova, A. I., Smith, A. G., Smith, H. A., Smith, P. S., Sun, W.-H., Thiele, U., Turner, T. J., Veilleux, S., Wagner, R. M., Weymann, R. J., Wilkes, B. J., Wills, B. J., Wills, D., & Younger, P. F. 1991, ApJ, 368, 119
- Peterson, B. M., Ferrarese, L., Gilbert, K. M., Kaspi, S., Malkan, M. A., Maoz, D., Merritt, D., Netzer, H., Onken, C. A., Pogge, R. W., Vestergaard, M., & Wandel, A. 2004, ApJ, 613, 682

Peterson, B. M. & Horne, K. 2006, in Planets to Cosmology: Essential Science in the Final Years of the Hubble Space Telescope, ed. M. Livio & S. Casertano, 89-+

Peterson, B. M. & Wandel, A. 1999, ApJ, 521, L95

Phillips, M. M. 1977, ApJ, 215, 746

—. 1978, ApJS, 38, 187

Reichert, G. A., Rodriguez-Pascual, P. M., Alloin, D., Clavel, J., Crenshaw, D. M., Kriss, G. A., Krolik, J. H., Malkan, M. A., Netzer, H., Peterson, B. M., Wamsteker, W., Altamore, A., Altieri, B., Anderson, K. S., Blackwell, Jr., J. H., Boisson, C., Brosch, N., Carone, T. E., Dietrich, M., England, M. N., Evans, I. N., Filippenko, A. V., Gaskell, C. M., Goad, M., Gondhalekar, P. M., Horne, K., Kazanas, D., Kollatschny, W., Koratkar, A. P., Korista, K. T., MacAlpine, G. M., Maoz, D., Mazeh, T., McCollum, B., Miller, H. R., Mendes de Oliveira, C., O'Brien, P. T., Pastoriza, M. G., Pelat, D., Perez, E., Perola, G. C., Pogge, R. W., Ptak, R. L., Recondo-Gonzalez, M. C., Rodriguez-Espinosa, J., Rosenblatt, E. I., Sadun, A. C., Santos-Lleo, M., Shields, J. C., Shrader, C. R., Shull, J. M., Simkin, S. M., Sitko, M. L., Snijders, M. A. J., Sparke, L. S., Stirpe, G. M., Stoner, R., Storchi-Bergmann, T., Sun, W.-H., Wang, T., Welsh, W. F., White, R. J., Winge, C., & Zheng, W. 1994, ApJ, 425, 582

Rodriguez-Pascual, P. M., Alloin, D., Clavel, J., Crenshaw, D. M., Horne, K., Kriss, G. A., Krolik, J. H., Malkan, M. A., Netzer, H., O'Brien, P. T., Peterson, B. M., Reichert, G. A., Wamsteker, W., Alexander, T., Barr, P., Blandford, R. D., Bregman, J. N., Carone, T. E., Clements, S., Courvoisier, T.-J., De Robertis, M. M., Dietrich, M., Dottori, H., Edelson, R. A., Filippenko, A. V., Gaskell, C. M., Huchra, J. P., Hutchings, J. B., Kollatschny, W., Koratkar, A. P., Korista, K. T., Laor, A., MacAlpine, G. M., Martin, P. G., Maoz, D., McCollum, B., Morris, S. L., Perola, G. C., Pogge, R. W., Ptak, R. L., Recondo-Gonzalez, M. C., Rodriguez-Espinoza, J. M., Rokaki, E. L., Santos-Lleo, M., Sekiguchi, K., Shull, J. M., Snijders, M. A. J., Sparke, L. S., Stirpe, G. M., Stoner, R. E., Sun, W.-H., Wagner, S. J., Wanders, I., Wilkes, B. J., Winge, C., & Zheng, W. 1997, ApJS, 110, 9

Schmidt, M. 1963, Nature, 197, 1040

Terrell, J. 1967, ApJ, 147, 827

Véron-Cetty, M.-P., Joly, M., & Véron, P. 2004, A&A, 417, 515

Vestergaard, M. & Peterson, B. M. 2005, ApJ, 625, 688

Vestergaard, M. & Wilkes, B. J. 2001, ApJS, 134, 1

Wamsteker, W., Rodriguez-Pascual, P., Wills, B. J., Netzer, H., Wills, D., Gilmozzi, R., Barylak, M., Talavera, A., Maoz, D., Barr, P., & Heck, A. 1990, ApJ, 354, 446

Wanders, I., Peterson, B. M., Alloin, D., Ayres, T. R., Clavel, J., Crenshaw, D. M., Horne, K., Kriss, G. A., Krolik, J. H., Malkan, M. A., Netzer, H., O'Brien, P. T., Reichert, G. A., Rodriguez-Pascual, P. M., Wamsteker, W., Alexander, T., Anderson, K. S. J., Benitez, E., Bochkarev, N. G., Burenkov, A. N., Cheng, F.-Z., Collier, S. J., Comastri, A., Dietrich, M., Dultzin-Hacyan, D., Espey, B. R., Filippenko, A. V., Gaskell, C. M., George, I. M., Goad, M. R., Ho, L. C., Kaspi, S., Kollatschny, W., Korista, K. T., Laor, A., MacAlpine, G. M., Mignoli, M., Morris, S. L., Nandra, K., Penton, S., Pogge, R. W., Ptak, R. L., Rodriguez-Espinoza, J. M., Santos-Lleo, M., Shapovalova, A. I., Shull, J. M., Snedden, S. A., Sparke, L. S., Stirpe, G. M., Sun, W.-H., Turner, T. J., Ulrich, M.-H., Wang, T.-G., Wei, C., Welsh, W. F., Xue, S.-J., & Zou, Z.-L. 1997, ApJS, 113, 69

